The Role of A-type Lamins in Normal Cardiac Function

Steven C. Chen

A dissertation
submitted in partial fulfillment of the
requirements for the degree of

Doctor of Philosophy

University of Washington
2012

Reading Committee:
Dr. Brian K. Kennedy, Chair
Dr. Paul D. Lampe
Dr. David R. Morris

Program Authorized to Offer Degree:
Department of Biochemistry

University of Washington

Abstract

The Role of A-type Lamins in Normal Cardiac Function

Steven C. Chen

Chair of the Supervisory Committee:
Associate Professor Brian K. Kennedy
Department of Biochemistry

A-type lamins, primarily represented by the proteins lamin A and lamin C, are unique intermediate filaments that localize to the inner nuclear membrane to form the nuclear lamina. The lamina helps maintain nuclear structure in addition to having regulatory roles in a range of nuclear processes. Point mutations in lamin A have been implicated in a wide variety of human diseases, termed laminopathies, which are categorized roughly into those affecting striated muscle tissue function, adipose tissue distribution, or pathologies associated with rapid aging in multiple tissues. The subset affecting striated muscle represents the majority of laminopathies, with patients often developing and eventually succumbing to cardiac failure resulting from progressive dilated cardiomyopathy with conduction disease. The A-type lamin knockout mouse (*Lmna*$^{-/-}$) exhibits many characteristics of striated muscle laminopathies, such as muscular dystrophy, dilated cardiomyopathy and premature death at 6-8 weeks. In this dissertation, I use the *Lmna*$^{-/-}$ mouse model to further dissect and understand the role of lamin A in cardiac function, proposing some potential mechanisms that may be suitable for further investigation in human patients.

Table of Contents

List of Figures

Appendix 1

List of Tables

Acknowledgements

This research would not be possible without the support of many people, as they say, "It takes a village to raise a doctoral student."

I would first express thanks to my compatriots in the Kennedy lab, who made J329 and J337 a great environment for science. I have to give special gratitude to Monique Stanfel, who somehow tolerated being seated one foot behind me and sharing a lab bay; Richard Frock, as we worked closely together for many years investigating the many roles of A-type lamins; and Vivian MacKay, the lab mother who provided much emotional support through the years. I also have to thank all the undergraduates who tolerated my mentorship. Firstly, Ellie Frett and Hannah Dzimitrowicz, the Amgen scholars, who did exceptional work and are starting their own journey into science. Secondly, Scott Tsuchiyama and Dennis Wang, the undergraduate researchers who helped me with all my mouse genotyping and experiments and are also pursuing science or medicine.

I should extend gratitude to the members of the Lampe lab, who were so welcoming to an orphaned graduate student and supported me in my research. I especially have to thank Joell Solan for being so passionate and available to talk science; Clay Dunn and Rachel Norris for sage postdoc advice; Perry Thornton the lab manager who so readily accepted the burden of my mouse colony; and Justin Mirus for being a fellow grad student and lover of beer.

I appreciated the many years of graduate students of the UW Department of Biochemistry who shaped and influenced my perspective on science, hopefully I was able to successfully pass the torch to the new generation of graduate students. A special thanks goes to Lucas Gray, my best man, fellow beer aficionado and constant companion; Phil Tai, who always asked the best questions and fought for the best answers; Dave Dranow, who somehow got his work done despite my best distractions; and Ken Lindsay, as a lover of fine board games and a fellow cocktailian.

Of course none of this work would be possible without the support of my mentors, Dr. Brian Kennedy and Dr. Paul Lampe. Brian, those first few years of graduate school were formative and seeing your unwavering dedication to advancing and advocating the field of science is admirable. Though our journey together took an atypical path, you've never ceased supporting and going to bat for me. Paul, you've been so gracious to allow me to join your lab and complete my project with your support. You made space for me on your own lab bench and gave me the corner window view of Lake Union and Gasworks Park. Of course I also extend thanks to my committee members for tolerating my presentations and providing very valuable help and insight. Never underestimate the wisdom of your elders.

Finally, to my family, for nurturing my love for science despite knowing the challenges I would face. To my mom for all the extra time she squeezed out of the day to support me, to my dad who helped shaped me as a man, and to my sister for being my co-conspirator in many mischievous deeds.

Dedication

Dedicated to my wife
Thank you for all you do

Introduction

The Nuclear Lamins

Lamins are a family of type V intermediate filament proteins that were discovered as the major component of the nuclear lamina, residing between chromatin and the inner nuclear membrane [1,2]. Originally hypothesized to help provide shape and structure to the nucleus, recent research has expanded their role to a variety of other functions, for instance either directly or indirectly influencing gene regulation, nuclear positioning in the cell through interactions with the cytoskeleton, and maintaining higher-order chromosome organization. Due to their many functions in the mammalian cell, it is not surprising that mutations in nuclear lamins can cause a wide variety of diseases collectively termed laminopathies. The spectrum of laminopathies can be broadly classified into those that affect the striated muscles, those that affect adipose tissue distribution and those leading to progeroid syndromes.

The family of nuclear lamin proteins currently consists of seven members, encoded by only three genes. The A-type lamins are encoded by the *LMNA* gene, which through alternative splicing, results in lamin A, lamin AΔ10, lamin C and lamin C2 [3,4,5]. B-type lamins are encoded by either the *LMNB1* or *LMNB2* genes, which encode lamin B1, lamin B2 and lamin B3 [6,7,8]. A-type lamins are primarily expressed in differentiated cells versus B-type lamins which are expressed in all cells through development [9]. Finally, lamins C2 and B3 are expressed only in germ-line cells [4,6,10]. The majority of laminopathies have implicated the *LMNA* gene and so research has focused on understanding the function and role of the A-type lamins in these diseases.

Lamins, being intermediate filament proteins, consist of a highly conserved α-helical coiled-coil rod domain, flanked by N-terminal and C-terminal globular domains [3]. Lamins initiate polymerization by lateral association of the rod domains to form head-to-tail dimers, which further polymerize in an end-to-end fashion, resulting in the meshwork of the nuclear lamina [11,12,13]. The C-terminal tail contains a nuclear localization signal, responsible for the active transport to the nucleus, and an immunoglobulin-like fold motif which is a hotspot for mutation in the group of laminopathies affecting adipose tissue. Lamin A is initially synthesized as a precursor, termed prelamin A, which ends with a CaaX amino acid motif at the C-terminus. This CaaX motif, also common to lamin B, is targeted for farnesylation, followed by cleavage of the –aaX, and carboxymethylation [14,15]. The farnesyl group is thought to be required to anchor and localize lamins properly to the nuclear envelope [16,17,18,19]. Finally, for prelamin A, the zinc metalloprotease ZMPSTE24 recognizes the farnesylated form of prelamin A and cleaves the carboxy-terminal 18 amino acids, ultimately removing the farnesyl group in mature lamin A [20]. Interestingly, lamin C is not synthesized with the CaaX motif, so it must undergo a different process to localize properly to the nuclear envelope.

Function of Nuclear Lamins

Nuclear lamins have a variety of essential roles in the cell, first and foremost being responsible for nuclear envelope assembly. The nuclear envelope, comprised of the inner nuclear membrane and outer nuclear membrane, functions as the interface between the nucleus and the cytoplasm [21]. The gap between them, known as the perinuclear space, is bridged by nuclear pore complexes, which regulate the flow of proteins in and out of the

nucleus [22]. The nuclear lamina, comprised of both A- and B-type lamins, forms a network underlying the inner nuclear membrane and interacts with many of the embedded integral membrane proteins. Many experiments utilizing cell-free extracts to study nuclear assembly *in vitro* have shown that, without lamins, there was a loss of chromosome decondensation, nuclear membrane formation and nuclear pore assembly [23,24,25,26,27]. In *Drosophila* and *C. elegans*, reduced lamin expression resulted in inhibition of nuclear membrane assembly or affected normal nuclear membrane organization, respectively [28,29]. Expressing the carboxy-terminal domain of lamin B3 in *Xenopus* affects the normal polymerization kinetics of A-type lamins, and subsequently altered the normal process of nuclear envelope formation by blocking the fusogenic nuclear membrane vesicle from interacting with chromatin [30]. These experiments demonstrate the essential role of lamins in the process of forming the nuclear lamina, likely dependent on some combination of the many inner nuclear membrane proteins with which it interacts.

In addition to its role in the physical formation of the nuclear envelope, lamins play an important role in regulating DNA synthesis and RNA transcription. *Xenopus* nuclei assembled *in vitro* lacking lamins do not replicate their DNA [31,32] and the addition of either *Xenopus* or human dominant-negative lamin A lacking the amino-terminal domain, do not rescue this defect [33,34,35]. During S phase, lamins have been observed to colocalize with PCNA, a factor essential during the elongation phase of replication [36], and the introduction of lamins lacking their amino-terminal domain induce the formation of nucleoplasmic aggregates containing PCNA [35]. However, highly concentrated *Xenopus* nucleoplasmic extract can support the replication of genomic DNA without the presence of a nuclear envelope and lamina [37]. It is

thus likely that the role of the lamina underlying the nuclear envelope is to retain and concentrate the factors necessary for DNA replication. The relationship between lamins and RNA transcription is less well-understood; however, many observations have been made that imply a significant interaction. As the isoforms of B-type lamins are expressed in different developmental stages and A-type lamins expressed in differentiated tissue, it is likely that the lamins are playing some role in regulating gene expression. Cancer cells, which tend to adopt a less differentiated state, have been shown to have lower expression of lamin A [38]. A number of transcription factors, such as *Oct-1* and *Rb*, have been shown to associate with nuclear lamins, further lending credence to the role of lamins in transcription [39,40,41]. Finally, the expression of the dominant negative lamin A reduces the amount of RNA polymerase II-dependent transcripts [42], though the mechanism by which this occurs and why it is specific to RNA polymerase II remains unknown. In summary, lamins likely serve as a scaffold for factors essential to both DNA synthesis and RNA transcription.

Peripheral heterochromatin has been shown to closely associate with nuclear lamins in a variety of animal species [1,43,44]. It has been shown that this may be occurring through specific DNA sequences known as matrix-attachment and scaffold-attachment regions [45,46,47]. Lamins tend to have a repressive role on the genes that they interact with, resulting in transcriptionally silent genes marked with repressive histone methylation [48,49]. The binding of lamins to specific chromosomal domains, combined with the concept of chromosomal territories, leads to speculation that lamins play an important role in the regulation of chromosomal domains and thus normal gene expression [50,51].

More recent biomechanical studies have revealed that lamins may play a crucial role in the concept of a “nucleoskeleton”, which confers specific mechanical properties and functionality to the nucleus similar to the cytoskeleton [52]. In fact, the mammalian cytoskeleton is dependent on the nucleoskeleton, as MEFS lacking A-type lamins have a significantly softer cytoskeleton, which implies an important role for the lamins in generating a functional cytoskeletal network [53]. Lamins have been shown to interact with the cytoskeleton through LINC (links the nucleoskeleton and cytoskeleton) protein complexes [54,55,56]. The LINC complexes are usually comprised of SUN (Sad1 and UNC-84) domain-containing proteins and KASH (Klarsicht, ANC-1 and SYNE homology) domain-containing nesprins. SUN domain-containing proteins, encoded by the *SUN*, *SUN2*, and *SUN3* genes, are embedded in the inner nuclear membrane and interact with other nuclear membrane proteins such as emerin and lamins. KASH domain-nesprins are embedded in the outer nuclear membrane, binding to both SUN domain-containing proteins and cytoskeletal proteins such as F-actin, thus forming a bridge through the nuclear membrane. Disrupting the LINC complex and the nucleoskeletal-cytoskeletal linkage can perturb normal gene expression in both myoblasts and cardiomyocytes [57,58].

Laminopathies

Given the many cellular roles in which A-type lamins are involved, it is perhaps surprising that mammals can survive at all without them. Instead, altered A-type lamin function is primarily limited to diseases affecting striated muscle or adipose tissue. Hundreds of different *LMNA* mutations have been catalogued (lamin mutation database can be accessed at

http://www.dmd.nl/lmna_seqvar.html) that are dispersed throughout the gene. The first disease-associated mutant, linking autosomal-dominant Emery-Dreifuss muscular dystrophy to the *LMNA* gene in 1999 [59], sparked a rash of discoveries over the next ten years linking *LMNA* to the wide variety of diseases we term laminopathies today [60].

The first group of laminopathies can be roughly characterized as those affecting striated muscle, including autosomal-dominant Emery-Dreifuss muscular dystrophy, limb-girdle muscular dystrophy, and dilated cardiomyopathy with conduction system disease. These diseases are the most common laminopathies, comprising over 60% of diagnosed cases. Emery-Dreifuss muscular dystrophy (EDMD) initially presents with joint contractures of the elbows, ankles and neck, in time progressing to muscle weakness and wasting of the muscles of the upper arms, lower legs, shoulders and hips [61]. Almost all patients eventually also develop dilated cardiomyopathy, which is the primary cause of mortality. There is also an X-linked Emery-Dreifuss muscular dystrophy, caused by mutations in emerin, another inner nuclear membrane protein [62]. From this, it has been inferred that EDMD is due to defects in the structural nature of lamins in the nuclear envelope, perhaps resulting in nuclear fragility and having a most pronounced effect in the repeatedly stressed myocyte.

Limb-girdle muscular dystrophy (LGMD) affects muscles of the hips and shoulders also known as the limb girdle muscles. Patients with limb-girdle muscular dystrophy can also develop cardiomyopathy, although at a lesser frequency than those with EDMD [63]. Other known causes of LGMD are mutations in genes encoding sarcoglycan proteins, which are transmembrane proteins responsible for connecting the cytoskeletal elements of the muscle fiber to the extracellular matrix. In addition, LGMD can be caused by mutations in the *SYNE1*

and *SYNE2* genes, which are components of the LINC complexes responsible for linking the nucleoskeleton and the cytoskeleton. Thus, we can speculate that lamins contribute to LGMD by affecting normal cytoskeleton organization through defects in the nucleoskeleton itself.

Interestingly, *LMNA* mutations can also cause dilated cardiomyopathy (DCM), without the development of skeletal muscle disease [63,64,65,66,67], making dilated cardiomyopathy the unifying theme among the laminopathies affecting striated muscle. DCM is a generalized condition describing an enlarged and weakened heart that is no longer able to efficiently pump blood. Laminopathy patients develop dilated cardiomyopathy with conduction system disease (DCM-CD), characterized by the addition of arrhythmic conduction defects and sudden cardiac death to the DCM pathology. Mutations in *LMNA* have been identified as the top identified genetic cause of DCM-CD [68], and conversely many patients with DCM-CD have an undiagnosed laminopathy [69,70]. Ultimately, most laminopathy patients with DCM-CD die from sudden cardiac death, causing death by ventricular fibrillation, which in certain cases can be rescued by the implantation of certain pacemakers [71,72,73,74]. The mechanism by which mutations in *LMNA* that cause EDMD or LGMD also leads to DCM-CD is still unclear, though some recent work shows that mutations do not affect structure significantly, thus implying DCM-CD arises from effects on binding partners of lamins [75]. Ultimately, as DCM-CD is the underlying cause of death in the majority of laminopathies, understanding this relationship will improve our understanding and perhaps lead to treatment in a wide variety of disease patients.

Shortly after the association of *LMNA* with muscular dystrophy, it was discovered in 2000 that *LMNA* mutations could also resulted in lipodystrophies, foremost among these Dunnigan-type familial partial lipodystrophy (FPLD) [76,77,78]. FPLD is characterized by the loss

of normal adipose tissue distribution and consequently insulin resistance and diabetes type 2 [79,80]. Most FPLD mutations occur in exon 8 of *LMNA*, which encodes the immunoglobulin-like fold domain of the globular C-terminal domain [81,82]. Mandibuloacral dysplasia (MAD), another disease with lipodystrophic-like symptoms, is also caused by mutations in this region and presents with the addition of congenital abnormalities and affecting normal development of facial bones [83]. As both FPLD and MAD are associated with mutations in the region of *LMNA* encoding the Ig-like fold domain, it is clear that this feature is somehow essential for normal lamin function, though the mechanism is currently unclear. MAD can also be the result of mutations in *ZMPSTE24*, required for the normal maturation process of lamin A, which may indicate that perturbing this process results in the abnormal bone development observed in MAD.

Mutations in *LMNA* can also result in Charcot-Marie-Tooth disease type 2 (CMT2), which results in dysfunctional axons and loss of normal nerve impulse conduction not necessarily due to demyelination [84]. Nerves of *Lmna*$^{-/-}$ mice exhibit a reduction of axonal density, enlargement of axons and loss of normal myelination, which may be similar to the human disease. Most of the genes associated with CMT encode neuronal proteins, but some of those associated with CMT2, such as *MFN2*, *KIF1B* and *RAB7A*, encode proteins essential for normal intracellular transport of either mitochondria or vesicles. As *LMNA* has been identified to interact with the cytoskeleton through the LINC complex, it is possible that CMT2 is the result of a disrupted normal cytoskeletal network and thus loss of normal trafficking of neuronal proteins.

The final group of diseases resulting from mutations in *LMNA* affects multiple organ systems and presents with signs of accelerated aging. The most recognizable is Hutchinson-Gilford progeria syndrome (HGPS), characterized by signs of accelerated aging such as alopecia, wrinkled skin, limited growth, loss of eyesight, atherosclerosis, and cardiovascular problems leading to premature death at 12-15 years of age due to myocardial infarction or stroke [85,86]. The predominant mutation associated with HGPS is G608G, which results in a truncated prelamin A protein that is farnesylated but not cleaved by ZMPSTE24 [87]. The permanently farnesylated prelamin A has been termed progerin. Accumulation of the progerin protein has been correlated with loss of normal DNA repair mechanisms and increased genomic instability [88,89,90,91]. In addition, progerin activates the Notch signaling pathway in both mouse models and human patients, which may affect normal stem cell proliferation and differentiation [92,93].

Mouse Models for Laminopathies

A number of mouse models have been generated to study the molecular pathology of laminopathies and DCM-CD in particular. By introducing the same mutations that cause disease in human patients, mouse models can help us understand the physiological consequences of each mutation and perhaps the molecular mechanism as well. One interesting point of note is that most laminopathies in humans are dominant genetic traits, while the same mutation in a mouse model requires homozygosity to exhibit disease pathology, indicating a recessive inheritance. Regardless, these mouse models have proven invaluable to furthering our understanding of laminopathies in general.

The first mouse line generated in 1999 was one that knocked out the *Lmna* gene, resulting in a mouse that did not express lamin A or C. These mice develop normally *in utero*, but begin to show a growth defect by 2 weeks of age and die at 6-7 weeks [94]. *Lmna*$^{-/-}$ mice exhibit severe muscular dystrophy, as indicated by the increase of fiber size variability and presence of centrally located nuclei. Initial characterization also revealed damage and atrophy of cardiomyocytes by histology. *Lmna*$^{-/-}$ myoblasts also demonstrate decreased differentiation potential [95]. Further studies confirmed cardiac involvement and the development of DCM-CD in these mice with hallmark characteristics such as ventricular dilation, decreased fractional shortening as measured by echocardiogram, and decreased heart conductivity as measured by electrocardiogram [96]. As previously mentioned, *Lmna*$^{-/-}$ mice also exhibit characteristics of a peripheral neuropathy which, combined with the muscular dystrophy and dilated cardiomyopathy, appear to make these mice recapitulate many of the disease phenotypes associated with laminopathies. However, most laminopathies are dominantly inherited and there have only been two patients with very early truncation of *LMNA* by either nonsense or premature stop codon [59,97]. This raises the question as to why the *Lmna*$^{-/-}$ mice seem like such a well-suited model for laminopathies. Is it simply coincidence that they develop the same disease pathology, could this be an effect of the mouse model or could this mouse not be a true null? Regardless, more recent studies have shown that *Lmna*$^{+/-}$ mice develop DCM-CD without muscular dystrophy, as measured by electrophysiology and death of AV node cells at 10 weeks of age, eventually succumbing to heart failure starting at one year of age [98].

A knock-in mouse line carrying the *LMNA* H222P mutation, which causes EDMD in humans, was generated in 2005 [99]. The *Lmna*$^{H222P/H222P}$ mouse develops normally without a

slight growth defect and lives significantly longer than *Lmna*$^{-/-}$ mice, dying at 7-9 months of age. These mice develop classical symptoms of dilated cardiomyopathy, showing decreased fractional shortening, ventricular dilation, and increased fibrosis in the myocardium. *Lmna*$^{H222P/H222P}$ also showed decreased heart conductivity as both PR interval and QRS duration were increased when measured by electrocardiogram. These mice also had decreased locomotion and performance on rotarod, which in combination with the wide variation in muscle fiber size and centrally located nuclei, are classical signs of muscular dystrophy. They later used microarray analysis to demonstrate increased expression of MAPK and JNK genes in *Lmna*$^{H222P/H222P}$ mice [100], which have been implicated in the development of cardiomyopathy [101,102,103], and then showed that inhibition of either the MAPK or JNK pathway could ameliorate the DCM-CD phenotype [104,105]. In addition, mice null for emerin, which is the protein responsible for X-linked EDMD, also show increased MAPK pathway activity [106]. From this work, it seems likely that the MAPK and JNK pathways play an important role in the development of muscular dystrophy and dilated cardiomyopathy in EDMD patients.

The *Lmna*$^{N195K/N195K}$ knock-in mouse, also generated in 2005, encodes a mutation known to cause DCM-CD in humans without skeletal muscle involvement. These mice develop normally until 4 weeks of age, whereupon they begin to exhibit a slight growth defect and die by 12 weeks of age [107]. The mice also exhibited dilated cardiomyopathy with ventricular dilation, decreased fractional shortening, increased expression of cardiac remodeling genes, and cardiac degeneration as gauged by histology. Through the implantation of continuous electrocardiographic monitoring transmitters, they demonstrated that the *Lmna*$^{N195K/N195K}$ mice have severe arrhythmic events, which became progressively worse and eventually resulted in

death. They then proceeded to show that connexin43, the primary protein of the cardiac gap junction responsible for conduction, was mislocalized and connexin40, found in the atria, was downregulated. In addition, there was a loss of the normal desmin network, which is a cytoskeletal element essential for proper force transduction and sarcomere organization. These findings help us to better understand the development of DCM-CD in laminopathy patients, which we can speculate may be due to disruption of the normal organization of the cardiomyocyte, though the exact mechanism by which this occurs still remains unclear.

A mouse expressing progerin (*Lmna*$^{HG/+}$), which cannot be properly cleaved by ZMPSTE24, was generated and characterized in 2005 to help study the development of HGPS [108]. These mice, in contrast with the other laminopathy disease mouse models, were symptomatic as heterozygous *Lmna*$^{HG/+}$ mice, showing symptoms characteristic of progeria such as retarded growth, osteoporosis, and alopecia, eventually dying prematurely at 6 months of age. However, these mice do not seem to suffer from cardiac disease, which differs from the human disease phenotype [109]. In 2002, two independent lines of *Zmpste24*$^{-/-}$ mice were generated, which are null for the protein responsible for the cleavage of the farnesylated prelamin A protein, share some of the same symptoms as the *Lmna*$^{HG/+}$ mice and appear to develop a progeroid syndrome [110,111], with retarded growth, alopecia, loss of bone density, and an increased frequency of bone fracture and muscle weakness. As it was hypothesized that the accumulation of farnesylated prelamin A protein was responsible for these observed effects, *Zmpste24*$^{-/-}$ mice were crossed with the *Lmna*$^{+/-}$ line, which exhibit a gene dosage effect and thus lower levels of lamin A protein. The *Zmpste24*$^{-/-}$ *Lmna*$^{+/-}$ mice appear completely normal [112], implying that there is a threshold of farnesylated prelamin A that triggers the

progeroid disorder. In addition, treatment of *Zmpste24*$^{-/-}$ mice with farnesyl transferase inhibitors, blocking the farnesylation of prelamin A, improved the growth, health and survival of the mice [113]. These three mouse models for the progeroid aspect of laminopathies confirm that perturbation of the normal maturation process of lamin A is responsible for the development of the progeroid syndrome associated with laminopathies.

Among other interesting mouse models utilized for the study of laminopathies is the lamin C-only mice (*Lmna*$^{LCO/LCO}$), in which expression of prelamin A is prevented entirely by blocking proper splicing of their knock-in allele after exon 10 [114]. These mice were characterized as completely physiologically normal, with no symptoms of any growth defect, muscular dystrophy, cardiomyopathy or premature death. In addition, the expression of a *Lmna*$^{LCO/+}$ allele in the *Zmpste24*$^{-/-}$ background prevented the accumulation of prelamin A entirely, while restoring A-type lamin function through lamin C. It is curious that lamin A appears to be disposable in this system, raising the question as to what is the distinct role of lamin A and why it requires farnesylation and cleavage for maturation.

The mTOR Pathway in Aging

The TOR pathway, initially discovered as the pathway inhibited by the antifungal drug rapamycin, consists of 2 complexes known as TOR complex 1 (TORC1) and TOR complex 2 (TORC2) [115,116]. TORC1's most well-known role is in promoting protein homeostasis through regulation of protein synthesis and, conversely, protein degradation by autophagy. TORC1 exists as a homodimer consisting of mTOR, regulatory associated protein of mTOR (raptor), proline-rich AKT substrate 40 kDa (PRAS40), mammalian lethal with Sec-13 protein 8 (mLST8)

and DEP domain TOR-binding protein (Deptor) [117]. The TOR pathway acts at a critical juncture integrating multiple signals from nutrient-sensing pathways and affecting key cellular processes.

The signaling events upstream of TOR include TSC1/TSC2, PI3K-AKT, amino acid levels, and cellular energy levels. TSC1 and TSC2, tuberous sclerosis complexes 1 and 2, normally act as the TSC1/2 complex promoting the GTPase activity of Rheb and preventing activation of mTOR. However, under growth conditions, the TSC1/2 complex is inactive, resulting in an increase of Rheb-GTP which promotes TORC1 activity [118]. PI3K, which responds to insulin and growth factor signaling, activates AKT which inactivates the previously mentioned TSC2, resulting in increased TORC1 signaling [119]. In addition, AKT can inactivate the TORC1 regulator PRAS40, which also increases TORC1 signaling [120]. The ability of TORC1 to respond to amino acid levels likely utilizes the Rag GTPase pathway, which in the presence of amino acids, dimerizes and binds to TORC1 and activates it through Rheb during positive growth conditions [121]. Finally, TORC1 is inhibited by low cellular ATP levels as the activation of AMPK activates the TSC1/2 complex and inhibits Rheb and TORC1 [122].

TOR signaling through TORC1 primarily affects protein translation and autophagy after integrating the upstream signals that indicate conditions for growth or starvation. Active TORC1 increases protein synthesis by phosphorylating eIF4E-binding protein (4E-BP) or ribosomal S6 kinase (S6K) [123]. 4E-BP normally sequesters the translation initiation factor eIF4E, but TORC1 phosphorylation of 4E-BP releases eIF4E, thereby increasing protein translation [124]. Activation of S6K by phosphorylation results in activation of eIF4B, a regulatory subunit of the RNA helicase eIF4A, which promotes translation initiation [125], although many other S6K

targets have been reported [126]. More recently, TORC1 has been shown to inhibit autophagy through phosphorylation of ULK1, the mammalian homolog of the yeast autophagy-specific gene 1 (ATG1) [127]. In summary, activation of TORC1 in nutrient-rich and growth-promoting conditions results in increased protein synthesis and decreased protein autophagy. Conversely, in low-nutrient or starvation conditions, TORC1 acts to inhibit protein synthesis and upregulate the recycling of proteins via autophagy.

The TOR signaling pathway has been implicated in normal mammalian aging as treatment of aged mice with rapamycin extended lifespan by 10-15% [128]. Both mean and maximal lifespan were increased in all strains of mice in the study, though currently the exact role that the TOR pathway has in aging is unclear. Ultimately, whether TOR results in decreased aging rates or postponing age-related diseases, the ability to extend lifespan in an aged population is promising. Recently, it has been shown that treatment of fibroblasts from patients with the lamin-associated progeroid disorder HGPS with rapamycin rescued many of the cellular defects caused by progerin [129]. The most dramatic cellular phenotype observed in HGPS fibroblasts is nuclear blebbing, described as irregular bulging of the nuclear membrane causing deviation from the normal ovoid structure of the nucleus, and treatment of these cells with rapamycin significantly decreased the frequency of nuclear blebs for well over 100 days. On a molecular level, the levels and solubility of the improperly processed prelamin A protein progerin were decreased in rapamycin-treated fibroblasts. Finally, autophagy was increased in the rapamycin-treated cells, contributing to the clearance of progerin. These experiments further illustrate the role of the TOR pathway in normal aging and the viability of HGPS as a model for the acceleration of normal aging.

Connexin Biology

The connexin family of proteins allows and regulates transfer of ions and small molecules between cells through an intercellular pathway termed the gap junction in essentially all tissues [130,131,132]. Connexin proteins have a highly conserved structure consisting of 4 transmembrane domains, two extracellular loops, one cytoplasmic loop and cytoplasmic N- and C-termini [133,134,135]. In order to form a gap junction, individual connexin proteins associate into a hexameric complex termed the connexon [136], which docks with a connexon on an adjoining cell to form a gap junction, eventually clustering with other gap junctions to form what is termed a gap junctional plaque [137]. Gap junctions typically allow molecules less than 1000 Da, which include ions, amino acids, simple sugars and short polypeptides, to freely travel between cells [138,139]. There are currently 21 identified members of the connexin family in humans [140,141], a number that may reflect the need for complex regulation of these proteins. One member, connexin43 (Cx43), is the most widely expressed connexin, found in at least 34 tissues and 46 cell types [142], and thus is the most well-studied connexin protein.

The process by which connexin proteins find their way into a gap junctional plaque is slightly different for each member of the connexin family. Cx32, for example, is assembled into a hexameric connexon at the endoplasmic reticulum, before it reaches the Golgi, whereas Cx43 is assembled in the trans-Golgi network [136,143]. This is further complicated by the fact that, in addition to connexons formed of identical connexin proteins, different members of the connexin family can also associate to form heteromeric channels, resulting in connexons

comprised of multiple different connexin proteins [144,145,146]. After assembly into connexons, they are then trafficked to the plasma membrane in either a Golgi-dependent or a microtubule-dependent manner [147,148]. The proper localization of connexins in the plasma membrane appears to be cadherin-dependent, with gap junctional communication being closely correlated with cadherin levels [149,150].

After being trafficked to the plasma membrane, connexins have a surprisingly short half-life of just 1-3 hours at the gap junction itself [151,152]. Gap junction degradation can occur by a number of different mechanisms, such as lysosomes, multivesicular bodies, or autophagosomal compartments [153,154,155,156]. There have also been reports of the ubiquitin-proteasome pathway being involved in gap junction degradation, but recently other investigators have shown a lack of dependence on the ubiquitin-proteasome pathway [157,158,159]. Ultimately, it is speculated that the presence of all of these distinct pathways in the degradation of Cx43 may mean that the preference is cell-type specific and may also depend on the current state of the cell itself. This complex series of events responsible for gap junction assembly and degradation may reflect the need for many levels of regulation when it comes to cellular communication.

Connexin proteins play an especially crucial role in the heart, as they are responsible for conducting the electrical coupling between cardiomyocytes that triggers the coordinated and regular contraction of the heart. Gap junctions in the heart are localized to specific regions located on the ends of the elongated cardiomyocytes known as intercalated disks, which are also the sites of the adherens junctions and desmosomes responsible for the mechanical coupling between cardiomyocytes. There are three connexins found to be expressed in the

heart, Cx43, Cx40 and Cx45. Cx43 is the major connexin in the ventricular myocardium and throughout most of the heart [160] and is absent from the specialized conducting regions of the sinoatrial (SA) and atrioventricular (AV) nodes [161,162]. In contrast, Cx40 is found limited to the atria and in the pacemaker cells of the SA and AV nodes [163,164], and Cx45 appears to be found primarily in the specialized cells of the His-Purkinje system [165].

The loss of Cx43 from the intercalated disk has been observed in patients suffering from cardiac disease. Patients with ischemic heart disease have disorganization and reduction in the surface area of their gap junctions [166,167], and this effect has also been observed in patients with congestive heart failure [168], ischemic or idiopathic dilated cardiomyopathy [169], and sudden cardiac death [170]. Many of these studies echo the hypothesis that heterogeneity in the levels of Cx43 may contribute to either loss of homogenous wave-front propagation or dispersion in repolarization and refractoriness. These factors may then subsequently cause asynchronous fiber contraction and poor force development, worsening any pre-existing heart condition and leading to tachycardia and arrhythmic defects.

There have been a few knockout mouse models generated to study the role of Cx43 in mice. The complete knockout developed normally, but shortly after birth became cyanotic and succumbed due to an obstruction of the right ventricular outflow tract, which indicates some sort of developmental role for Cx43 [171]. Mice heterozygous for the knockout allele develop normally, but exhibit slowed conduction and prolongation of the QRS complex [172]. Other models have used either tissue-specific or drug-induced deletion of Cx43, in which the mice develop normally, but exhibit slowed conduction velocity, arrhythmic events and death from ventricular tachycardia [173,174,175,176,177].

Phosphorylation of Connexin43

The short half-life of the gap junction indicates a need for post-translational regulation of both assembly and turnover. As with many other proteins in the cell, this is accomplished through phosphorylation events. The phosphorylation of Cx43 is readily observed by SDS-PAGE, as there appear to be multiple electrophoretic isoforms, termed P0, P1 and P2. The slower migrating P1 and P2 bands can be abolished by treatment with alkaline phosphatase, which demonstrates that phosphorylation is responsible for the change in the electrophoretic migration of Cx43 [178,179]. As phosphate groups are on the order of 80 Da and the differences between the phospho-isoforms of Cx43 are 2-4 kDa, it is clear that these shifts must be due to conformational changes induced by phosphorylation rather than the added weight of the phosphate group itself. The regulation of Cx43 likely occurs through phosphorylation in the C-terminal domain which contains over 20 serine or tyrosine residues that serve as potential phosphorylation sites. These conformation changes induced by serine phosphorylation may be linked to Cx43 function, as different phosphorylation patterns are found in different regions of the cell [180,181]. Cx43 without phosphorylation of Ser364/Ser365 was found in the trans-Golgi network, presumably as untrafficked connexons. Phosphorylation of Ser365 is necessary for the shift to the P1 isoform and is found in the plasma membrane, but not entirely in gap junction plaques [182]. Subsequent phosphorylation of Ser325/Ser328/Ser330 then shifts Cx43 to the P2 isoform and is found exclusively in gap junctions [183]. There are many other combinations of phosphorylation of Cx43 and a handful of kinases that seem to regulate this event, but phosphorylation appears to play a major role in the maturation and life cycle of Cx43.

There are a number of kinases whose phosphorylation sites on Cx43 have been identified and, despite the potential combinatorial effects of multiple phosphorylated residues, these kinases can generally be considered to promote or inhibit gap junction. Phosphorylation by CK1 on Ser325/Ser328/Ser330 seems to be required to traffic Cx43 to the plasma membrane and successfully form gap junctions as either inhibition of CK1 or a mutation of the Ser325/Ser328/Ser330 residues to alanine resulted in a dramatic loss in the ability to form gap junctions [184]. PKA, through cAMP levels, likely interacts with connexin proteins increasing both gap junctional permeability and gap junction plaque size [185]. It has been shown recently that Akt may be responsible for regulating gap junction stability as blocking Akt degradation by inhibiting proteasome activity resulted in increased gap junction plaque size and conversely inhibiting Akt resulted in reduced gap junction plaque size [159]. The phosphorylation site for Akt has not yet been described, but is likely occurring on Ser373 (personal communication C. Dunn).

Phosphorylation of Cx43 by MAPK, PKC or Src has been shown to generally inhibit gap junction activity through lowering channel conductance or increasing internalization. The MAPKs ERK1/2 are responsible for phosphorylation of Ser255/Ser279/Ser282 [186] which results in a reduction in both conductance and channel open probability [187,188], though there are conflicting reports that attribute this phosphorylation to BMK5, a different MAPK protein [189]. PKC phosphorylation of Cx43 occurs on Ser262/Ser368, resulting in decreased channel conductance [190,191]. Src activation results in phosphorylation of Tyr247/Tyr265 and results in down-regulation of gap junctions [192,193], though activation of Src also results in

phosphorylation of S262/S279/S282/S368, indicating that the MAPK and PKC phosphorylation of Cx43 are activated in conjunction with Src activation [194].

Summary

The majority of this dissertation is focused on further understanding the role that A-type lamins play in the heart to better understand the disease pathology of laminopathies. As covered in the laminopathy portion of the introduction, many patients with a laminopathy develop dilated cardiomyopathy [68]. In the first part of this dissertation, working in conjunction with Richard Frock, we investigated and determined that A-type lamins are essential for normal cardiac function, for both physical contraction and electrical conduction. Using *Lmna*$^{-/-}$ mice, we found that expression of the human *LMNA* gene in cardiomyocytes improved many parameters of contractility as measured by echocardiogram, eliminated inappropriate cytoplasmic aggregation of the cytoskeletal protein desmin, restored normal localization of the gap junction protein connexin43, improved conduction velocity as measured by ECG, and ultimately resulted in a 12% improvement in lifespan.

In the second part of my dissertation, I worked with Fresnida Ramos and we began to delve into the mTOR pathway as a potential molecular mechanism that may contribute to the cardiomyopathy phenotype, as mTOR has been shown to play a role in normal heart and muscle function [195,196]. In addition, exposing fibroblasts derived from Hutchinson-Gilford progeria patients to rapamycin, an inhibitor of mTORC1, ameliorated many of the cellular defects observed in untreated fibroblasts [129]. We observed that the mTOR pathway was activated in *Lmna*$^{-/-}$ mice and that inhibition of mTORC1 by rapamycin improved many of the

cardiac defects previously observed. By feeding *Lmna*$^{-/-}$ mice rapamycin-encapsulated chow starting at 3-4 weeks of age, we observed that the increased mTORC1 activity of *Lmna*$^{-/-}$ mice was ameliorated in both heart and skeletal muscle, which resulted in improved contractility as measured by echocardiogram and improved rotarod performance, respectively. Treatment with dietary rapamycin resulted in a 35% increase in median lifespan of *Lmna*$^{-/-}$ mice and a 55% increase if administered by intraperitoneal injection.

In the final portion of my dissertation, I focused on the conduction disease aspect of laminopathies, which is likely mediated by connexins and specifically phosphorylation of connexins. It has recently been shown that one of the functions of A-type lamins is to bind activated ERK1/2 [197] and activity of these MAPK proteins has been shown to be increased in *Lmna*$^{H222P/H222P}$ mice [100]. In addition, signaling through the MAPK pathway is associated with cardiac hypertrophy [101] and causes phosphorylation of connexin43, the primary connexin in the heart, in an inhibitory fashion [188]. I have shown that the loss of A-type lamins results in release of pERK1/2 from the nuclear membrane and increases phosphorylation of connexin43 in both cultured cells and mice. I believe this may be a mechanism that contributes to the arrhythmic profile of *Lmna*$^{-/-}$ mice and potentially human patients, resulting in their premature and sudden death.

Chapter 1

Cardiomyocyte-specific Expression of Lamin A Improves Cardiac Function in *Lmna*$^{-/-}$ Mice

As it has been previously described that loss of *Lmna* in mice results in dilated cardiomyopathy with conduction defect (DCM-CD) [96], I endeavored to determine whether the cardiac effects observed were solely due to the loss of A-type lamins in the heart, or whether the generalized stress of muscular dystrophy and other effects were contributing to the disease phenotype. In order to address this, the *Lmna*$^{-/-}$ mouse strain was crossed with a transgenic mouse line that expressed FLAG-tagged human lamin A under the α-myosin heavy chain promoter, obtained and previously described from the lab of Howard Worman (Columbia University) [198]. The resulting mouse, termed *Lmna*$^{-/-}$; Tg, would be deficient in A-type lamins throughout the body, it would have expression of lamin A specifically in the cardiomyocytes that comprise the heart. Using this mouse, I would be able to determine the heart-specific effects of lacking lamin A. In summary, I was able to demonstrate that lamin is essential for cardiac function, both in terms of contraction and conduction.

I performed these experiments with my co-author, Richard Frock, and they are presented here in manuscript form which is currently in resubmission to *PLoS ONE*.

Cardiomyocyte-specific expression of lamin A improves cardiac function in *Lmna*$^{-/-}$ mice

Richard L. Frock, PhD [1]; Steven C. Chen, BS [1]; Dao-Fu Dai, MD, PhD [2]; Ellie Frett, BS [5]; Carmen Lau, BS [1]; Christina Brown, BS [1]; Diana N. Pak, BS [1]; Yuexia Wang, PhD [7]; Antoine Muchir, PhD [7]; Howard J. Worman, MD [7]; Luis F. Santana, PhD [3]; Warren C. Ladiges, DVM [4]; Peter S. Rabinovitch, MD [2], PhD; Brian K. Kennedy, PhD* [1,6]

Departments of [1] Biochemistry, [2] Pathology, [3] Physiology and Biophysics, and [4] Comparative Medicine, University of Washington, Seattle, WA

[5] Department of Pharmacology and Physiology, University of Rochester, Rochester, NY

[6] Buck Institute for Age Research, Novato, CA

[7] Department of Medicine and Department of Pathology and Cell Biology, College of Physicians and Surgeons, Columbia University, New York, NY

Abstract

Lmna$^{-/-}$ mice display multiple tissue defects and die by 6-8 weeks of age reportedly from dilated cardiomyopathy with associated conduction defects. We sought to determine whether restoration of lamin A in cardiomyocytes improves cardiac function and extends the survival of *Lmna*$^{-/-}$ mice.

We observed increased total desmin protein levels and disorganization of the cytoplasmic desmin network in ~20% of *Lmna*$^{-/-}$ ventricular myocytes, rescued in a cell-autonomous manner in *Lmna*$^{-/-}$ mice expressing a cardiac-specific *LMNA* transgene (*Lmna*$^{-/-}$; Tg) . *Lmna*$^{-/-}$; Tg mice displayed significantly increased contractility and preservation of myocardial performance compared to *Lmna*$^{-/-}$ mice. *Lmna*$^{-/-}$; Tg mice attenuated ERK1/2 phosphorylation relative to *Lmna*$^{-/-}$ mice, potentially underlying the improved localization of connexin43 to the intercalated disc. Electrocardiographic recordings from *Lmna*$^{-/-}$ mice revealed arrhythmic events and increased frequency of PR interval prolongation, which is partially rescued in *Lmna*$^{-/-}$; Tg mice. These findings support our observation that *Lmna*$^{-/-}$; Tg mice have a 12% median extension in lifespan compared to *Lmna*$^{-/-}$ mice. While significant, *Lmna*$^{-/-}$; Tg mice only have modest improvement in cardiac function and survival likely stemming from the observation that only 40% of *Lmna*$^{-/-}$; Tg cardiomyocytes have detectable lamin A expression.

Cardiomyocyte-specific restoration of lamin A in *Lmna*$^{-/-}$ mice improves heart-specific pathology and extends lifespan, demonstrating that cardiac pathology of *Lmna*$^{-/-}$ mice limits survival. The expression of lamin A is sufficient to rescue certain cellular defects associated with loss of A-type lamins in a cardiomyocyte cell-autonomous fashion.

Introduction

Nuclear lamins are type V intermediate filament proteins that are implicated in a variety of cellular processes, including DNA replication, gene transcription and chromatin organization [34,42,199,200]. Mutations within the A-type lamin gene, *LMNA*, are associated with over 13 different tissue-specific diseases, collectively termed laminopathies. These include autosomal Emery-Dreifuss muscular dystrophy (EDMD2/3), limb-girdle muscular dystrophy type 1B (LGMD1B), and dilated cardiomyopathy with conduction defects 1A (CMD1A). Adipose, bone, and neural tissues can also be affected in laminopathies, which may resemble aspects of accelerated or premature aging (for review see Worman, et al. 2010) [60,201].

Mice lacking the *Lmna* gene appear normal at birth but progressively display multiple tissue defects, including muscular dystrophy and dilated cardiomyopathy, with a noticeable reduction in growth rate beginning as early as 2 weeks of age followed by premature death at 6-8 weeks [94]. Further analysis of hearts from $Lmna^{-/-}$ mice has revealed a rapid development of left ventricular dilatation coupled with decreased systolic function beginning after 2 weeks of age [96]. Dosage of A-type lamins can also influence cardiac function as $Lmna^{+/-}$ mice display cardiac conduction defects with a late onset of dilated cardiomyopathy [98]. However, expression of either major isoform alone, lamin A only [202] or lamin C only [114], is sufficient to prevent phenotypes observed in $Lmna^{-/-}$ mice, indicating that either isoform can largely compensate for the other. Interestingly, only homozygous—but not heterozygous—knock-in mouse models for either muscular dystrophy-associated or cardiac-specific *LMNA* mutations [99,107] display dilated cardiomyopathy with conduction defects and premature death. In contrast, humans heterozygous for the corresponding missense mutations [64,203] develop

cardiac and skeletal muscle pathology, indicating that there are subtle differences in disease manifestation between rodents and humans.

In this study, we tested whether cardiomyocyte-specific expression of lamin A [198] can improve cardiac function and result in increased lifespan in *Lmna*$^{-/-}$ mice. We show better preservation of myocardial performance and reduced occurrence of conduction abnormalities for *Lmna*$^{-/-}$ mice expressing the cardiac transgene. These observations are consistent with a partial restoration of localization and protein levels of desmin, connexin43 and ERK1/2 phosphorylation. The heterogenic expression of cardiac lamin A in *Lmna*$^{-/-}$ hearts underlies this partial restoration and limits improvement of lifespan, however, with this model we are able to investigate cell-autonomous and non-cell autonomous roles which lends new insight into the biology of A-type lamins in the cardiac system.

Results

Cardiac-specific expression of FLAG-tagged human lamin A in Lmna$^{-/-}$ mice

To determine whether cardiac-specific expression of lamin A can improve heart function in *Lmna*$^{-/-}$ mice, we crossed transgenic mice expressing FLAG-tagged human lamin A under the α-myosin heavy chain promoter [198] with *Lmna*$^{+/-}$ mice to ultimately produce litters containing both *Lmna*$^{-/-}$ and *Lmna*$^{-/-}$ mice expressing the cardiac-specific *LMNA* transgene (*Lmna*$^{-/-}$; Tg) mice. FLAG-lamin A is highly expressed in *Lmna*$^{-/-}$; Tg cardiac tissue as measured by Western analysis using an A-type lamin antibody **(Figure 1A),** and expression is restricted to cardiac tissue in both *Lmna*$^{+/+}$; Tg and *Lmna*$^{-/-}$; Tg mice **(Figure 1B)**. Indirect immunofluorescence microscopy using antibodies against myosin heavy chain (MF-20) and FLAG **(Figure 1C)** indicate

that ~35% of ventricular myocytes express the FLAG-lamin A transgene in both *Lmna*$^{+/+}$; Tg and *Lmna*$^{-/-}$; Tg hearts **(Figure 1D)**. Finally, expression of the cardiac-specific transgene in *Lmna*$^{-/-}$; Tg mice does not improve the growth defect of *Lmna*$^{-/-}$ mice as measured by their body weights compared to *Lmna*$^{+/+}$ mice **(Figure 1E)**. Collectively, these results show that the FLAG-lamin A transgene is highly – though mosaically – expressed and specific to cardiomyocytes.

***Characterization of molecular phenotypes associated with cardiac structure and remodeling in Lmna*$^{-/-}$ *and Lmna*$^{-/-}$; Tg hearts**

Western analysis was performed on lysates derived from hearts of 5-7 week old *Lmna*$^{+/+}$ control, transgenic and non-transgenic *Lmna*$^{-/-}$ mice to determine whether molecular phenotypes are restored in the presence of cardiac lamin A expression. Desmin, previously determined to be mislocalized in *Lmna*$^{-/-}$ cardiomyocytes [96], exhibits an approximately 3-fold increase in total protein levels from *Lmna*$^{-/-}$ hearts **(Figure 2A)**. This finding in cardiomyocytes contrasts with skeletal muscle myoblasts from *Lmna*$^{-/-}$ mice, where desmin levels are reduced [95]. Expression of FLAG-lamin A in the heart results in attenuation of total desmin that is only approximately 2-fold increased compared to *Lmna*$^{+/+}$ hearts. Desmin is mislocalized in *Lmna*$^{-/-}$ ventricular myocytes, resulting in diminished staining in the majority of intercalated discs **(Figures 2B vs. 2C)** as well as increased cytoplasmic desmin staining in ~21% of ventricular myocytes ($P<0.001$) **(Figure 2E)**. Less than 1% of transgene-expressing ventricular myocytes from *Lmna*$^{-/-}$; Tg mice display increased cytoplasmic desmin ($P<0.001$) **(Figures 2D and 2E)**, suggesting cell-autonomous rescue of desmin localization. Due to the mosaic nature of our transgene expression, we continued to observe increased cytoplasmic desmin in the transgene-

non-expressing ventricular myocytes, but also noted a 38% reduction in the fraction of these cells, possibly due to neighboring transgene-expressing ventricular myocytes (P<0.01; see Discussion). These observations are consistent with the observed increase in desmin in hearts of *Lmna*$^{-/-}$ mice and the partial attenuation of desmin levels in hearts of *Lmna*$^{-/-}$; Tg mice.

Improved cardiac contractile function in transgenic Lmna*$^{-/-}$ *mice

To determine whether transgenic expression of FLAG-lamin A improves cardiac function in *Lmna*$^{-/-}$ mice, transthoracic echocardiograms were performed at 4-8 weeks of age. Echocardiographic measurements comparing *Lmna*$^{+/+}$ and *Lmna*$^{+/+}$; Tg mice showed no significant difference **(Supplemental Figure 1A-1C).** *Lmna*$^{-/-}$ mice display impaired contractility and left ventricular dilatation **(Figure 3A)**. They have significantly increased (P<0.001) left ventricular end-systolic diameters (LVESD) and left ventricular end-diastolic diameters (LVEDD) normalized for body weight between *Lmna*$^{-/-}$ and *Lmna*$^{+/+}$ littermates **(Figures 3B & 3C)**. Additionally, *Lmna*$^{-/-}$ hearts are enlarged as shown by the ~55% increase in the left ventricular mass index (LVMI) (**Supplementary Figure 2**). Fractional shortening declined by 50% in *Lmna*$^{-/-}$ mice compared to *Lmna*$^{+/+}$ littermates (P<0.001) **(Figure 3D)** and consistent with the 80% decrease observed previously [96]. As a second measure of cardiac function, the myocardial performance index (MPI) was calculated (See methods for further details; increased MPI scores have been shown previously to reflect LV systolic and/or diastolic dysfunction [204]). *Lmna*$^{-/-}$ mice display 100% increase in MPI compared to *Lmna*$^{+/+}$ littermates (P<0.001) **(Figure 3E)**, consistent with decreased cardiac contractility in *Lmna*$^{-/-}$ mice.

The expression of FLAG-lamin A partially restores cardiac contractility in *Lmna*$^{-/-}$ mice **(Figures 3A, 3B, 3D)**. Compared to *Lmna*$^{-/-}$ mice, *Lmna*$^{-/-}$; Tg mice significantly attenuate dilation of LVESD by ~25% (P<0.01) **(Figure 3B)** and display ~60% improvement in fractional shortening (P<0.001) although fractional shortening is still significantly lower in comparison to control littermates by 20% (P<0.001) **(Figure 3D)**. Similarly, the MPI is partially improved by ~25% in *Lmna*$^{-/-}$; Tg mice compared to *Lmna*$^{-/-}$ mice (P<0.01) **(Figure 3E).** However, hearts of *Lmna*$^{-/-}$; Tg mice still exhibit cardiac enlargement, as LVEDD **(Figure 3C)** and LVMI **(Supplemental Figure 2)** are not significantly changed compared to hearts of *Lmna*$^{-/-}$ mice. Furthermore, mRNA expression of atrial natriuretic factor and brain natriuretic peptide, hallmarks of cardiac remodeling and physical stress, are not significantly changed in hearts of *Lmna*$^{-/-}$; Tg mice compared to those from *Lmna*$^{-/-}$ mice **(Supplemental Figure 3)**. Collectively, these data indicate that the mosaic expression of FLAG-lamin A in *Lmna*$^{-/-}$ cardiomyocytes results in partial but significant restoration of cardiac contractility compared to *Lmna*$^{-/-}$, yet fails to ameliorate cardiac dilation and remodeling.

Characterization of molecular phenotypes associated with cardiac conduction in both Lmna$^{-/-}$ ***and Lmna***$^{-/-}$**; Tg mice**

Increased ERK signaling as reflected by increased levels of phosphorylated ERK1/2 (pERK1/2) has been observed in hearts from *Lmna*$^{H222P/H222P}$ mice [100] and in other cell systems with knockdown of A-type lamin or emerin expression [205]. Consistently, we observe a 2.5-fold increase of pERK1/2 in *Lmna*$^{-/-}$ hearts relative to total ERK1/2 levels (P<0.01) **(Figure 4A and 4B)**. Although we were unable to achieve significance, *Lmna*$^{-/-}$; Tg hearts (n=11) trend

towards a reduced pERK1/2 level compared to hearts from *Lmna*$^{-/-}$ mice (n=16), suggesting that there may be a partially decreased cellular stress response. Increases in ERK1/2 activity have been shown to negatively affect gap junction communication through phosphorylation of connexin43 (Cx43) [188,206]. We observe no significant change in levels of total Cx43 as detected by the NT1 antibody. However, in *Lmna*$^{-/-}$ hearts we detect a significant increase in CT1 signal, an antibody which predominantly recognizes Cx43 found in the cytoplasm and is increased in ischemic hearts [180] **(Figure 4A)**. The increase in CT1 signal is not significantly attenuated in the hearts from *Lmna*$^{-/-}$; Tg mice. In addition to changes detectable by immunoblot, we also observe a decreased amount of gap junctional Cx43 in hearts from 5-7 week old *Lmna*$^{-/-}$ mice compared to similarly aged *Lmna*$^{+/+}$ mice (representative images from 6-week old mice shown) via immunofluorescence **(Figures 4C and 4D)**. Hearts from *Lmna*$^{-/-}$; Tg mice appear to have more gap junctional Cx43 than hearts from *Lmna*$^{-/-}$ mice **(Figure 4E)**. To quantitatively assay the extent of Cx43 mislocalization in ventricular myocytes from 5-7 week old *Lmna*$^{-/-}$ mice, we formulated a co-association index for scoring Cx43 at intercalated discs (see methods). Intercalated discs from *Lmna*$^{+/+}$ ventricular myocytes display a mean Cx43 index of 0.70, which is reduced to 0.39 in *Lmna*$^{-/-}$ ventricular myocytes **(Figure 4F)**. Intercalated discs from *Lmna*$^{-/-}$; Tg ventricular myocytes display a mean Cx43 index of 0.53. When normalized against the mean index for *Lmna*$^{+/+}$ ventricular myocytes for each experiment, ventricular myocytes from *Lmna*$^{-/-}$ mice display 45% decrease in Cx43 localization at the intercalated disc ($P<0.01$) **(Figure 4G)**. In contrast, ventricular myocytes from *Lmna*$^{-/-}$; Tg mice display 25% decrease in Cx43 localization at the intercalated disc compared to *Lmna*$^{+/+}$ ventricular myocytes ($P=0.11$), suggesting a partial restoration of Cx43 localization at the intercalated disc.

Transgenic Lmna$^{-/-}$ mice have less severe conduction defects

We hypothesized that if Cx43 localization was partially restored in *Lmna*$^{-/-}$; Tg mice, there may be improvements in cardiac conduction. To test this hypothesis, we took electrocardiography (ECG) recordings of 5-7 week old mice and measured a number of parameters associated with cardiac conduction, including PR and QRS intervals. Despite the previous study reporting a significant increase in the average PR and QRS intervals for *Lmna*$^{-/-}$ mice [7], we were unable to observe a significant increase in the average PR or QRS intervals of similarly aged *Lmna*$^{-/-}$ mice after analyzing 300 beats per mouse (N=5) using this method **(Supplemental Table 1)**. However, intermittent prolongation of the PR interval was noted in *Lmna*$^{-/-}$ mice. Since there is no consensus on the normal reference values for PR intervals, we derived the reference values by analyzing 1,500 beats from 5 *Lmna*$^{+/+}$ littermates, which display a Gaussian distribution. PR intervals from single mice were then compared against the derived reference value and values greater than 95% of our normal reference were considered abnormally prolonged **(Figure 5A)**. Using the cut-off value of >30% abnormally prolonged PR intervals, 5 out of 6 *Lmna*$^{-/-}$ mice displayed PR prolongation (Fisher's exact test, P=0.0476), suggesting the presence of first degree atrioventricular block **(Figure 5B)**. In contrast, 2 out of 5 *Lmna*$^{-/-}$; Tg mice exhibited PR prolongation (Fisher's exact test, P=0.2222), suggesting partial improvement in atrioventricular conduction due to cardiac-specific FLAG-lamin A expression. One *Lmna*$^{+/+}$; Tg mouse exhibited >30% PR interval prolongation and a second mouse displayed a dropped beat **(Supplemental Figure 4)**, which might be a manifestation of sinus pause, sinoatrial or atrioventricular block, suggesting that increased expression of lamin A in a subset

of normal myocytes can also result in conduction abnormalities. We also observe several arrhythmic events in *Lmna*$^{-/-}$ mice. Compared to a normal ECG tracing from a representative *Lmna*$^{+/+}$ mouse **(Figure 5C)**, the ECG of *Lmna*$^{-/-}$ mice display intermittent atrial premature beat **(Figure 5D)** and a multifocal atrial rhythm **(Figure 5E)**. We were unable to locate any similar arrhythmic occurrences in *Lmna*$^{-/-}$; Tg mice, potentially due to improved cardiac function.

Transgene expression of FLAG-lamin A in* Lmna$^{-/-}$ *cardiomyocytes extends lifespan

Concurrent with our studies of cardiac function and molecular restoration in cardiomyocytes from *Lmna*$^{-/-}$; Tg mice, we sought to determine whether this improvement would translate into an increased lifespan. Kaplan-Meier curves were generated from a cohort of 24 and 28 mice each for transgenic and non-transgenic *Lmna*$^{-/-}$ mice, respectively. Despite the mosaic expression of FLAG-lamin A in *Lmna*$^{-/-}$; Tg cardiomyocytes, we observe a 12% mean increase and a 15% maximal increase in lifespan ($P<0.011$) of *Lmna*$^{-/-}$; Tg mice compared to non-transgenic *Lmna*$^{-/-}$ littermates **(Figure 6)**.

Discussion

In this study, we tested the hypothesis that cardiomyocyte-specific expression of lamin A in *Lmna*$^{-/-}$ mice can improve cardiac function and increase lifespan. Through the generation of *Lmna*$^{-/-}$ mice with cardiomyocyte-specific expression of FLAG-lamin A, we observed significantly improved fractional shortening and myocardial performance index by echocardiogram, restored localization of both desmin and Cx43, and attenuated protein levels of both pERK1/2 and desmin, collectively indicating improved cardiac function compared to

Lmna$^{-/-}$ mice. Despite improved cardiac contractility, cardiac remodeling in transgenic *Lmna*$^{-/-}$ mice was still evident with no amelioration of chamber dilation. We observed less Cx43 localized to the intercalated disk in ventricular myocytes of *Lmna*$^{-/-}$ mice which was partially restored in ventricular myocytes of *Lmna*$^{-/-}$; Tg mice. This modest improvement in Cx43 localization was also consistent with our finding that the stochastic PR interval prolongation observed in *Lmna*$^{-/-}$ mice is less frequent in *Lmna*$^{-/-}$; Tg mice. These improvements to cardiac function due to the expression of lamin A resulted in a significant—though modest—improvement in lifespan compared to *Lmna*$^{-/-}$ littermates. Collectively, these data suggest that cardiomyocyte-specific expression of lamin A in *Lmna*$^{-/-}$ mice can partially improve cardiac function and that the cardiac pathology present in *Lmna*$^{-/-}$ mice is lifespan limiting.

Mosaic expression of lamin A in *Lmna*$^{-/-}$ cardiomyocytes was very likely a limiting factor in many of our incompletely rescued phenotypes, but also allowed us to observe a juxtaposition of cardiomyocytes either expressing or not expressing the lamin A transgene. Other studies had previously used this approach to address cell autonomy roles in the cardiac system [173,207]. In our study, *Lmna*$^{-/-}$; Tg mice displayed ~30-40% heterogeneity of lamin A transgene expression in ventricular cardiomyocytes, and we observed both cell-autonomous and non-cell-autonomous phenotypes. In general, our findings suggest the contractile defect of *Lmna*$^{-/-}$ mice can be rescued in a cell-autonomous fashion, as indicated by restoration of the desmin cytoskeletal network in lamin A-expressing *Lmna*$^{-/-}$ cardiomyocytes. We also observed a significantly decreased fraction of non-transgene expressing *Lmna*$^{-/-}$; Tg cardiomyocytes with disorganized desmin, which we postulate as being propagated from neighboring cardiomyocytes expressing the lamin A transgene. Since mechanotransduction relies on

communication between the nucleus and extracellular interactions from cell-cell contact, extracellular matrix composition, and secreted factors [208,209], we propose that A-type lamins may play an additional role by modulating these extracellular properties to coordinate mechanosensing and transduction in a non-cell-autonomous manner.

Altered A-type lamin function also results in increased activity of ERK1/2. Although this phenomenon is universal to many cell types with abnormal A-type lamin composition [197,205,210,211], the administration of the MEK inhibitor, PD98059, improves the dilated cardiomyopathy of *Lmna*$^{H222P/H222P}$ mice [104,105], which strongly supports the notion that altered ERK1/2 activity is a critical component associated with pathogenesis. Indeed, increased ERK1/2 activity is associated with cardiac hypertrophy in other heart disease models [212]. Cx43 is the most widely distributed member of the connexin family of proteins, which forms gap junctions, facilitates cell-to-cell communication, and is found in a variety of different tissues and cell types [142]. Phosphorylation of Cx43 by ERK1/2 inhibits gap-junctional communication [188,206], and decreased Cx43 activity at the intercalated disc in *Lmna*$^{-/-}$ mice may play a critical part in the conduction defects and premature death observed. Electrical conduction of the heart cannot be completely rescued in a cell-autonomous fashion as gap junctions must form stable connexons with neighboring cells in order to maintain a functioning channel, making it an attractive example of non-cell-autonomous function. Mice carrying a heterozygous deletion for Cx43 [172] as well as cardiac-restricted inactivation of Cx43 in adult mice [175,177] has resulted in slowing of ventricular conduction and eventual death by ventricular tachycardia. In addition, heterogeneous or mosaic expression of Cx43 resulted in similar spontaneous ventricular arrhythmia and altered conduction velocity [173,213]. We

observed heterogeneity in the rescue of gap-junctional Cx43 levels, which we speculate contributes to the continued premature death phenotype of *Lmna*$^{-/-}$; Tg mice through terminal arrhythmic events. Interestingly, a similar phenotype describing loss of Cx43 localization to the intercalated disc coupled with desmin aggregation has been described in D7-des mice, which encode a deletion that causes human dilated cardiomyopathy [214]. Additionally, we observed arrhythmia in two *Lmna*$^{+/+}$; Tg mice suggesting that increased expression of lamin A in a fraction of cardiomyocytes can alter conduction—and possibly connexin activity—in an otherwise normal heart. These examples demonstrate the importance of assessing non-cell-autonomous outcomes in any transgenic and gene therapy models.

ERK1/2 activity can also result in the activation of different transcriptional pathways depending on the context of the tissue type and origin of ERK1/2 activation [215]. A-type lamins can bind and sequester c-Fos, the immediate downstream effector of pERK1/2, thereby inhibiting the activity of AP-1 [216]. Further studies have shown that active ERK1/2 can also co-localize with lamin A and c-Fos at the nuclear envelope, and the loss of A-type lamins results in increased AP-1 activity and reduced c-Fos phosphorylation [211]. Finally, ERK1/2 may additionally act upon Cx43 in a cell survival pathway, as ERK1/2 activity enhances translocation of Cx43 to the mitochondria, where Cx43 has been shown to play a protective role against cell death [217,218,219]. Although it is currently not known whether ERK1/2 signaling can modulate desmin filament formation in cardiomyocytes, it is becoming increasingly clear that loss of or mutation of A-type lamins may impinge on multiple pathways that lead to cardiac dysfunction.

Our data highlight the role of A-type lamins in cardiomyocyte function to both maintain efficient contraction and preserve a functional conductive network. These findings also re-emphasize the need for uniform expression in gene therapy models correcting conduction diseases.

Methods

Animals

Lmna$^{+/-}$ mice were obtained from Dr. Colin Stewart [94] and were backcrossed on C57BL/6J for 9 additional generations. The resulting *Lmna*$^{+/-}$ mice, B6.129S1(Cg)-Lmna^{tm1Stw}/BkknJ, were crossed with transgenic mice (founder line 903; B6/CBA F1 hybrids) expressing FLAG-lamin A under the control of the α-myosin heavy chain promoter, which have been described elsewhere [198]. The resulting transgenic *Lmna*$^{+/-}$ mice were crossed with *Lmna*$^{+/-}$ mice to generate *Lmna*$^{-/-}$ mice expressing the cardiac-specific transgene (*Lmna*$^{-/-}$; Tg). Details for genotyping can be found in the Supplemental Methods section. Mice were bred and maintained under specific pathogen-free conditions. Euthanasia of mice was accomplished by administration of CO_2. For dissection, mice were additionally subjected to cervical dislocation following CO_2 euthanasia. All experiments were performed in compliance with the University of Washington Institutional Animal Care and Use Committee (Protocol Number: 2174-23).

Tissue preparation and indirect immunofluorescence

Hearts of transgenic and non-transgenic *Lmna*$^{-/-}$ and control mice were rapidly excised and rinsed in phosphate-buffered saline (PBS) prior to mounting in Tissue-Tek O.C.T. compound and subsequent freezing in liquid nitrogen-cooled isopentane. Heart ventricle sections 8 μm in

thickness were collected and mounted on Superfrost plus glass slides (Fisher). Antibodies used and detailed methods for staining and scoring desmin and connexin can be found in the Supplemental Methods Section.

Western analysis

Tissues were homogenized using the TH homogenizer (Omni International) in a lysis buffer (10 µL/mg tissue) containing the following: 2% SDS, 250 mM sucrose, 75 mM urea, 1 mM DTT, 50 mM Tris (pH 7.5), 25 µg/mL aprotinin, and 10 µg/mL leupeptin [99,100]. Antibodies used and further details can be found in the Supplemental Methods Section.

Echocardiography

Transgenic and non-transgenic *Lmna*$^{-/-}$ mice and control littermates received echocardiography examination (Siemens Acuson CV70) at two time points: 4-6 weeks and 6-8 weeks of age. A mixture of 0.5% isoflurane with O_2 was administered through a nose cone to provide adequate sedation but minimal cardiac suppression during echocardiography. Heart rate was monitored and kept above 400 bpm to minimize any effect on any parameters [220]. Pathologists performing the echocardiography examination were blinded to the transgene genotype for *Lmna*$^{-/-}$ mice. Further details can be found in the Supplemental Methods Section.

ECG recordings

Electrocardiography was recorded using TA11ETA-F10 transmitters (Data Science International, St.Paul, MN). ECG data were recorded using Dataquest A.R.T^{TM} software (Data Sciences International) and the first 300 beats were analyzed using LabChart7 Pro (ADInstruments). Further details can be found in the Supplemental Methods Section.

Statistical analysis

Data are expressed as mean ± S.E.M. and one-way ANOVA analyses were performed where relevant with Bonferroni post tests to compare genotypes of specific age groups. A value of $P<0.05$ was considered statistically significant. For lifespan analysis, a Kaplan-Meier curve was generated and Log Rank Tests were performed with a value of $P <0.05$ that was considered statistically significant. All statistical analyses and graphs were performed using GraphPad Prism 5.02.

Acknowledgements

The authors would like to thank Sara Mamman, Rubysue Mangalindan, Ashot Safarli and other members of the Ladiges lab in the Department of Comparative Medicine for handling and maintenance of mouse colonies. The MF20 myosin antibody (Fischman) was obtained from the Developmental Studies Hybridoma Bank under the auspices of the NICHD, maintained by University of Iowa (Biological Sciences, Iowa City, IA 52242).

Online Supplement

Cardiomyocyte-specific expression of lamin A improves cardiac function in *Lmna*$^{-/-}$ mice

Richard L. Frock, PhD; Steven C. Chen, BS; Dao-Fu Dai, MD, PhD; Ellie Frett, BS; Carmen Lau, BS; Christina Brown, BS; Diana N. Pak, BS; Yuexia Wang, PhD; Antoine Muchir, PhD; Howard J. Worman, MD; Luis F. Santana, PhD; Warren C. Ladiges, DVM; Peter S. Rabinovitch, MD, PhD; Brian K. Kennedy, PhD

Contents:

Supplemental Methods

Animals

Genotyping of transgenic mice was performed by using PCR using primers against the FLAG-lamin A transgene: FLAG – ATGGACTACAAGGACGACGATGAC; Lamin A – AGTTCAGCAGAGCCTCCAGGTCCTT yielding a ~500 bp fragment. Primers for the detection of *Lmna* and its knockout allele [94]: 5'-wild-type – TGCTGATGCCATGGATACTC; 5'-knockout – GCACGAGACTAGTGAGACGTG; 3'-common – GAGAAGGCAGAGGTGTGAGCAGC yielding ~1 kb and 700 bp fragments respectively.

Tissue preparation and indirect immunofluorescence

Primary antibodies were myosin heavy chain (DSHB MF20; 1:100), desmin (Abcam 15200; 1:250), pan-cadherin (Sigma CH-19; 1:200), FLAG (Sigma M2; 1:50), and connexin 43 (Invitrogen 71-0700; 1:200). Sections were fixed in cold acetone for 20 min at –20°C, washed in PBS prior to blocking in 20% goat serum, 0.1% BSA, PBS for 20 min for desmin and FLAG staining. Blocking with 1% BSA, 0.3% TritonX-100 in PBS for 15 minutes was done for staining of pan-cadherin and connexin 43.

For nuclear staining of the FLAG-tagged transgenic protein, sections were boiled for 10 minutes in antigen unmasking solution (Vector labs) prior to blocking. Samples were viewed on a Zeiss 200M Axiovert and images were acquired using Axiovision. Scoring of desmin phenotypes from collected images was performed using ImageJ (NIH). Scoring of desmin accumulation was accomplished using tools from ImageJ to differentially mark fibers with

qualitatively increased desmin staining in the cytoplasm or loss of normal striated pattern (include total number here if not apparent in the legend) compared to control animal hearts. The co-association index was determined by measuring the ratio of fluorescence intensities of connexin 43 overlapping with pan-cadherin at the intercalated discs of sectioned ventricular myocytes using the "Outline Spline" tool to trace intercalated discs and then calculated the “Densitometric Mean” for each channel utilizing Axiovision software. Images were taken for each group at equivalent exposure times for connexin 43 and pan-cadherin. Fluorescence intensity ratios were binned into 0.05 increments from 0-1.0, where 1.0 represents equal intensity of connexin 43 with pan-cadherin. A non-linear regression for Gaussian distribution was applied to each group to determine mean co-association indices per experiment. To compare multiple experiments, mean co-association indices for each experiment were normalized to their respective mean index for *Lmna*$^{+/+}$ and averages of the normalized means were graphed.

Western analysis

Protein concentrations of lysates were quantitated using a DCA assay kit (Biorad). Approximately 10 μg of total protein was loaded for detection of desmin protein and 50 μg of total protein was loaded for detection of other less abundant proteins. Protein samples were separated on 4-12% SDS-PAGE gradient gels (Invitrogen) and transferred onto nitrocellulose. The following antibodies and dilutions were used in this study for Western analysis: pan-lamin A/C (Cell signaling 2032; 1:1000), desmin (Abcam 15200; 1:25000), pERK1/2 (Cell Signaling 9101; 1:500), ERK1/2 (Santa Cruz sc-94; 1:2500), connexin 43 (Invitrogen 71-0700; 1:250), α-

tubulin (Cell Signaling 2125; 1:1000), Cx43 NT1 and Cx43 CT1 (gifts from Paul Lampe, FHCRC, Seattle, WA; 1:1000). pERK/ERK ratio was quantified utilizing the "Measure" tool in ImageJ (NIH) to calculate pixel densitometry. CT1/NT1 ratio was quantified utilizing the “Rectangle Feature” in Odyssey software (LI-COR) to calculate pixel densitometry.

Quantitative RT-PCR

Hearts were homogenized using the TH homogenizer (Omni International) in RLT buffer (600 µL/30 mg tissue; Qiagen). Approximately 5 OD_{260} units of the RNA/protein mixture were used for the RNeasy kit with the remaining steps performed as per the manufacturer’s instructions (Qiagen). Reverse transcription reactions were performed with 2 µg total RNA using Superscript III (Invitrogen) at 42^{o}C for 50 min. Quantitative RT-PCR (qPCR) samples were normalized against the housekeeping gene ribosomal protein, large, P0 (RPLP0; ARBP). qPCR primers are listed in the following or cited elsewhere: ANF Forward 5’-GAAAAGGCAGTCGATTCTGC-3’, Reverse: 5’-CAGAGTGGGAGAGGCAAGAC-3’; BNP [221]; RPLP0 Forward: 5’-TGTTTGACAACGGCAGCATTT-3’ Reverse: 5’-CCGAGGCAACAGTTGGGTA-3’.

Echocardiography

M-mode and Doppler imaging was performed to evaluate cardiac morphometry, systolic function, and myocardial performance index, which is calculated as the ratio of the sum of isovolemic contraction and relaxation time (IVCT + IVRT) to LV ejection time (LVET). An increase in MPI indicates that a larger fraction of systole is spent during isovolemic phases, which is the ineffective time fraction.

ECG recordings

Due to the small size of the *Lmna*$^{-/-}$ mice, 5 min recordings were collected for anesthetized mice using 0.5% isoflurane with ECG leads placed at the modified lead II position of the chest cavity underneath the skin.

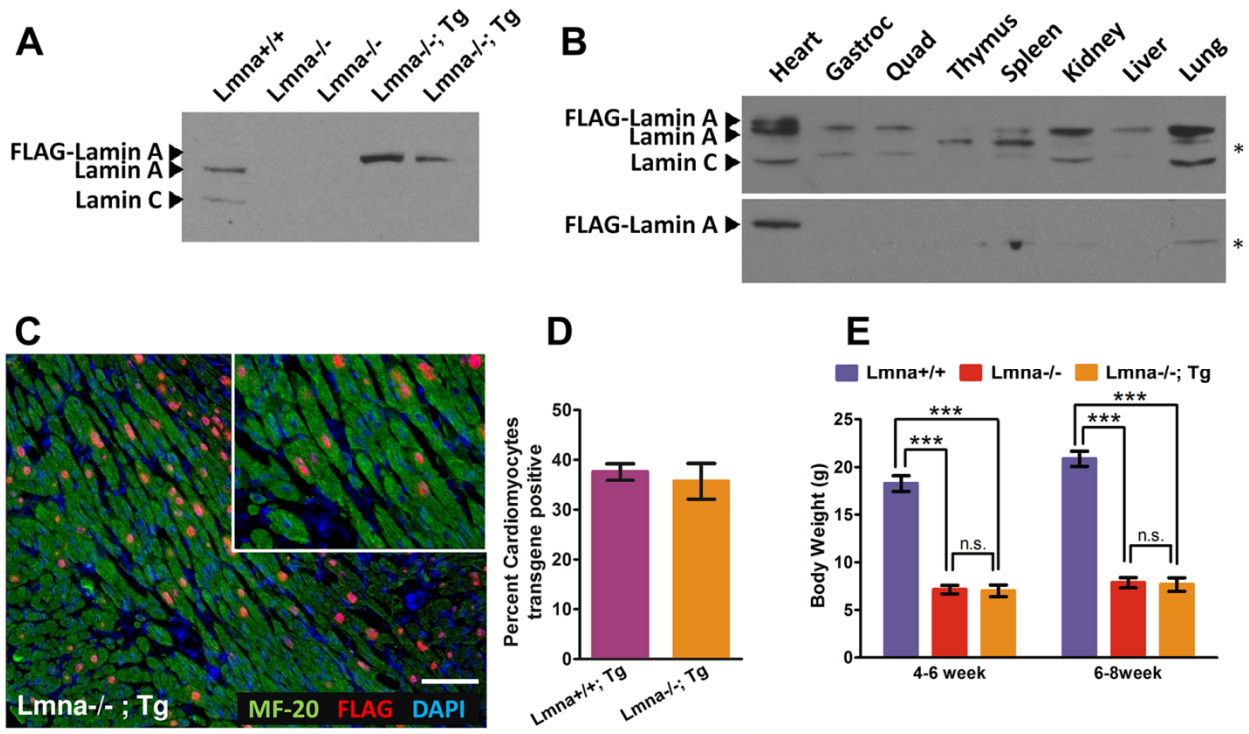

Figure 1. FLAG-lamin A is highly expressed, tissue-specific, and mosaic. **(A)** Western blot analysis of *Lmna*$^{+/+}$, *Lmna*$^{-/-}$, and *Lmna*$^{-/-}$; Tg heart lysates that were probed with lamin A/C antibody. **(B)** Western blot analysis of heart, gastrocnemius, quadriceps, thymus, spleen, kidney, liver, and lung from *Lmna*$^{+/+}$; Tg (upper panel) and *Lmna*$^{-/-}$; Tg (lower panel) mice probing with lamin A/C antibody. The asterisk indicates a cross-reactive band present in all lanes. **(C)** Indirect immunofluorescence micrograph of *Lmna*$^{-/-}$; Tg heart cross-section stained for MF-20 (cardiomyocytes; green), FLAG (transgene; red), and DAPI (nuclei, blue). Note that the mosaic expression of the transgene is limited to only cardiomyocytes. Scale bar denotes 100 µm. Inset is zoomed in view from the same image. **(D)** Quantitation of the percent of cardiomyocytes expressing FLAG-lamin A (N=3 each; ~500 cardiomyocytes were scored for each group) (E) Body weights of *Lmna*$^{+/+}$, *Lmna*$^{-/-}$, and *Lmna*$^{-/-}$; Tg mice (N=10, 11, and 8 at 4-6 weeks respectively and N=10, 7, and 5 at 6-8 weeks respectively).

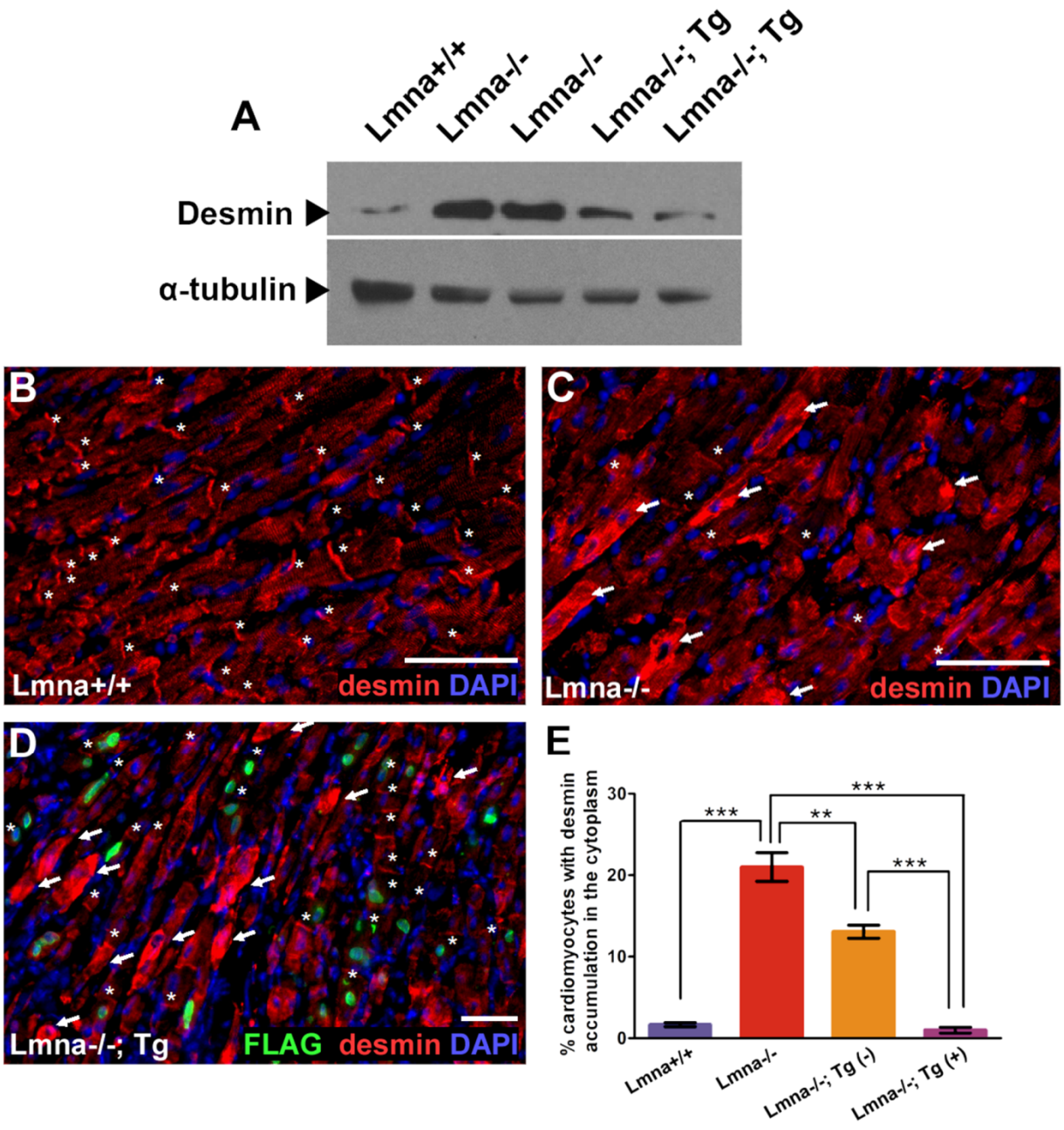

Figure 2. Transgenic expression of lamin A in *Lmna*$^{-/-}$ cardiomyocytes results in partial restoration of desmin phenotype but not cardiac remodeling markers. (A) Western blot analysis of *Lmna*$^{+/+}$, *Lmna*$^{-/-}$, and *Lmna*$^{-/-}$; Tg whole heart lysates. Desmin is increased in *Lmna*$^{-/-}$ heart lysates compared to *Lmna*$^{+/+}$ and is partially attenuated in *Lmna*$^{-/-}$; Tg mice (middle blot). α-tubulin is shown as a loading control (bottom blot). **(B-D)** Indirect immunofluorescence

micrographs showing desmin (red), FLAG (green), and DAPI (blue) in *Lmna*$^{+/+}$ (B), *Lmna*$^{-/-}$ (C), and *Lmna*$^{-/-}$; Tg (D) heart ventricle sections. Asterisks mark intercalated discs, which co-localize with a pan-cadherin antibody (not shown) and arrows indicate ventricular myocytes with accumulated desmin in the cytoplasm. Scale bar denotes 50 μm. (D) Note the lack of ventricular myocytes positive for both desmin cytoplasmic accumulation and transgene expression. **(E)** Graph summarizing the desmin cytoplasmic accumulation phenotype observed in *Lmna*$^{-/-}$ ventricular myocytes across different mouse backgrounds aged 5-7 weeks (N=3 for *Lmna*$^{+/+}$, *Lmna*$^{-/-}$, and *Lmna*$^{-/-}$; Tg; ** P<0.01; *** P<0.001).

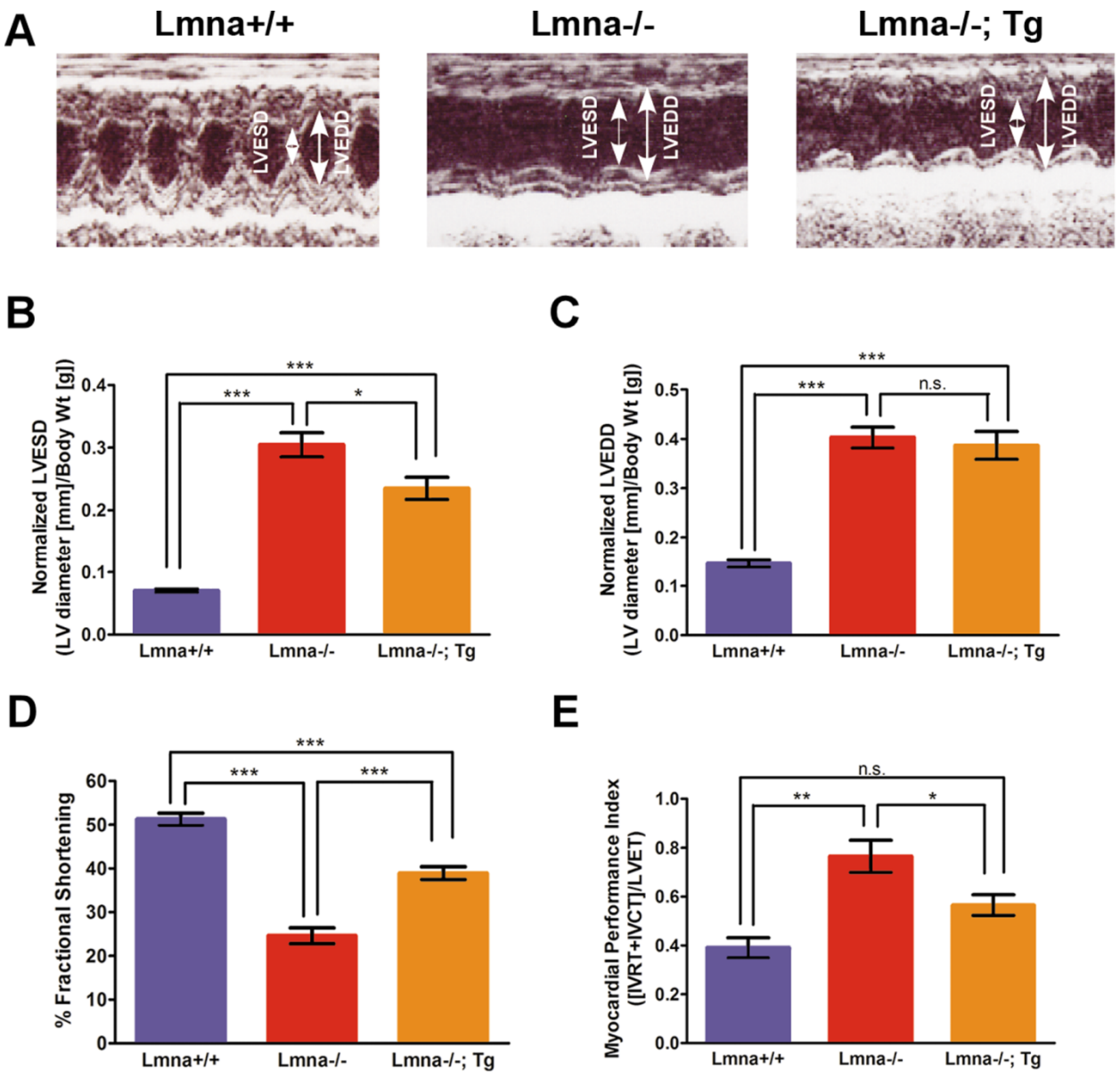

Figure 3. *Lmna*$^{-/-}$; Tg mice display improved contractile function compared to *Lmna*$^{-/-}$ littermates. **(A)** Representative echocardiograms of *Lmna*$^{-/-}$, *Lmna*$^{-/-}$; Tg, and control littermates. **(B)** Normalized left ventricular end-systolic diameter (LVESD) measurements are increased in *Lmna*$^{-/-}$ hearts compared to control hearts and are improved in *Lmna*$^{-/-}$; Tg hearts. **(C)** Normalized left ventricular end-diastolic diameter (LVEDD) measurements are increased in *Lmna*$^{-/-}$ hearts and are not improved in *Lmna*$^{-/-}$; Tg hearts. **(D)** Fractional shortening is

decreased in *Lmna*$^{-/-}$ hearts compared to control hearts and is improved in *Lmna*$^{-/-}$; Tg hearts. **(E)** Myocardial performance index (MPI) is increased (worse) in *Lmna*$^{-/-}$ mice, but is improved in *Lmna*$^{-/-}$; Tg mice. For all of the above experiments: Control, N=13; *Lmna*$^{-/-}$, N=15; *Lmna*$^{-/-}$; Tg, N=12 for 4-8 weeks of age. One-way ANOVA analyses were performed (B-E) and significant genotype differences are listed above for each panel. Post-tests were performed between genotypes and significance is listed as follows: * $P<0.05$; ** $P<0.01$; *** $P<0.001$; n.s. not significant.

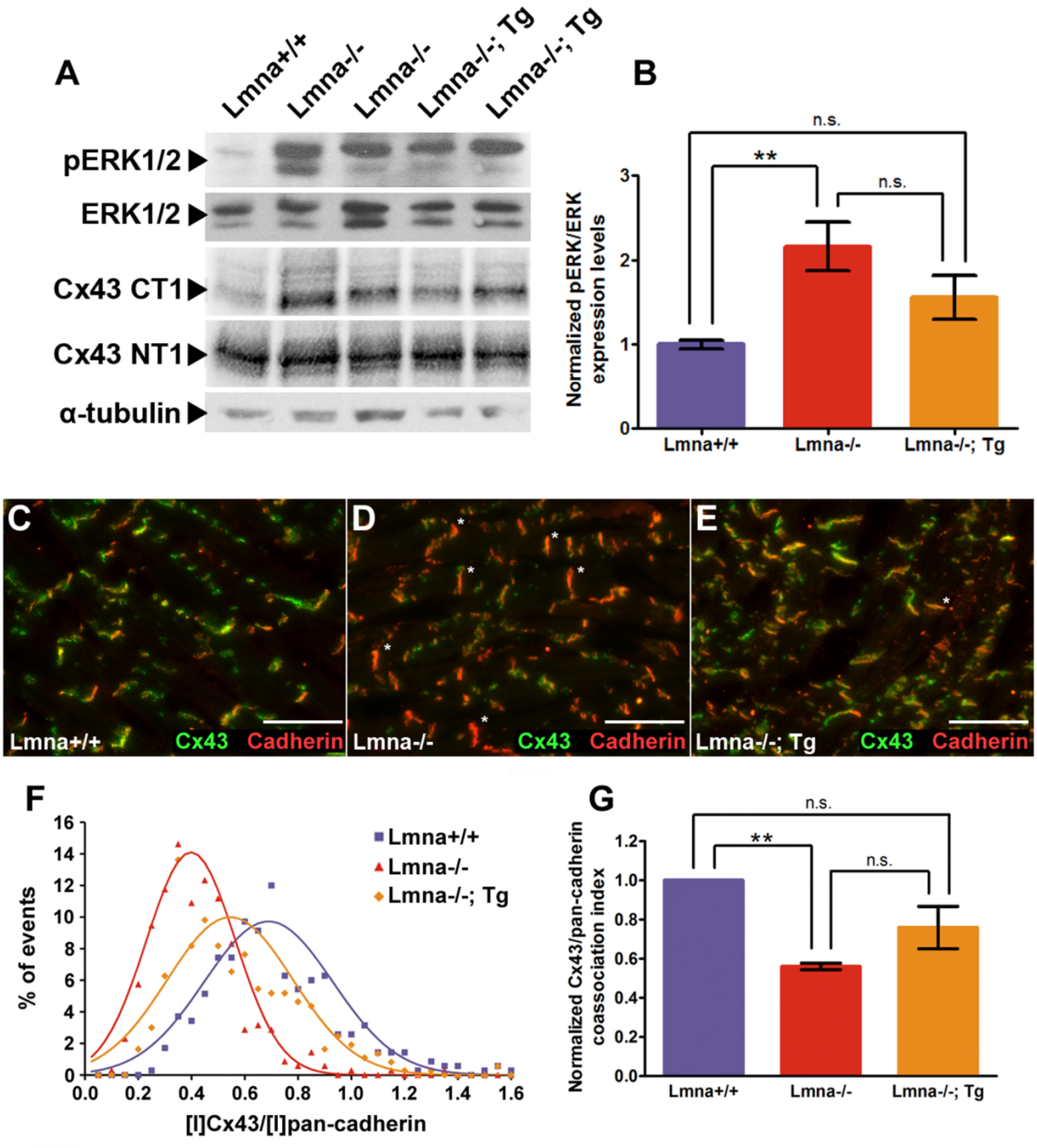

Figure 4. Transgenic expression of lamin A in *Lmna*$^{-/-}$ cardiomyocytes partially restores ERK1/2 activation and gap junction protein localization. (A) Western blot analysis of *Lmna*$^{+/+}$, *Lmna*$^{-/-}$, and *Lmna*$^{-/-}$; Tg mouse heart lysates. Phosphorylated-ERK1/2 (pERK1/2) levels are increased in *Lmna*$^{-/-}$ compared to *Lmna*$^{+/+}$ and are decreased in *Lmna*$^{-/-}$; Tg hearts while total ERK1/2 levels

are unchanged. Total Cx43 protein levels detected by NT1 are unchanged, while cytoplasmic levels of Cx43 as detected by CT1 are increased. α-tubulin is shown as a loading control. **(B)** Quantification of pERK1/2 levels normalized to total ERK1/2 levels in 5-7 week old *Lmna*$^{+/+}$ (N=13), *Lmna*$^{-/-}$ (N=16), and *Lmna*$^{-/-}$; Tg (N=11) mouse heart lysates. One-way ANOVA analyses were performed for significance with post-test significance values as follows: ** P<0.01; n.s. not significant. **(C-E)** Indirect immunofluorescence micrographs of pan-cadherin (red) and Cx43 (green) in *Lmna*$^{+/+}$ (C), *Lmna*$^{-/-}$ (D), and (E) *Lmna*$^{-/-}$; Tg heart ventricle sections taken at equivalent exposure times from 6-week old mice. Asterisks mark intercalated discs with qualitative decreases in Cx43 relative to pan-cadherin staining. White scale bar denotes 50 μm. **(F)** Distribution of individual intercalated disks summarizing relative frequency of Cx43 co-association index in 5-7-week old *Lmna*$^{+/+}$ (N=3; 350 intercalated discs analyzed total), *Lmna*$^{-/-}$ (N=3; 349 intercalated discs analyzed total), and *Lmna*$^{-/-}$; Tg (N=3; 367 intercalated discs analyzed total) mice. A non-linear regression for Gaussian distribution was fitted for each group tested (*Lmna*$^{+/+}$ R^2=0.91; *Lmna*$^{-/-}$ R^2=0.96; *Lmna*$^{-/-}$; Tg R^2=0.80). **(G)** Combined Cx43 co-association indices from multiple experiments normalized against their respective *Lmna*$^{+/+}$ control (N=3). One-way ANOVA analyses were performed for significance with post-test significance values as follows: ** P<0.01; n.s. not significant.

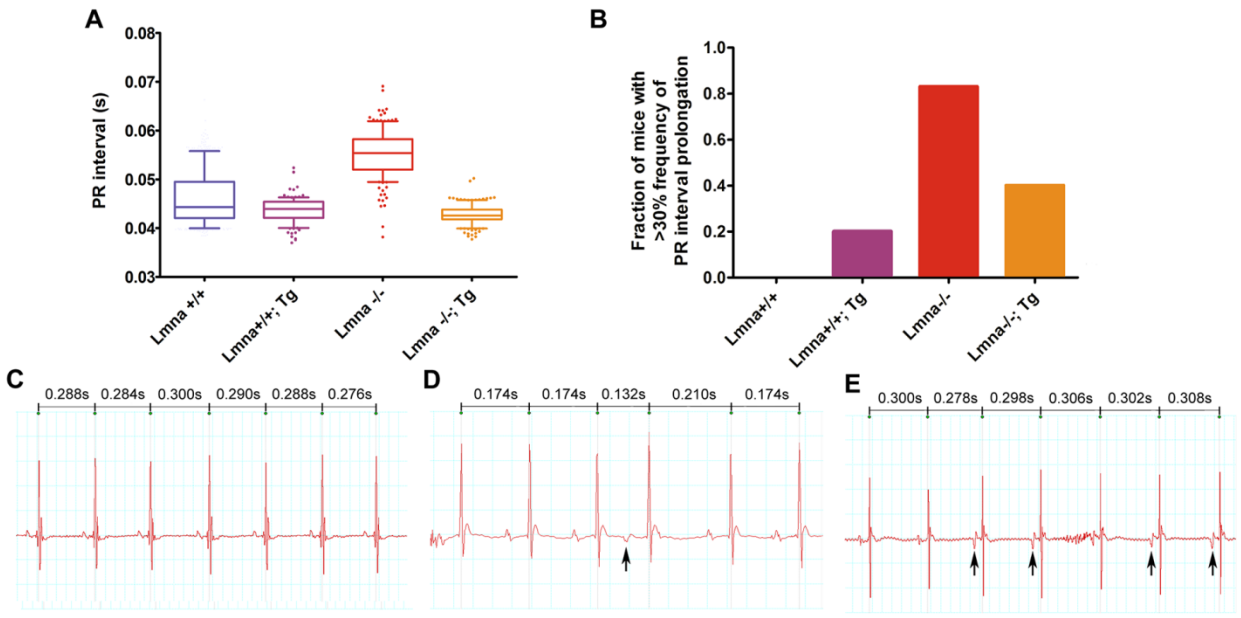

Figure 5. *Lmna*$^{-/-}$; Tg mice show improved conduction parameters compared to Lmna$^{-/-}$ mice by ECG analysis. (A) Box-and-whiskers plot of pooled *Lmna*$^{+/+}$ PR intervals (N=5) compared with single animal PR intervals for each of the following genetic backgrounds at 5-7 weeks of age: *Lmna*$^{+/+}$; Tg, *Lmna*$^{-/-}$ and *Lmna*$^{-/-}$; Tg. The whiskers represent at 5-95% confidence interval and individual outliers are represented by their respective dots. **(B)** Fraction of mice which display >30% abnormally prolonged PR interval. *Lmna*$^{+/+}$ (N=5), *Lmna*$^{+/+}$; Tg (N=5), *Lmna*$^{-/-}$ (N=6), and *Lmna*$^{-/-}$; Tg (N=5). **(C-E)** ECG traces from a *Lmna*$^{+/+}$ mouse (C), a *Lmna*$^{-/-}$ mouse exhibiting an atrial premature beat (D) and a *Lmna*$^{-/-}$ mouse displaying multifocal atrial rhythm (E). Note the changes in P-wave morphology and cycle length. Arrows denote ectopic P-waves. RR intervals are shown above.

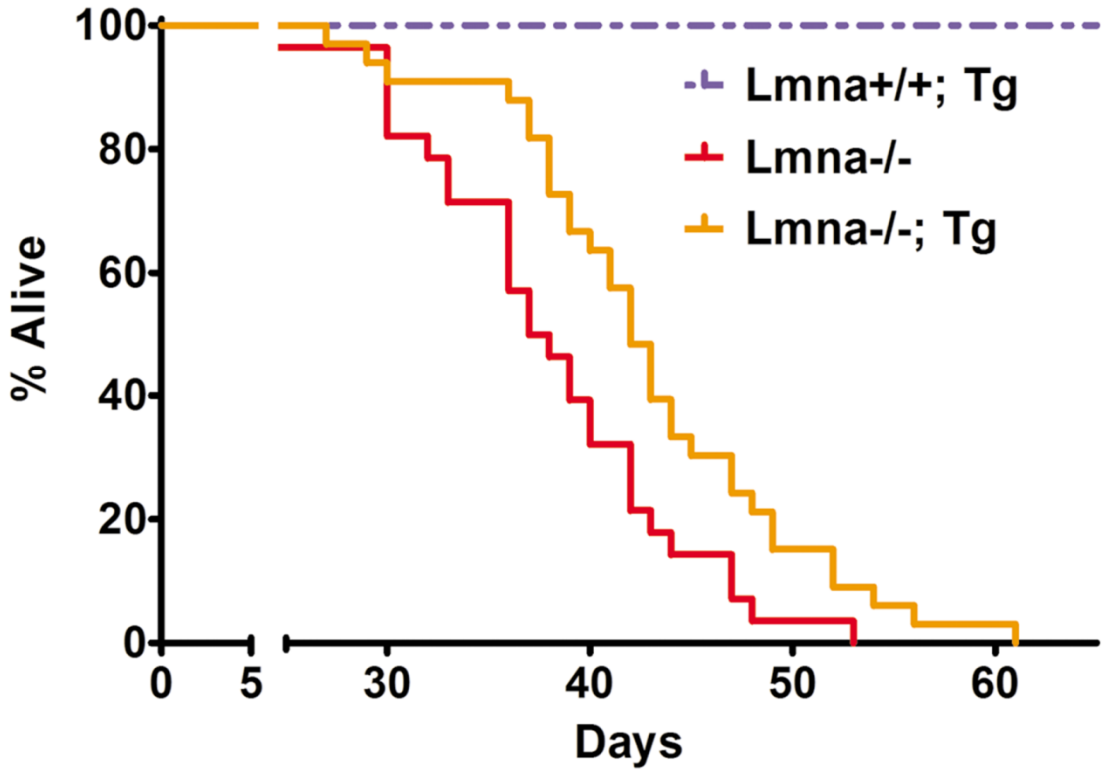

Figure 6. Extension of median and maximal lifespan in *Lmna*$^{-/-}$ mice expressing cardiac lamin A. *Lmna*$^{-/-}$; Tg mice display a 12% and 15% increase in median and maximal lifespans, respectively, compared to *Lmna*$^{-/-}$ littermates (*Lmna*$^{+/+}$; Tg N=10; *Lmna*$^{-/-}$ N=24; *Lmna*$^{-/-}$; Tg N=28). The Log-Rank test, which measures significance evenly across all time points, reports a significance probability of P<0.0114

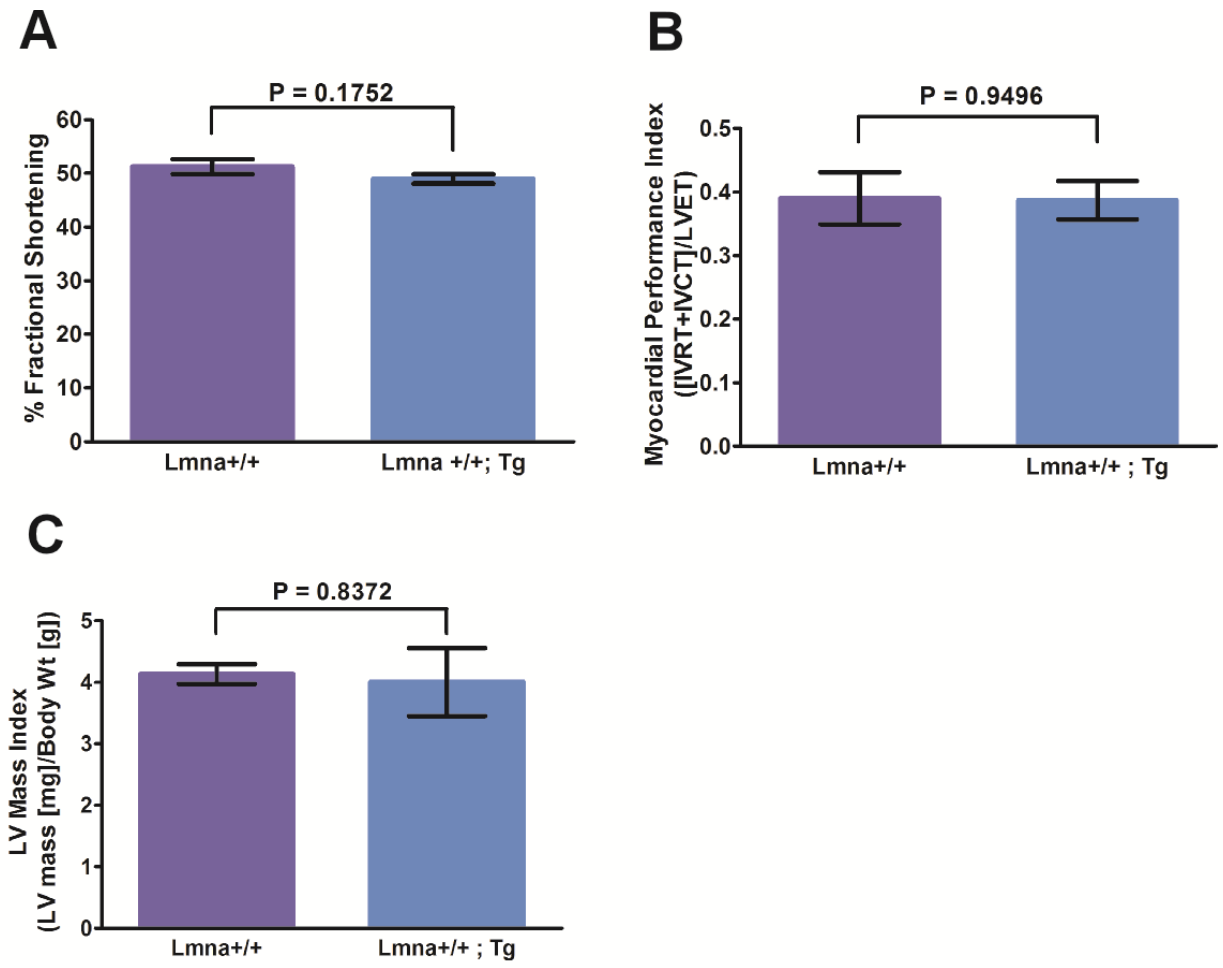

Supplemental Figure 1. *Lmna*$^{+/+}$ and *Lmna*$^{+/+}$; Tg hearts show no significant difference in cardiac function. (A & B) No significant difference is noted in (A) fractional shortening, (B) myocardial performance index (MPI), or **(C)** left ventricular mass index (LVMI) of *Lmna*$^{+/+}$ and *Lmna*$^{+/+}$; Tg hearts at 4-8 weeks of age as measured by echocardiography. Two-tailed unpaired t-tests were used to determine P-values which are listed for each panel. (*Lmna*$^{+/+}$, N=6; *Lmna*$^{+/+}$; Tg, N=7)

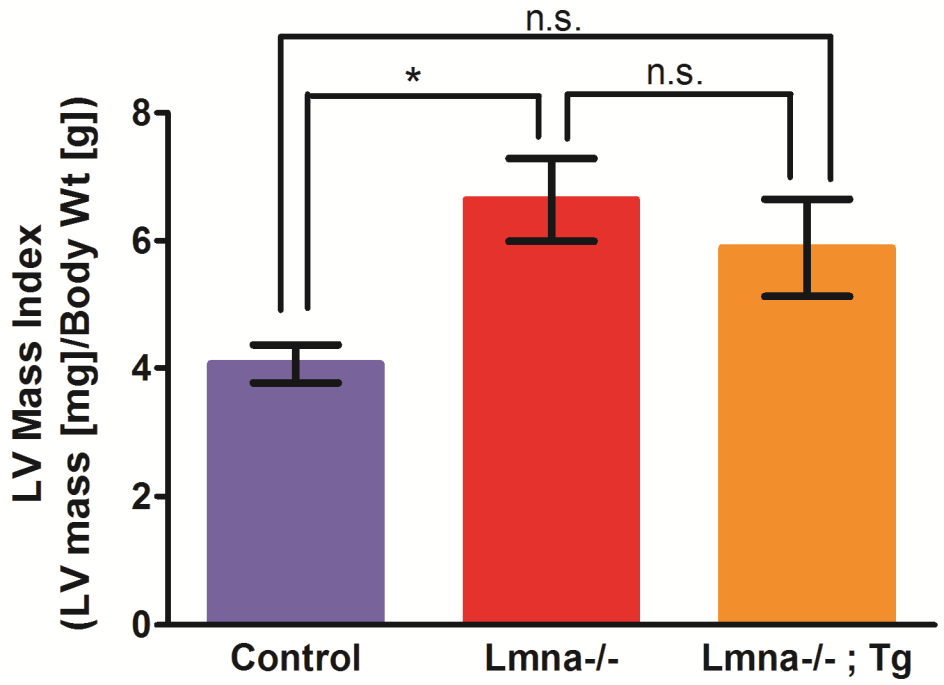

Supplemental Figure 2. *Lmna*$^{-/-}$ hearts are enlarged relative to control littermates and *Lmna*$^{-/-}$; Tg hearts are not significantly improved. Left ventricular mass of 4-8 week old mice was measured and normalized to body weight to resolve the LVMI. One-way ANOVA was performed and significant genotype differences are listed for each panel. Bonferonni post-tests were performed between genotypes and significance is listed as follows: * P<0.05; n.s. not significant. (Control, N= 13; *Lmna*$^{-/-}$, N=15; *Lmna*$^{-/-}$; Tg, N=12)

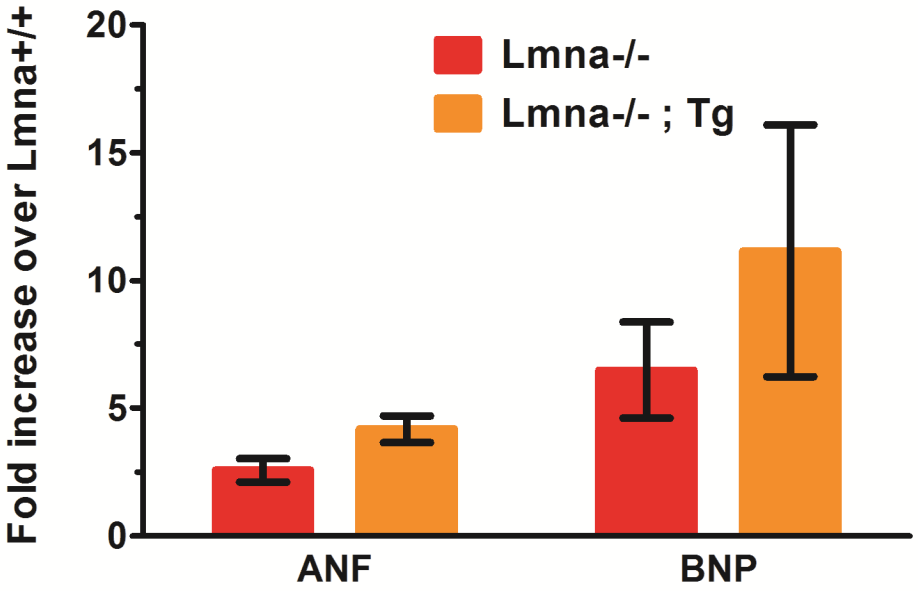

Supplemental Figure 3. mRNA levels of global remodeling markers, ANF and BNP, are enriched in *Lmna*$^{-/-}$ and *Lmna*$^{-/-}$; Tg mice. qPCR of cardiac remodeling mRNA's for *Lmna*$^{-/-}$ and *Lmna*$^{-/-}$; Tg hearts. Data are presented as fold-increase over *Lmna*$^{+/+}$ hearts. Global cardiac remodeling mRNA's, ANF and BNP, are all increased in *Lmna*$^{-/-}$ hearts and are not significantly changed in *Lmna*$^{-/-}$; Tg hearts. (*Lmna*$^{+/+}$, N= 4; *Lmna*$^{-/-}$, N=7; *Lmna*$^{-/-}$; Tg, N=5)

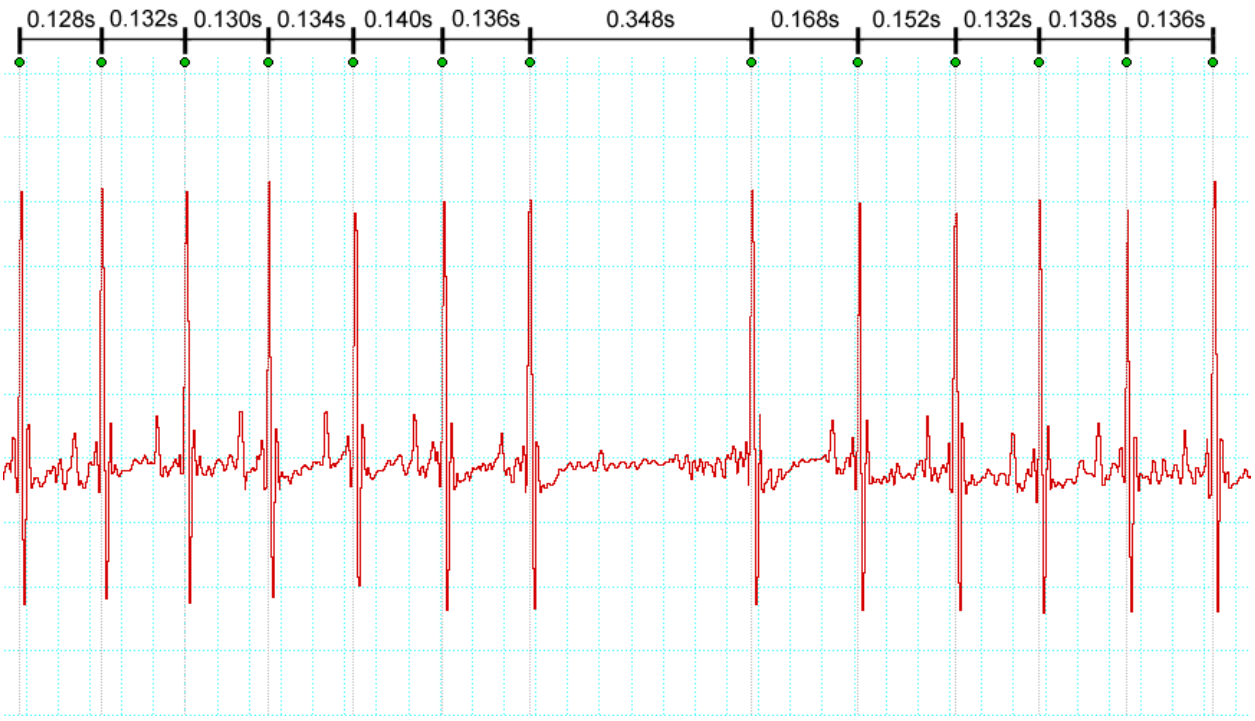

Supplemental Figure 4. Dropped beat in *Lmna*$^{+/+}$; Tg heart. An isolated case of a dropped heartbeat was noted in a single *Lmna*$^{+/+}$; Tg heart during ECG recording which could reflect either a sinus pause or sino-atrial block.

Average ECG parameters from 5-7 week old mice (first 300 beats/mouse analyzed)

Lmna $^{+/+}$	RR Interval (s)	Heart Rate (BPM)	PR Interval (s)	P Duration (s)	QRS Interval (s)
52731	0.1380	434.9	0.0481	0.0113	0.0080
52733	0.1754	342.0	0.0426	0.0112	0.0085
53045	0.1431	419.6	0.0446	0.0123	0.0084
52168	0.2669	225.3	0.0548	0.0155	0.0153
52721	0.1668	359.8	0.0406	0.0125	0.0121
Average	*0.178 ± 0.052*	*356.3 ± 83.0*	*0.046 ± 0.006*	*0.013 ± 0.002*	*0.010 ± 0.003*
Lmna $^{+/+}$; Tg	RR Interval (s)	Heart Rate (BPM)	PR Interval (s)	P Duration (s)	QRS Interval (s)
53049	0.1244	482.5	0.0405	0.0117	0.0077
53055	0.2033	302.2	0.0437	0.0111	0.0083
53057	0.1135	528.9	0.0396	0.0091	0.0077
52167	0.1604	375.6	0.0421	0.0112	0.0123
50907	0.1698	355.9	0.0534	0.0087	0.0099
Average	*0.154 ± 0.036*	*409.0 ± 93.7*	*0.044 ± 0.006*	*0.010 ± 0.001*	*0.009 ± 0.002*
Lmna $^{-/-}$	RR Interval (s)	Heart Rate (BPM)	PR Interval (s)	P Duration (s)	QRS Interval (s)
53052	0.1722	349.8	0.0698	0.0080	0.0087
53053	0.1913	313.7	0.0485	0.0100	0.0080
52570	0.1775	338.7	0.0412	0.0144	0.0125
50716	0.1546	388.4	0.0502	0.0094	0.0087
50721	0.3031	198.1	0.0547	0.0093	0.0090
50904	0.2826	212.5	0.0502	0.0085	0.0085
Average	*0.214 ± 0.063*	*300.2 ± 77.5*	*0.052 ± 0.010*	*0.010 ± 0.002*	*0.009 ± 0.002*
Lmna $^{-/-}$; Tg	RR Interval (s)	Heart Rate (BPM)	PR Interval (s)	P Duration (s)	QRS Interval (s)
53054	0.4066	148.7	0.0917	0.0149	0.0152
53224	0.3745	160.5	0.0707	0.0132	0.0125
53234	0.1529	392.4	0.0427	0.0081	0.0079
53240	0.1504	398.9	0.0431	0.0187	0.0087
52732	0.1423	421.8	0.0342	0.0111	0.0124
Average	*0.245 ± 0.133*	*304.5 ± 137.3*	*0.057 ± 0.024*	*0.013 ± 0.004*	*0.011 ± 0.003*

Supplemental Table 1. Average ECG parameters from 5-7 week old mice. ECG parameters of individual mice from *Lmna*$^{+/+}$ and *Lmna*$^{-/-}$ mice either expressing or not expressing FLAG-lamin A in cardiomyocytes. Similar mouse genotypes are grouped together with mouse ID displayed and parameters are averaged. Each parameter from an individual mouse represents an

averaged value from the first 300 beats recorded. Parameters include RR interval, Heart Rate, PR interval, P duration, and QRS interval.

Chapter 2

Rapamycin Reverses Elevated mTORC1 Signaling in *Lmna*$^{-/-}$ Mice, Rescuing Cardiac and Skeletal Muscle Function and Extending Survival

Given the association that lamin has with progeroid syndromes such as Hutchinson-Gilford progeria, I was curious as to whether any of the observed pathologies in the *Lmna*$^{-/-}$ mouse could be attributed to progeria. Since it had recently been shown that administration of rapamycin to aged mice extended lifespan [128], it would be interesting to see if rapamycin would also extend lifespan in *Lmna*$^{-/-}$ mice. Rapamycin is a specific inhibitor of mTORC1, which is responsible for regulating cell growth and protein synthesis through the mTOR pathway. The mTOR pathway has also been shown to be activated during skeletal and cardiac remodeling, which are part of the *Lmna*$^{-/-}$ mouse phenotype. Therefore, giving rapamycin to *Lmna*$^{-/-}$ mice seemed like it could not only improve any progeroid defect, but improve the described skeletal and cardiac muscle defect. In summary, we were able to demonstrate increased mTOR signaling in *Lmna*$^{-/-}$ mice, contributing to loss of both cardiac and skeletal muscle function, and that rapamycin was able to ameliorate some of these effects and extend lifespan by 35%.

In this manuscript, I performed the immunofluorescence experiments which showed that rpS6 is increased in the hearts of *Lmna*$^{-/-}$ mice and is rescued by rapamycin treatment. I also demonstrated that the desmin accumulation, as described in the previous chapter, is increased in both heart and muscle of *Lmna*$^{-/-}$ mice, but that rapamycin only restores normal organization in the heart. Using immunohistochemistry, I confirm the heart dilation previously

described in *Lmna*$^{-/-}$ mice. Finally, I show that the muscular dystrophy phenotype is potentially improved by rapamycin treatment as cross-sectional area of individual muscle fibers in treated *Lmna*$^{-/-}$ mice is increased. This chapter is presented in manuscript form and is currently under resubmission to *Science Translational Medicine*.

Rapamycin reverses elevated mTORC1 signaling in *Lmna*$^{-/-}$ mice, to rescue cardiac and skeletal muscle function and extend survival

Fresnida J. Ramos[1], Steven C. Chen[2], Michael G. Garelick[2,3], Dao-Fu Dai[1], Vincent M. Damian[1], Vivian L. MacKay[2], Elroy H. An[1], Randy Strong[4,5,6],Warren C. Ladiges[7], Peter S. Rabinovitch[1], Matt Kaeberlein[1], and Brian K. Kennedy[2,3]

Departments of Pathology[1], Biochemistry[2] and Comparative Medicine[5], University of Washington, Seattle, WA 98195; [3]Buck Institute for Research on Aging, Novato, CA 94945; [4]The Barshop Institute for Longevity and Aging Studies, University of Texas Health Science Center at San Antonio, San Antonio, TX; [5]Department of Pharmacology, University of Texas Health Science Center at San Antonio, San Antonio, TX; [6]Geriatric Research, Education and Clinical Center and Research Service, South Texas Veterans Health Care System, San Antonio, TX;

Abstract

Mutations in *LMNA*, encoding A-type lamins, cause multiple diseases including dystrophies of the skeletal muscle and fat, dilated cardiomyopathy, progeria-like syndromes and others (collectively termed laminopathies). Reduced A-type lamin function, however, is most commonly associated with skeletal muscle dystrophy and dilated cardiomyopathy rather than lipodystrophy or progeria. The mechanisms underlying these diseases are only beginning to be unraveled. Here we report that *Lmna*$^{-/-}$ mice have enhanced mTORC1 signaling specifically in tissues linked to pathology, namely cardiac and skeletal muscle. Pharmacologic reversal of elevated mTORC1 signaling by rapamycin improves parameters of cardiac and skeletal muscle function and enhances survival in mice lacking A-type lamins. At the molecular level, rapamycin decreases the number of myocytes with abnormal desmin accumulation and decreases desmin protein levels in both muscle and cardiac tissue of *Lmna*$^{-/-}$ mice. In addition, inhibition of mTORC1 signaling with rapamycin enhances productive autophagy in *Lmna*$^{-/-}$ mice. Together, these findings identify aberrant mTORC1 signaling as a mechanistic component of laminopathies associated with reduced A-type lamin function and offer a potential therapeutic approach involving rapamycin-related, clinically approved mTORC1 inhibitors.

Introduction

A-type lamins are type V intermediate filament proteins that form part of the nuclear lamina, providing structural integrity to the nucleus[30,222] and regulating chromatin organization[223], transcription[42,224], and DNA replication[35]. In humans, mutations in *LMNA*, result in several diseases including autosomal dominant limb-girdle muscular dystrophy (LGMD1B)[63], Emery-Dreifuss muscular dystrophy (EDMD2/3)[59], dilated cardiomyopathy and conduction-system disease (CMD1A)[64], familial partial lipodystrophy[76], Charcot-Marie-Tooth disease[84], and Hutchinson-Gilford progeria syndrome (HGPS)[225]. Skeletal muscle dystrophy and dilated cardiomyopathy (DCM) are two phenotypes commonly associated with *LMNA* missense mutations that impair the activity of the protein (often in a dominant negative fashion) [70,226,227]. Stop codons, splice site variants, or insertions/deletions can also result in reduced lamin A/C protein levels[70,226,227]. *Lmna*$^{-/-}$ mice also develop both DCM and skeletal muscle dystrophy, succumbing to complications related to cardiac dysfunction by 6-8 weeks of age[96]. Thus, *Lmna*$^{-/-}$ mice are a clinically relevant model to investigate the molecular mechanisms involved in skeletal muscle dystrophy and DCM caused by reduced lamin A protein levels.

Cardiac and skeletal muscle tissues are highly adaptable and many signaling pathways are involved in regulating muscle remodeling. One such pathway involves the mammalian target of rapamycin complex 1 (mTORC1), which is a major regulator of protein synthesis. The mTORC1 complex consists of mTOR, regulatory associated protein of mTOR (Raptor)[228,229], and mlst8/GβL[230]. Among other events, activation of the mTORC1 signaling cascade results in the phosphorylation of downstream substrates, such as p70 S6 kinase and 4E-BP1[231,232], which in

turn affect protein synthesis. Activation of S6 kinase by phosphorylation, for instance, results in the phosphorylation of ribosomal protein S6 (rpS6) and other components of the translational machinery, while phosphorylation of 4E-BP1 decreases its binding to eif4E, freeing this initiation factor to promote cap-dependent translation[231]. Enhanced mTOR-mediated phosphorylation of 4E-BP1 and S6 kinase is evident during non-pathological cardiac and skeletal muscle remodeling as well as in disease-related cardiac and skeletal remodeling[233,234,235,236,237].

Another important function of the mTORC1 signaling pathway is the regulation of autophagy, a process involving the degradation of damaged or excess cellular components, ranging from individual proteins and protein aggregates to whole organelles, through lysosomal machinery. When cells have sufficient nutrients, autophagy is inhibited by mTORC1; on the other hand, lack of nutrients inhibits the mTORC1 pathway and autophagy is initiated to reallocate nutrients from non-essential components to those that are vital to survival[238]. Activation of mTORC1 in mammalian cells results in the phosphorylation of ULK1 and disruption of the ULK1/Atg13 complex, thereby inhibiting autophagy [239]. Autophagy plays an important role in protein homeostasis in cardiac and skeletal muscle and changes in autophagic markers in these tissues can be detected due to non-pathological stimulation such as exercise, as well as in disease-induced situations such as dilated cardiomyopathy and muscular dystrophy[240,241,242,243].

Because of the important roles that mTORC1 signaling plays in skeletal and cardiac tissue, we hypothesized that dysregulation of mTORC1 signaling may contribute to the cardiac and skeletal muscle pathology of *Lmna*$^{-/-}$ mice. Here we examine mTORC1 signaling in *Lmna*$^{-/-}$

mice and test the effects of pharmacological manipulation of this pathway by rapamycin on *Lmna*$^{-/-}$ disease phenotypes.

Results

To test the hypothesis that dysregulation of mTORC1 signaling may contribute to the cardiac and skeletal muscle pathology of *Lmna*$^{-/-}$ mice, we looked at phosphorylation of downstream signaling components of the mTORC1 pathway by western blot analysis. Consistent with this hypothesis, we observed significantly increased phosphorylation of S6 kinase$^{(T389)}$ (P=0.044), rpS6$^{(S235/S236)}$ (P=0.0178), and 4E-BP1$^{(S65)}$ (P=0.0047) in heart and increased phosphorylation of rpS6$^{(S235/S236)}$ (P=0.026) and 4E-BP1$^{(S65)}$ (P=0.011) in skeletal muscle of 4 week old *Lmna*$^{-/-}$ animals, compared to wild type controls (**Fig. 1A and B**). Hyperactivation of the mTORC1 pathway in *Lmna*$^{-/-}$ mice was not observed in non-diseased tissue such as liver **(Supplemental Fig. 1A)**. Increased mTORC1 signaling in *Lmna*$^{-/-}$ mouse hearts was associated with early signs of left and right ventricle dilatation rather than hypertrophy **(Supplemental Fig. 1B)**. Indeed, other studies have noted the absence and/or attenuation of a hypertrophic response in both *Lmna*$^{-/-}$ mice and *Lmna*$^{+/-}$ mice subjected to pressure overload by transverse aortic constriction[96,244]. To further understand the impact of increased mTORC1 signaling in *Lmna*$^{-/-}$ mice, we performed polysome profile analysis on heart tissue using a protocol that was able to detect an angiotensin-induced increase in protein synthesis in wild-type heart tissue. Consistent with a lack of hypertrophy, hyperactivated mTORC1 signaling in *Lmna*$^{-/-}$ mice does not result in an alteration of global protein synthesis

since polysome profiles of heart tissue from *Lmna*$^{-/-}$ mice were not significantly different from *Lmna*$^{+/+}$ mice **(Supplemental Fig. 1C and D)**.

The small molecule rapamycin is a specific inhibitor of mTORC1 activity and derivatives are used clinically in cancer treatment, prevention of organ transplant rejection, and prevention of restenosis after angioplasty[245,246,247,248]. Dietary treatment with rapamycin has also been found to extend lifespan in genetically heterogeneous mice[128,249]. In order to determine whether hyperactivation of the mTORC1 pathway plays a causal role in pathologies associated with loss of *Lmna*, we fed *Lmna*$^{-/-}$ mice chow containing encapsulated rapamycin beginning at an age of 3-4 weeks. By 2 weeks of treatment, rapamycin was detectable in the blood of *Lmna*$^{-/-}$ mice (6.9 ± 0.45ng/ml) and inhibition of mTORC1 signaling was apparent in heart tissue of rapamycin-treated animals relative to controls (**Fig. 2A**). Specifically, there was a significant decrease in phosphorylated mTOR$^{(S2448)}$ (P= 0.000014), S6 kinase$^{(T389)}$ (P= 0.020), and rpS6$^{(S235/S236)}$ (P=0.034) in *Lmna*$^{-/-}$ mice fed the rapamycin diet compared to *Lmna*$^{-/-}$ mice fed the control diet. However, phosphorylation of 4E-BP1$^{(S65)}$ was not significantly reduced by rapamycin treatment (P=0.074), consistent with prior *in vivo* evidence suggesting that rapamycin has stronger effects on S6 kinase phosphorylation than on 4E-BP1[250]. Reduction of phosphorylated rpS6$^{(S235/S236)}$ in cardiomyocytes was confirmed by immunohistochemistry of heart tissue sections from *Lmna*$^{-/-}$ mice fed the rapamycin diet compared to those fed control diet (P=0.024) (**Fig. 2B**).

Transthoracic echocardiography was used to determine the effect of dietary rapamycin on heart function in *Lmna*$^{-/-}$ mice. Echocardiographic analysis confirmed previous studies

showing impaired cardiac function and left ventricular dilatation at 6 weeks of age in *Lmna*$^{-/-}$ mice compared to *Lmna*$^{+/+}$ mice[96] (**Fig. 3A and B**). This is reflected in a significant increase in left-ventricular end diastolic diameter (LVEDD) and systolic diameter (LVESD) (normalized to body weight) in *Lmna*$^{-/-}$ mice (both P<0.001), which results in a significant decrease in fractional shortening (P<0.001) (**Fig. 3B**). *Lmna*$^{-/-}$ mice treated with rapamycin showed a significant decrease in LVESD (P<0.001) relative to untreated animals and suppression of the defects in both fractional shortening (P<0.001) and myocardial performance index (P<0.05). These data suggest that rapamycin improves cardiac function in mice lacking A-type lamins.

The rotarod test of motor coordination was used to assess the effects of dietary rapamycin on skeletal muscle function in *Lmna*$^{-/-}$ mice. The test represents a complex motor task involving muscle coordination and balance, as well as motor learning, and it has been used to determine the effectiveness of treatments for mouse muscular dystrophy models[251,252]. As expected, *Lmna*$^{-/-}$ mice are unable to stay on the rotating rod as long as *Lmna*$^{+/+}$ mice (P<0.05), and they cannot reach the same maximum speed as *Lmna*$^{+/+}$ mice given the same amount of time (P<0.01) **(Fig. 3C)**. Interestingly, latency to fall off the rotating rod was significantly improved in rapamycin treated *Lmna* $^{-/-}$ mice compared to control fed *Lmna*$^{-/-}$ mice (P<0.05). In addition, rapamycin fed *Lmna*$^{-/-}$ mice were able to reach a significantly higher speed than control fed *Lmna*$^{-/-}$ mice by the cut off time of 5 minutes (P<0.01)**(Fig. 3C)**.

Since *Lmna*$^{-/-}$ mice treated with rapamycin show improved cardiac and muscle function, we examined the effect of rapamycin on the lifespan of these animals. *Lmna*$^{-/-}$ mice fed rapamycin chow lived significantly longer than animals fed an identical diet without rapamycin

(P=0.0013) **(Fig. 4A)**. Rapamycin feeding resulted in a 35% increase in median lifespan (62 days vs. 46 days) and a 23% increase in mean lifespan (62 days vs. 50 days). Maximum lifespan was also increased by rapamycin treatment, as analysis of *Lmna*$^{-/-}$ mice surviving to the 90th percentile revealed a significantly greater proportion of rapamycin fed mice surviving compared to mice fed the control diet (P=0.049). Survival was significantly increased in both male *Lmna*$^{-/-}$ mice fed dietary rapamycin (P=0.0068) and in female *Lmna*$^{-/-}$ mice fed dietary rapamycin (P=0.036) **(Supplemental Fig. 2A and B).** Analysis of weekly body weights while on the diet revealed that male and female *Lmna*$^{-/-}$ mice fed rapamycin were better at maintaining their body weight over time than *Lmna*$^{-/-}$ mice fed the control diet (P= 0.048 and P=0.0060, respectively), although individual values at specific time points were not significantly different by Bonferroni *post-hoc* test **(Supplemental Fig. 2C and D)**.

Lmna$^{-/-}$ mice backcrossed to C57BL/6J for 9 generations have a more severe phenotype and a shorter lifespan than the *Lmna*$^{-/-}$ mice in the mixed background used in the dietary rapamycin studies reported above. To ascertain whether rapamycin could also be effective in a *Lmna*$^{-/-}$ model with a more severe phenotype, we administered rapamycin to *Lmna*$^{-/-}$ mice in the C57BL/6J background. Since the diet was only available in one dose, we increased rapamycin concentration by administering 8mg/kg rapamycin by intraperitoneal injection every other day starting at 3-4 weeks of age. Analysis of blood from rapamycin treated *Lmna*$^{-/-}$ mice resulted in levels of 85.7 ± 17.7 ng/ml. In addition, phosphorylation of S6 kinase$^{(T389)}$ and rpS6$^{(S235/S236)}$ was significantly decreased in heart by rapamycin injections (P=0.017 and 0.016, respectively) **(Supplemental Fig. 2E)**. While body weights of rapamycin treated *Lmna*$^{-/-}$ mice were not significantly different than control treated mice **(Supplemental Fig. 2F),** injection of

rapamycin significantly increased the survival of *Lmna*$^{-/-}$ mice (p=0.0002) **(Fig. 4B)**, resulting in a 56% increase in mean lifespan (58 days vs. 37 days) and a 60.5% increase in median lifespan (61 days vs. 38 days). Although maximum lifespan of *Lmna*$^{-/-}$ mice at the 90th percentile was not significantly different (due to low sample size), analysis of the 80th percentile revealed a significantly increased proportion of rapamycin treated mice compared to control mice (P=0.035). These data indicate that the beneficial effects of rapamycin in this disease model may be further enhanced by continued drug optimization.

To further understand the effects of rapamycin on the heart and muscle of *Lmna*$^{-/-}$ mice, we examined tissues at the molecular level. *Lmna*$^{-/-}$ mice have previously been shown to have defects in the desmin filaments linking the cytoskeleton to the nucleus in both heart and muscle tissue, resulting in accumulation of desmin aggregates in the cytoplasm and disruption of the Z-disc cross-striation pattern[96]. We also observed this phenomenon in our control fed *Lmna*$^{-/-}$ mice; however, with rapamycin treatment, we detect a significant reduction in desmin protein levels in both cardiac and skeletal muscle tissue by western blot analysis (P=0.042 and P=0.012) **(Fig. 5A)**. We also looked at desmin staining in tissue by immunohistochemistry and found that rapamycin was able to diminish abnormal desmin conglomerates in skeletal muscle **(Fig. 5B)** but not the cardiac tissue of *Lmna*$^{-/-}$ mice (P=0.025 and P=0.68) **(Fig. 5C)**. The differences in the effect of rapamycin in cardiac tissue by the two assays suggests that although the number of cardiomyocytes containing desmin conglomerates did not change, there was a reduction in the total amount of desmin present. Lastly, we examined whether rapamycin rescued aberrant cross-sectional area of the *Lmna*$^{-/-}$ skeletal muscle fibers. While there was a trend towards an increase in cross-sectional area of skeletal muscle fibers in rapamycin-fed

Lmna$^{-/-}$ mice, it did not achieve significance at a P-value of 0.05 (P=0.071) **(Supplemental Fig. 2G)**.

Because autophagy is implicated in mouse models of desmin-related cardiomyopathies[253] and because autophagy is regulated by mTORC1[254], we examined autophagy markers LC3 and p62 in *Lmna*$^{-/-}$ mice. We found an increase in LC3-I (P=0.0078) and LC3-II (P=0.0019) protein levels, as well as increased p62 (P=0.00099) protein levels in the heart tissue of *Lmna*$^{-/-}$ mice compared to *Lmna*$^{+/+}$ mice **(Fig. 6A and B)**. The increase in LC3-II levels, the lipidated form of LC3 localized to autophagosome membranes, suggests an increase in the formation of autophagosomes since LC3-II is believed to be required for autophagosome closure[255]. The increase in p62 protein levels suggests a reduction in autophagic flux because p62, a protein that binds ubiquitinated proteins targeted for autophagic degradation, is itself degraded during the autophagic process[255]. In *Lmna*$^{-/-}$ mice treated with rapamycin, there is a significant decrease in LC3-I levels (P=0.029), while there is no change in LC3-II levels (P=0.48) **(Fig. 6C)**. In addition, there is a significant decrease in p62 levels (P=0.0062) in rapamycin treated *Lmna*$^{-/-}$ mice **(Fig. 6D)**. Together, these data suggest that loss of A type lamins causes defects in productive autophagy in cardiac tissue and that treatment with rapamycin suppresses this defect.

Discussion

Our findings indicate that hyperactivation of the mTORC1 signaling pathway in *Lmna*$^{-/-}$ mice contributes to the heart and muscle-specific defects in these mice and that inhibition of

this pathway with rapamycin can significantly counteract this dysfunction and ultimately improve survival. Initially, activation of the mTORC1 pathway can be a beneficial response in muscle and cardiac tissue when hypertrophy is needed. In cardiac tissue, the hypertrophic response is activated due to hemodynamic overload and this provides temporary relief in terms of heart function. However, sustained activation of the hypertrophic response may not always result in the long-term maintenance of heart function. For example, acute induction of hypertrophy by activation of Akt-1 specifically in the heart results in the preservation of heart function, while chronic activation leads to dilated cardiomyopathy[256]. Moreover, treatment with rapamycin prevents the effects of both acute and chronic activation of Akt-1, suggesting that the mTORC1 pathway may be involved in both physiological responses[256]. In addition, a recent report showed that mTORC1 signaling is elevated in a mouse model (LS/+ mice) of LEOPARD syndrome, an autosomal dominant disorder which manifests with congenital heart disease, among other symptoms[257]. LS/+ mice initially develop hypertrophic hearts with sustained heart function; without treatment, however, this progresses to dilated cardiomyopathy and impaired heart function by 52 weeks of age[257]. Interestingly, treatment of LS/+ mice with rapamycin reversed hypertrophic cardiomyopathy and rescued aberrant signaling through the Akt/mTOR pathway. In the case of *Lmna*$^{-/-}$ mice, activation of mTORC1 signaling and the hypertrophic response appears to be uncoupled since *Lmna*$^{-/-}$ mice bypass hypertrophy and instead develop dilated cardiomyopathy. It has been suggested that the lack of hypertrophy may be due in part to the disorganization of the desmin filament network and accumulation of desmin aggregates [96]. Desmin, a major cytoskeletal protein in cardiac and muscle tissue that connects the contractile apparatus to other organelles of the cell (including

the mitochondria and nucleus), is highly involved in the cytoskeletal rearrangements required for adaptive hypertrophy[258]. Accordingly, dilated cardiomyopathy and skeletal myopathy is observed in humans with gene mutations (encoding desmin or desmin interacting proteins like αB-crystallin) that lead to desmin disorganization and aggregation[259,260], and desmin aggregates are often observed in human idiopathic dilated cardiomyopathy[261]. Autophagy is upregulated in response to desmin aggregation and increases in autophagic markers such as autophagosomes, LC3-II levels, and p62 levels can be found in mouse models of desmin-related cardiomyopathies[253]. While similar increases in LC3-II levels and p62 are noted in *Lmna*$^{-/-}$ mice, due to the potentially antagonizing effect of aberrant mTORC1 signaling on autophagy, the efficiency of this process may be compromised. Thus, we propose that non-productive autophagy contributes to the disease phenotypes observed in *Lmna*$^{-/-}$ mice and that treatment with rapamycin suppresses mTORC1 hyperactivation and promotes productive autophagy. This in turn has positive effects on desmin in the heart and skeletal muscle of *Lmna*$^{-/-}$ mice, resulting in improvements in heart and skeletal muscle function and ultimately, survival.

There are currently no effective treatments for CDM1A and the two muscular dystrophies linked to *LMNA* mutation (EDMD2/3 and LGMD1B), with affected individuals succumbing to sudden cardiac failure in their 4th and 5th decade[262] . Our findings point to a potential means of clinical intervention which could benefit individuals who suffer from these diseases. Rapalogs, derivatives of rapamycin with better pharmacokinetics, are clinically approved for use in an increasing range of human diseases. We propose that these agents may be efficacious for improving cardiac function in *LMNA*-associated CDM1A, EDMD2/3, and LGMD1B patients, as well as in other diseases associated with reduced A-type lamin function.

Materials and Methods

Animals and experimental protocols

Lmna$^{-/-}$ mice and *Lmna*$^{+/+}$ littermate controls were produced by mating *Lmna*$^{+/-}$ mice of a mixed 129Sv-C57BL/6J genetic background. For analysis of mTORC1 signaling in *Lmna*$^{-/-}$ mice and *Lmna*$^{+/+}$ littermate controls, tissues were dissected from mice aged 4 weeks and analyzed by western blot. For behavioral and biochemical studies, *Lmna*$^{-/-}$ mice and *Lmna*$^{+/+}$ littermate controls were fed either a control diet or a diet containing encapsulated rapamycin *ad libitum* starting at 3-4 weeks of age for 2 weeks prior to analysis. For survival studies, *Lmna*$^{-/-}$ mice were fed either a control diet or a diet containing encapsulated rapamycin[128] (Courtesy of R. Strong, UTHSCSA) *ad libitum* starting at 3-4 weeks of age for the duration of their lifespan. Mice were weighed weekly when their cage was changed and food was added to the cage. Mice were examined daily for signs that they were reaching the end of their natural lifespan and were euthanized for humane reasons before they succumbed to disease. For studies with 8mg/kg injections of rapamycin (LC laboratories), *Lmna*$^{-/-}$ mice and *Lmna*$^{+/+}$ littermate controls were produced by mating *Lmna*$^{+/-}$ mice of C57BL/6J genetic background. For biochemical studies, *Lmna*$^{-/-}$ mice and *Lmna*$^{+/+}$ littermate controls (3-4 weeks of age) were given intraperitoneal injections of 8mg/kg rapamycin or vehicle control every other day for 1 week (4 injections). 24 hours after the last injection, tissues were dissected from the mice and immediately frozen in liquid nitrogen. For survival studies, *Lmna*$^{-/-}$ mice (3-4 weeks of age) were given intraperitoneal injections of 8mg/kg rapamycin or vehicle control every other day for the duration of their lifespan. Endpoint was determined as stated above.

Polysome analysis

Heart polysome protocol was adapted from Zomzely et al[263]. Frozen hearts were homogenized with a dounce homogenizer in 1.5 ml of homogenization buffer composed of 250 mM sucrose, 50 mM Tris HCl, pH 7.4, 100 mM KCl, 12 mM $MgCl_2$, 0.1 mg/ml cycloheximide, and 400 units/ml RiboLock (Fermentas). Samples were centrifuged at 10,000 X g for 10 minutes at 4°C. Deoxycholate was then added to supernatant to a final concentration of 1%. Samples were incubated for 10 minutes at 4°C then re-centrifuged at 16,000 X g. The supernatant was loaded on a 10.8 ml sucrose gradient with 50 mM Tris-HCl, 100 mM KCl, and 15 mM $MgCl_2$ with 100 μg/ml cycloheximide and 1mg/ml heparin. Samples were centrifuged in an SW41 Ti rotor (Beckman) at 39,000 rpm at 4°C for 2 hrs.

Western blot analysis

Mouse tissues were dissected and immediately frozen in liquid nitrogen. For tissue homogenization, frozen tissues were placed into the pre-chilled chamber of a cryogenic tissue pulverizer (RPI) and instantly turned into fine powder using the compression force of a pestle struck by a mallet. The finely ground tissue was transferred to a dounce homogenizer containing ice-cold homogenization buffer (50mM HEPES pH 7.6, 150mM NaCl, 20mM sodium pyrophosphate, 20mM beta-glycerophosphate, 10mM NaF, 2mM EDTA, 1% igepal, 10% glycerol, 1mM $MgCl_2$, 1mM $CaCl_2$, 2mM sodium orthovanadate, 2mM PMSF, 10ug/ml leupeptin, 10ug/ml aprotinin, and 1:100 serine/threonine phosphatase inhibitor cocktail (Sigma)). The tissues were dounce homogenized on ice and then centrifuged at 13,000 rpm for 15 minutes at 4°C. The supernatants were collected and protein concentration was determined by BCA protein assay (Thermo Scientific #23227). Equal amounts of protein were resolved by SDS-PAGE (4-12% gel) and

western blot analysis was performed using protein/phospho-protein specific antibodies. Anti-mTOR (#2972, 1:1000), anti-phospho mTOR$^{(S2448)}$(#5536, 1:1000), anti-p70 S6 kinase (#2708, 1:1000), anti-phospho p70 S6 kinase$^{(T389)}$ (#9234, 1:500), anti-rpS6 (#2217, 1:1000), anti-phospho-rpS6$^{(S235/236)}$ (#2211, 1:1000), anti-4EBP1 (#9452, 1:1000), anti-tubulin (#2125; 1:1000) and anti-phospho 4EBP1$^{(S65)}$ (#9451, 1:500) were from Cell Signaling Technologies. Anti-desmin (sc-23879, 1:1000) was from Santa Cruz Biotechnologies. Anti-p62 (H00008878-M01, 1:1000) was from Abnova. Anti-LC3 (NB100-2331, 1:1000) was from Novus Biologicals. Anti-actin was from Chemicon (MAB1501R, 1:10,000).

Transthoracic echocardiography

Echocardiography examination was performed using a Siemens Acuson CV70. A mixture of 0.5% isoflurane with O_2 was used to provide adequate sedation with minimal cardiac suppression during echocardiography. M-mode and Doppler imaging was performed to evaluate cardiac morphometry, systolic function, and myocardial performance index, which is calculated as the ratio of the sum of isovolemic contraction and relaxation time (IVCT + IVRT) to LV ejection time (LVET). An increase in MPI indicates that a larger fraction of systole is spent during isovolemic phases, which is the ineffective time fraction.

Rotarod

The day before the actual rotarod testing, the mice were placed on the rotarod set to a beginning speed of 5rpm, with an acceleration rate of 0.1 rpm/s. The max speed was set at 25 rpm. They were allowed to practice the rotarod 5 times, one repetition every 5 minutes. If the animal did not fall off, each repetition would end at 5 min. The test day occurred 24 hrs after

the practice day, and the procedure was the same except scores were recorded. The score for each repetition was the time in seconds when the animal fell off the rotarod. The average of all five repetitions was used to score the sessions.

Tissue preparation and indirect immunofluorescence

Hearts and gastrocnemius muscles were rapidly excised and rinsed in phosphate-buffered saline (PBS) prior to mounting in Tissue-Tek O.C.T. compound and subsequent freezing in liquid nitrogen-cooled isopentane. Special care was taken to prevent deformation of the hearts when dissecting by using a plastic bulb pipette with the tip cut off to gently grasp the heart by suction rather than using forceps. Mounted samples were stored at -80^{O}C until further processing. For analysis of ventricle wall thickness and ventricular dilatation, heart sections 10 µm in thickness were mounted on Superfrost plus glass slides (Fisher) and then stained with *hematoxylin* and eosin. For immunohistochemistry, heart ventricle or gastrocnemius muscle sections 8 µm in thickness were collected and mounted on glass slides. Primary antibodies were desmin (Santa Cruz Biotech sc-23879; 1:100), dystrophin (kindly gifted from Chamberlain, JS; 1:600), phospho-rpS6$^{(S240/244)}$ (Cell Signaling 2215; 1:100) and β-sarcoglycan (Leica NCL-b-SARC; 1:100). Sections were fixed in cold acetone for 20 min at –20°C, followed by blocking in 5% BSA in PBS with 0.3% Triton X-100. After staining was complete, tissues were mounted in Fluoromount (Southern Biotech). Samples were viewed on a Zeiss 200M Axiovert and images were acquired using Axiovision (Zeiss). Images were then scored for cross-sectional area in Axiovision by utilizing the “Outline Spline” tool to trace individual muscle fibers and calculate area. All fibers of an individual image were outlined until total fibers scored was >100 per

mouse. Scoring of desmin and phospho-rpS6 accumulation was accomplished in a similar fashion using the cell counter tool in ImageJ to mark fibers with increased staining until >500 total fibers were scored per mouse. Increased desmin staining in muscle fibers was considered when there was any detectable cytoplasmic desmin or if there was significant desmin associated with the plasma membrane, as these features were not detected in the control animals. Increased desmin staining in the heart was considered when loss of normal striated pattern of desmin in the cytoplasm or accumulations of desmin was noted anywhere within the outline of the fiber.

Rapamycin analysis

HPLC/MS/MS on whole blood samples was performed by Rocky Mountain Labs (http://www.rockylab.com/).

Statistical analysis

A two-tailed student's t-test was used for comparisons between two groups. Two-way ANOVA with Bonferroni post-hoc analysis was used for comparisons between more than two groups. Log-rank test was used for comparisons of survival curves. Quantile regression with a two-tailed Fisher's exact test was used for analysis of maximum lifespan. For all statistics, $P< 0.05$ was considered significant.

Acknowledgements.

The authors would like to thank Rubysue Mangalindan, Ashot Safarli, James Harrington, Dylan Vathana Touch, Heather Hopkins and other members of the Ladiges lab in the

Department of Comparative Medicine for their help and expertise in the maintenance of mouse colonies. These studies have been supported by NIA grant R01 AG024287 to B.K.K and U01 AG022307 to R.S. F.J.R. and M.G.G. are supported by NIH Training Grant T32AG000057. S.C.C. is supported by the cardiovascular and pathology training grant NIH T32 HL007312. MK is an Ellison Medical Foundation New Scholar in Aging.

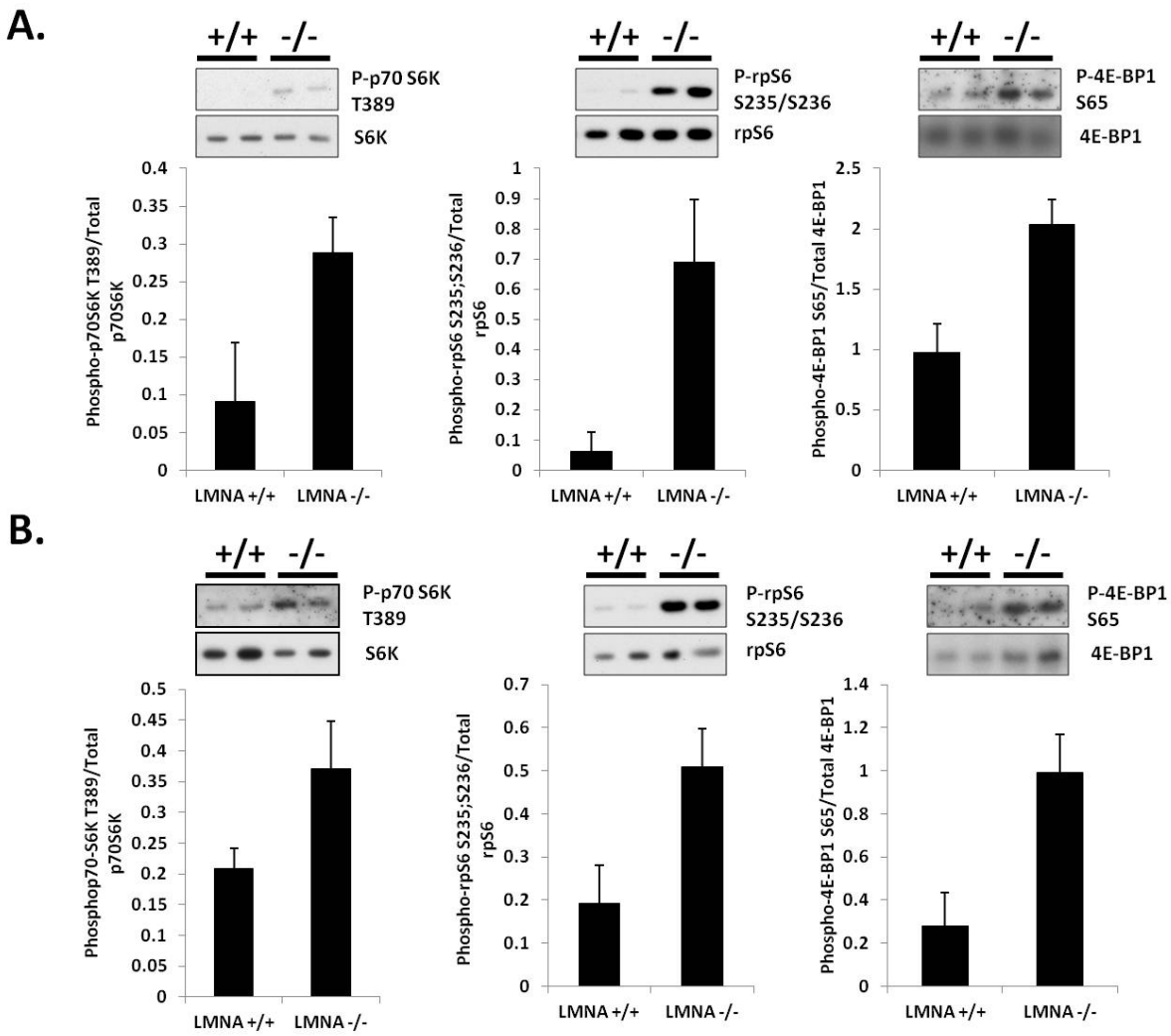

Figure 1. Signaling through the mTORC1 pathway is increased in *Lmna*$^{-/-}$ mice. (A) Western blot analysis of *Lmna*$^{+/+}$ (N=7) and *Lmna*$^{-/-}$ (N=8) mice heart tissue lysates. Phosphorylated S6 kinase$^{(T389)}$ (P= 0.044), rpS6$^{(S235/S236)}$ (P=0.0178), and 4E-BP1$^{(S65)}$ (P=0.0047) are increased in *Lmna*$^{-/-}$ mice compared to *Lmna*$^{+/+}$ mice. **(B)** Western blot analysis of *Lmna*$^{+/+}$ (N=7) and *Lmna*$^{-/-}$ (N=8) mice skeletal muscle (quadriceps) tissue lysates. Phosphorylated rpS6$^{(S235/S236)}$ (P=0.026), and 4E-BP1$^{(S65)}$ (P=0.011) are increased in *Lmna*$^{-/-}$ mice compared to *Lmna*$^{+/+}$ mice. However, phosphorylated S6 kinase$^{(T389)}$ (P= 0.087) is not significantly increased.

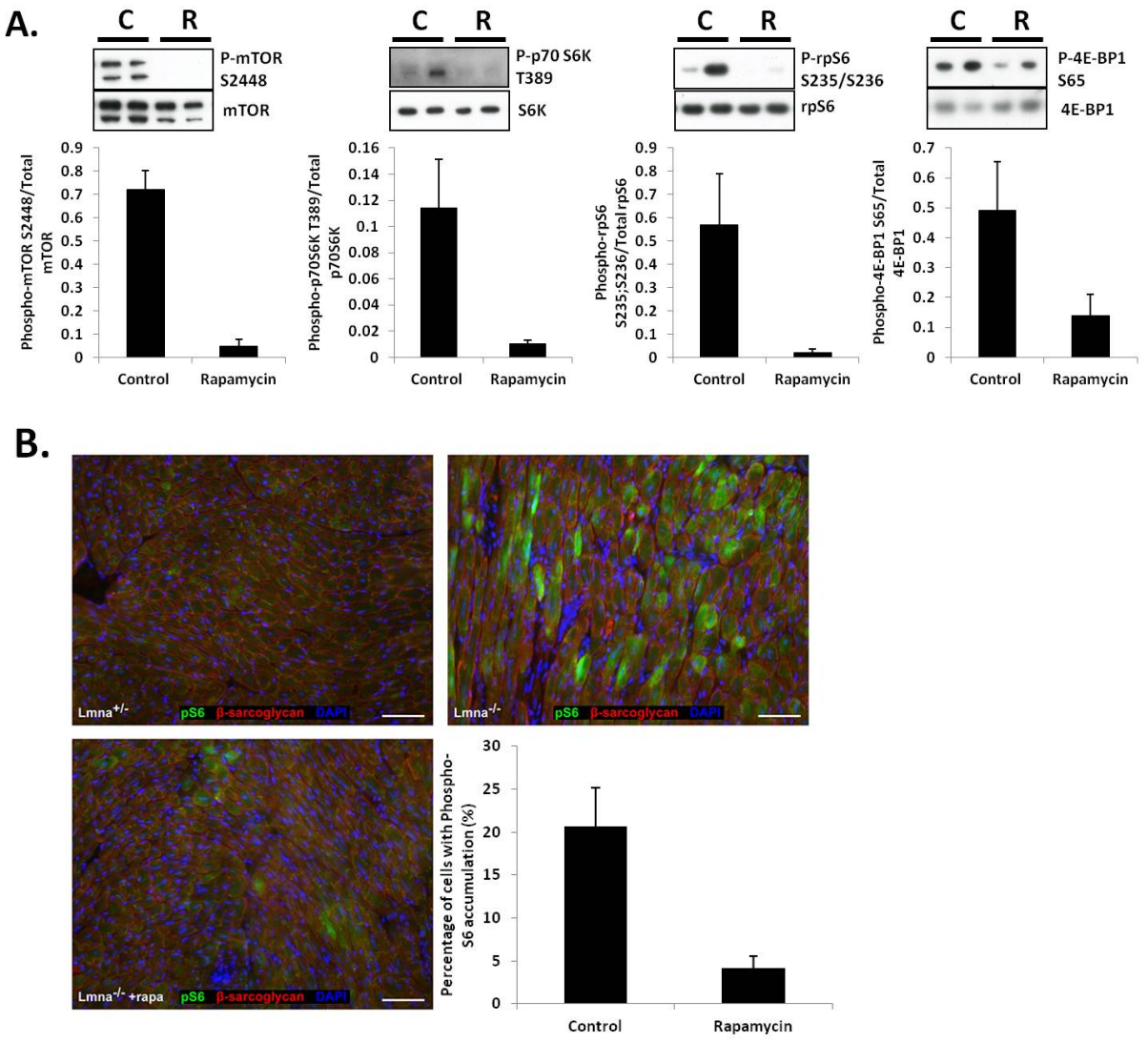

Figure 2. **Signaling through the mTORC1 pathway in *Lmna*$^{-/-}$ mouse heart is reduced by rapamycin treatment.** **(A)** Phosphorylated mTOR$^{(S2448)}$ (P= 0.000014), S6 kinase$^{(T389)}$ (P= 0.020), and rpS6$^{(S235/S236)}$ (P=0.034) are decreased in *Lmna*$^{-/-}$ mice fed the rapamycin diet (R, N=6) compared to *Lmna*$^{-/-}$ mice fed the control diet (C, N=6). However, phosphorylation of 4E-BP1$^{(S65)}$ (P=0.074) is not significantly reduced. **(B)** Immunohistochemistry of heart tissue sections from *Lmna*$^{-/-}$ mice fed the rapamycin diet (N=3) shows a significant decrease in the percentage of

cardiomyocytes with accumulation of phosphorylated rpS6 compared to *Lmna*$^{-/-}$ mice fed the control diet (N=3) (P=0.024).

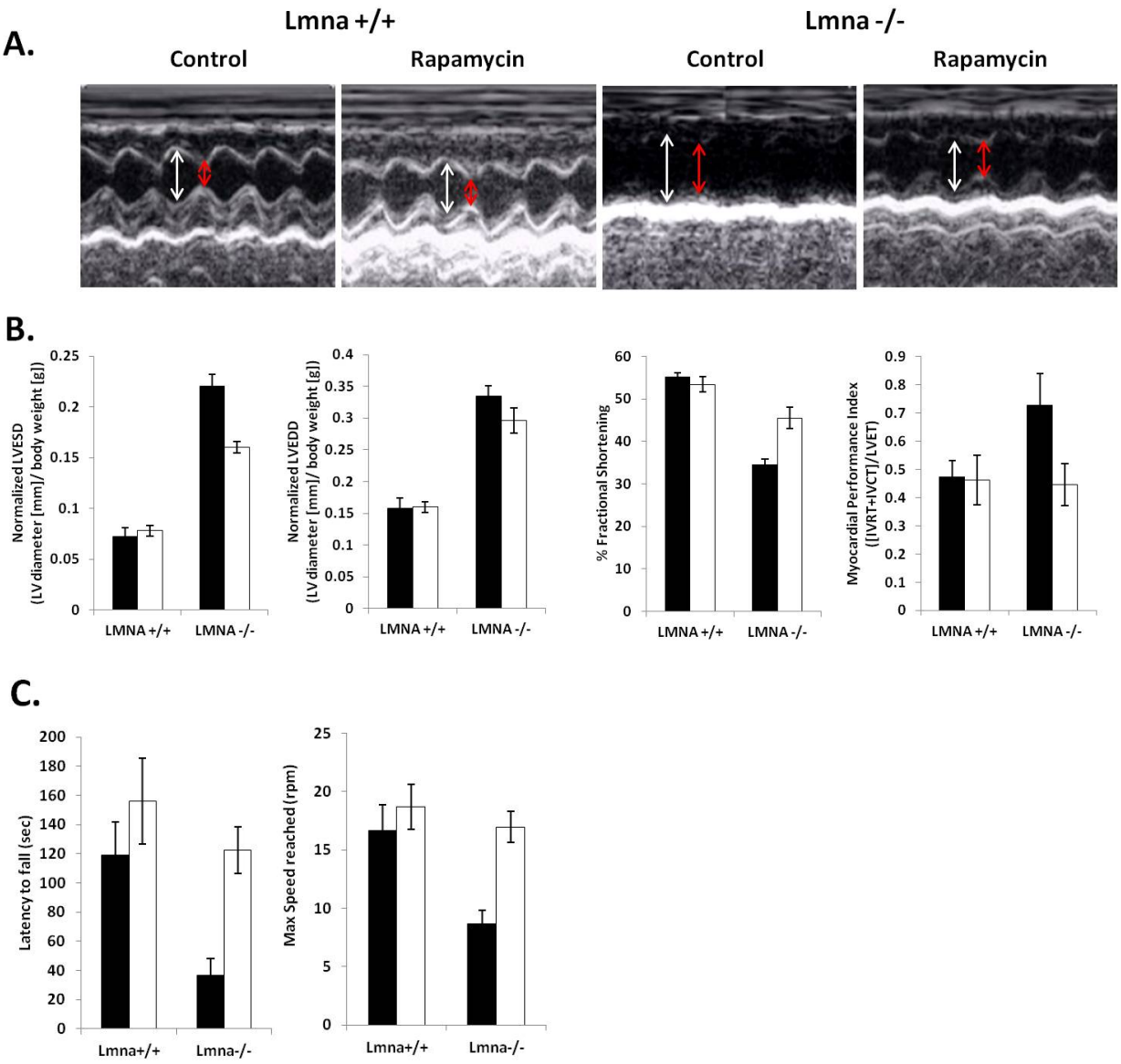

Figure 3. Treatment of *Lmna*$^{-/-}$ mice with rapamycin improves heart and skeletal muscle function. (A) Representative echocardiograms of *Lmna*$^{+/+}$ and *Lmna*$^{-/-}$ mice fed control or rapamycin diet. White arrow= LVEDD; red arrow= LVESD. **(B)** Normalized left-ventricular end systolic diameter (LVESD) ($P<0.001$), normalized left-ventricular end diastolic diameter (LVEDD) ($P<0.001$), and fractional shortening (FS) ($P<0.001$) are significantly different in *Lmna*$^{-/-}$ mice fed control diet (N=7) compared to *Lmna*$^{+/+}$ mice fed control diet (N=4). Dietary rapamycin

significantly improves normalized left-ventricular end systolic diameter (P<0.001), fractional shortening (P<0.001), and myocardial performance index (MPI) (P<0.05) in *Lmna*$^{-/-}$ mice (N=7) compared to *Lmna*$^{-/-}$ mice fed the control diet (N=7). Black bars= control fed; white bars= rapamycin fed. **(C)** Analysis of muscle function by rotarod test shows a significant decrease in latency to fall (P<0.05) and maximum speed reached (P<0.01) in *Lmna*$^{-/-}$ mice fed control diet (N=5) compared to *Lmna*$^{+/+}$ mice fed control diet (N=5). Dietary rapamycin significantly increases latency to fall (P<0.05) and maximum speed reached (P<0.01) in *Lmna*$^{-/-}$ mice (N=4) compared to *Lmna*$^{-/-}$ mice fed the control diet (N=5). Black bars= control fed; white bars= rapamycin fed.

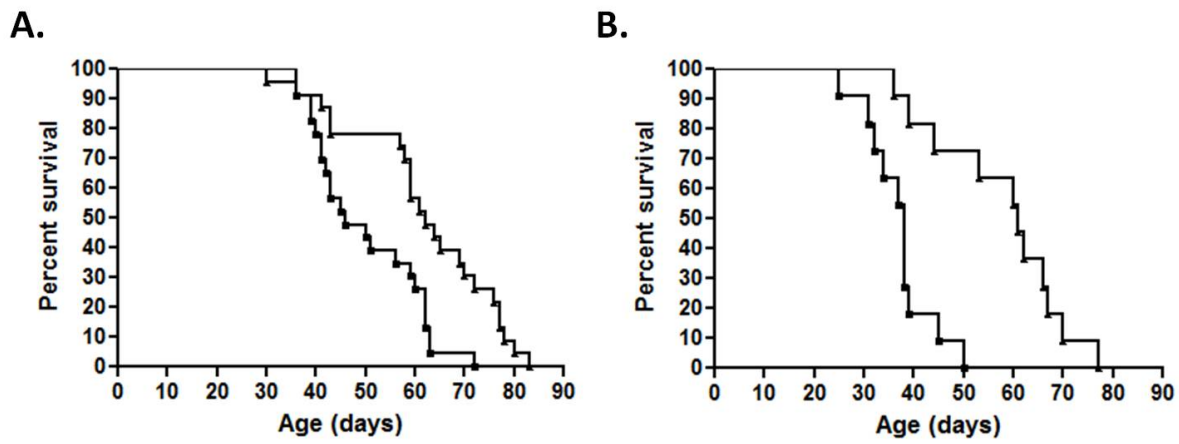

Figure 4. Treatment of *Lmna*$^{-/-}$ mice with rapamycin increases survival. (A) Kaplan-Meier plot of *Lmna*$^{-/-}$ mice fed control (N=23) or rapamycin diet (N=23). Survival is significantly increased in *Lmna*$^{-/-}$ mice fed dietary rapamycin (p=0.0013). Control diet=square marker and rapamycin diet=triangle marker. **(B)** Kaplan-Meier plot of *Lmna*$^{-/-}$ mice (C57BL/6 background) injected with vehicle (N=11) or 8mg/kg rapamycin (N=11). Survival is significantly increased in *Lmna*$^{-/-}$ mice injected with rapamycin (P=0.0002). For Kaplan-Meier plot, vehicle control=square marker and 8mg/kg rapamycin=triangle marker.

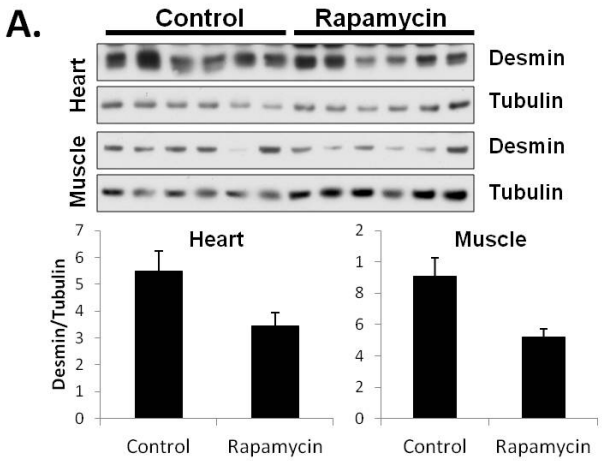
A.
Control
Rapamycin
Heart
Muscle
Desmin
Tubulin
Desmin
Tubulin
Heart
Muscle
Desmin/Tubulin
Control
Rapamycin
Control
Rapamycin

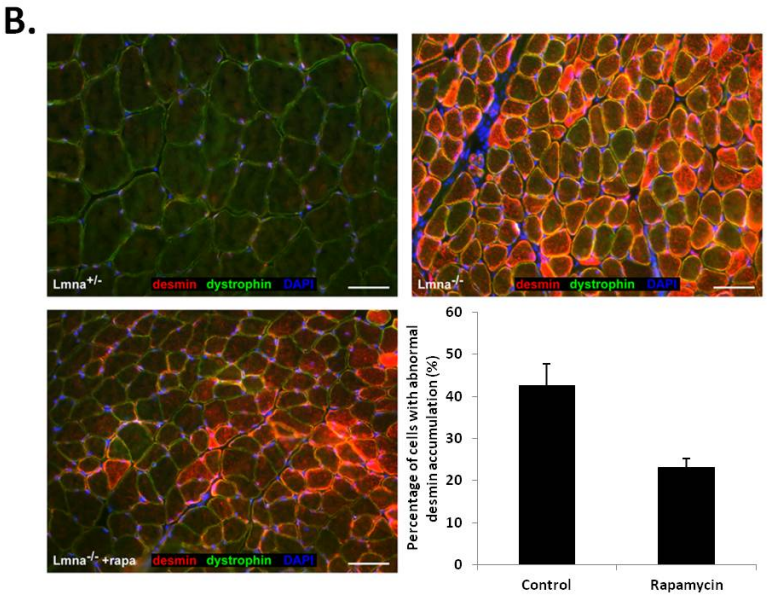
B.
Lmna+/-
desmin dystrophin DAPI
Lmna-/-
desmin dystrophin DAPI
Lmna-/-+rapa
desmin dystrophin DAPI
Percentage of cells with abnormal desmin accumulation (%)
Control
Rapamycin

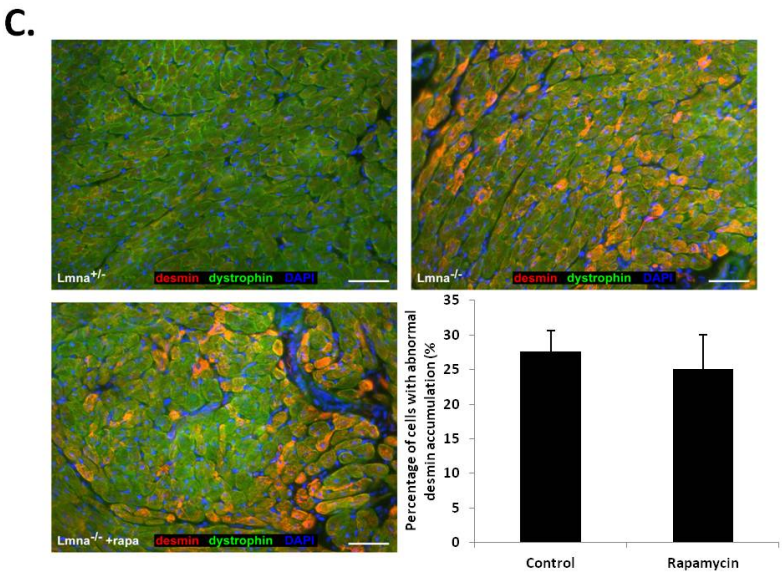

Figure 5. Rapamycin reduces abnormal desmin accumulation in *Lmna*$^{-/-}$ mice. **(A)** Western blot analysis shows a significant decrease in desmin protein levels in heart (P=0.043) and skeletal muscle (P=0.012) of rapamycin treated *Lmna*$^{-/-}$ mice (N=6) compared to control fed *Lmna*$^{-/-}$ mice (N=6). **(B)** Immunohistochemistry of muscle sections shows abnormal accumulation of desmin in the myocytes of *Lmna*$^{-/-}$ mice compared to control *Lmna*$^{+/-}$ mice. Abnormal accumulation of desmin in the myocytes of *Lmna*$^{-/-}$ mice fed rapamycin (N=4) was significantly reduced compared to *Lmna*$^{-/-}$ mice fed the control diet (N=4) (P=0.025). **(C)** Immunohistochemistry of heart sections shows abnormal accumulation of desmin in the cardiomyocytes of *Lmna*$^{-/-}$ mice compared to control *Lmna*$^{+/-}$ mice. The percentage of cells with abnormal accumulation of desmin in the cardiomyocytes of *Lmna*$^{-/-}$ mice fed rapamycin (N=4) was not improved compared to *Lmna*$^{-/-}$ mice fed the control diet (N=4) (P=0.67).

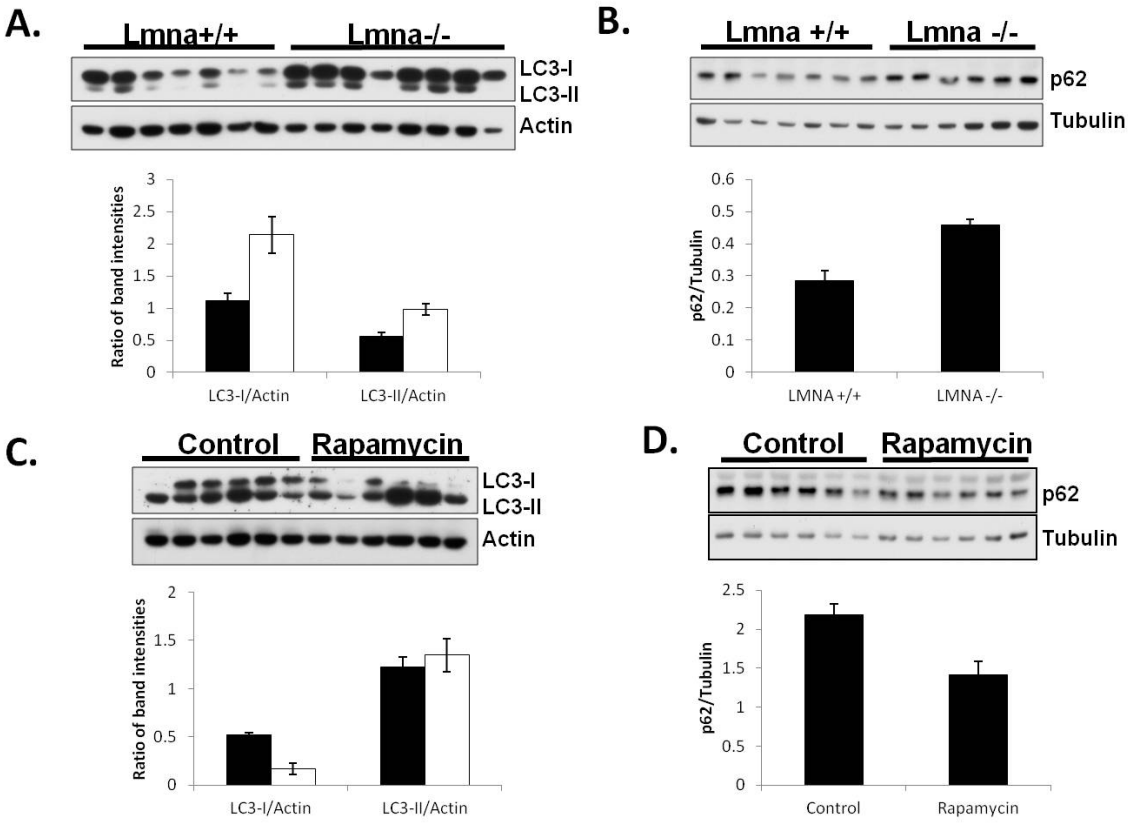

Figure 6. Rapamycin increases productive autophagy in *Lmna*$^{-/-}$ mice. **(A)** Western blot analysis of heart tissue lysates shows a significant increase in LC3-I (P=0.0078) and LC3-II (P=0.0019) protein levels in *Lmna*$^{-/-}$ mice (N=7) compared to *Lmna*$^{+/+}$ mice (N=8). **(B)** Western blot analysis of heart tissue shows a significant increase in p62 protein levels (P=0.00099) in *Lmna*$^{-/-}$ mice (N=7) compared to *Lmna*$^{+/+}$ mice (N=6). **(C)** Western blot analysis of heart tissue shows a significant decrease in LC3-I protein levels (P=0.029) and no change in LC3-II (P=0.48) protein levels in *Lmna*$^{-/-}$ mice (N=6) treated with rapamycin compared to control treated *Lmna*$^{-/-}$ mice (N=6). **(D)** Western blot analysis of heart tissue shows a significant decrease in p62 protein levels (P=0.0062) in *Lmna*$^{-/-}$ mice treated with rapamycin (N=6) compared to control treated *Lmna*$^{-/-}$ mice (N=6). For all figures, error bars are ± s.e.m.

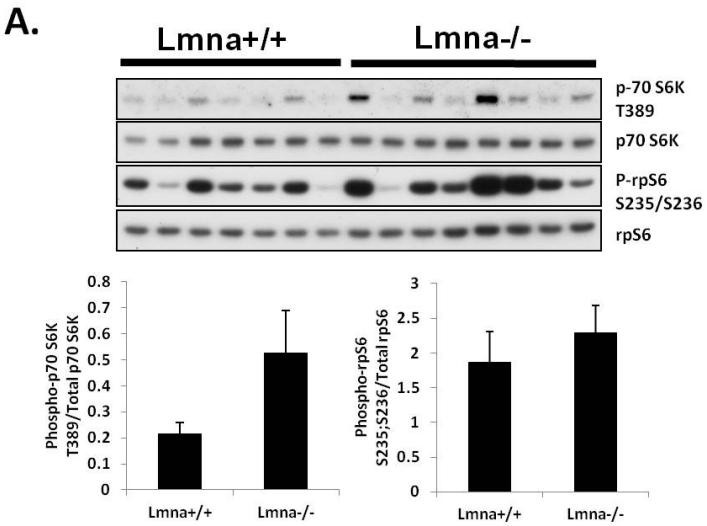
A.
Lmna+/+
Lmna-/-
p-70 S6K T389
p70 S6K
P-rpS6 S235/S236
rpS6
Phospho-p70 S6K T389/Total p70 S6K
Phospho-rpS6 S235;S236/Total rpS6
Lmna+/+
Lmna-/-

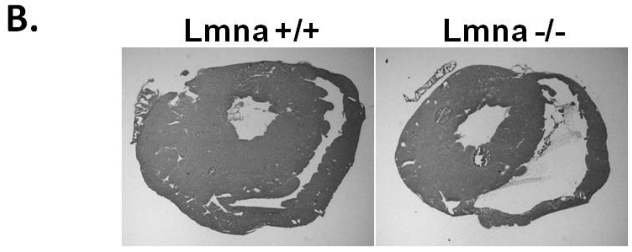
B.
Lmna +/+
Lmna -/-

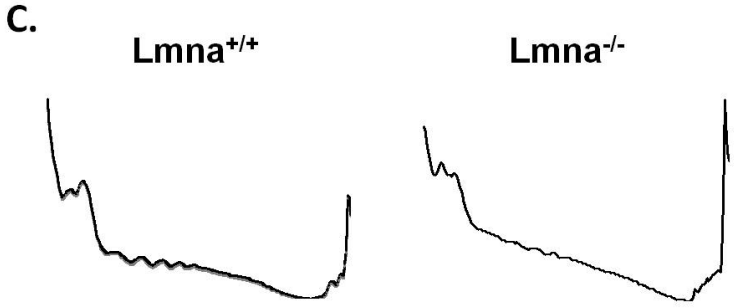
C.
Lmna+/+
Lmna-/-

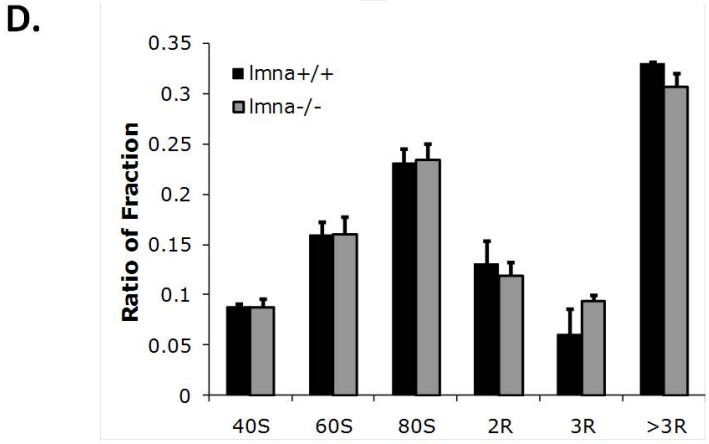
D.
lmna+/+
lmna-/-
Ratio of Fraction
40S
60S
80S
2R
3R
>3R

Supplemental Figure 1. Protein translation is not increased in dilated *Lmna*$^{-/-}$ hearts. (A) Representative western blots of *Lmna*$^{+/+}$ (N=7) and *Lmna*$^{-/-}$ (N=8) mice liver tissue lysates and quantification. Phosphorylated S6 kinase$^{(T389)}$ (P= 0.11) and rpS6$^{(S235/S236)}$ (P=0.48) are not significantly different in *Lmna*$^{-/-}$ mice compared to *Lmna*$^{+/+}$ mice. Error bars are ± s.e.m. **(B)** Heart sections of *Lmna*$^{+/+}$ and *Lmna*$^{-/-}$ mice stained with hematoxylin and eosin demonstrate left and right ventricular dilatation in *Lmna*$^{-/-}$ mice. **(C)** Representative polysome profiles of *Lmna*$^{+/+}$ (N=3) and *Lmna*$^{-/-}$ (N=3) mice. **(D)** Polysome analysis of *Lmna*$^{+/+}$ and *Lmna*$^{-/-}$ mice heart tissue shows that protein translation is not increased in *Lmna*$^{-/-}$ mice. Solid black bars= *Lmna*$^{+/+}$ mice; solid gray bars= *Lmna*$^{-/-}$ mice. For all figures, error bars are ± s.e.m.

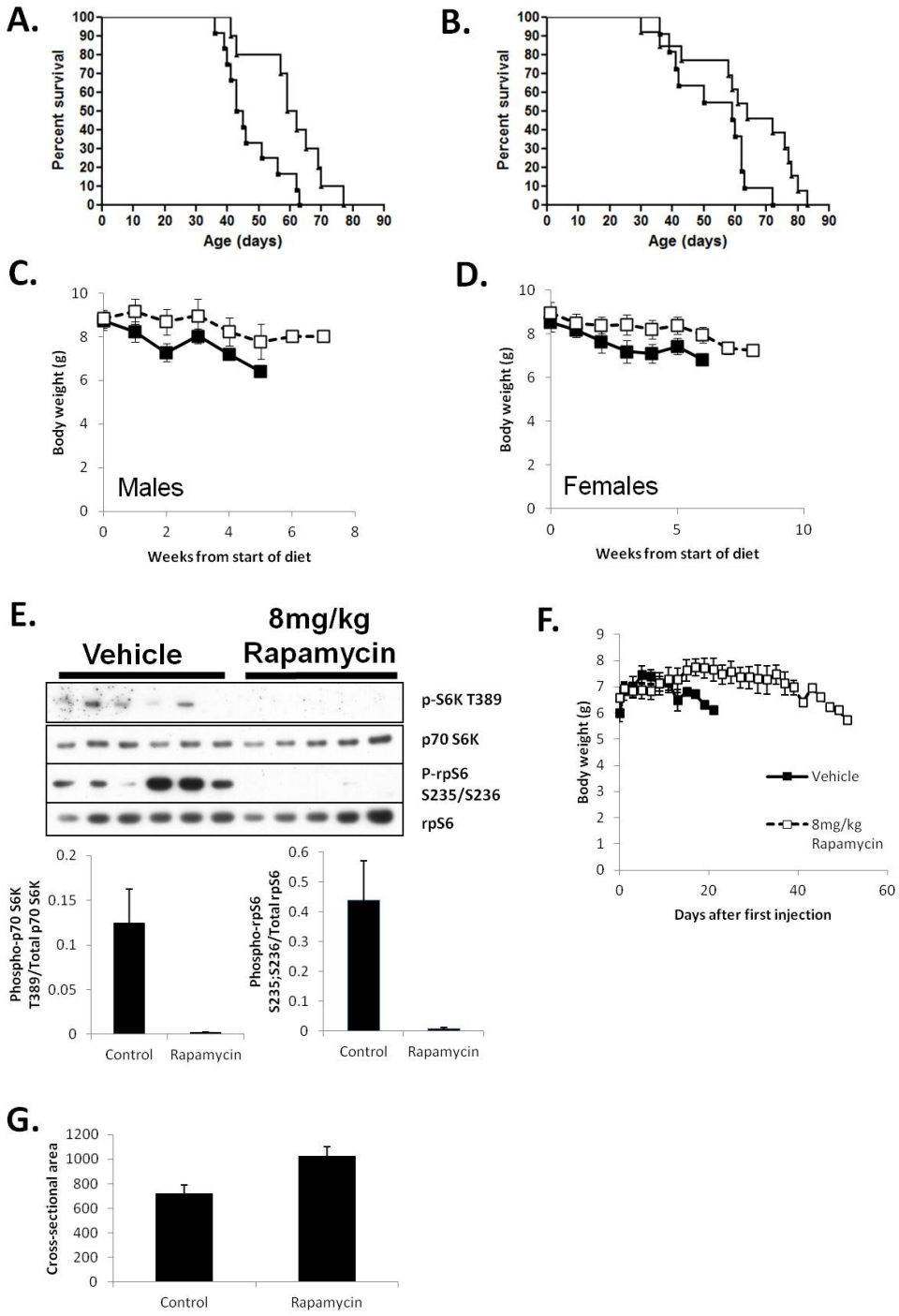

Supplemental Figure 2. Rapamycin-mediated lifespan extension in *Lmna*$^{-/-}$ mice is not sex-specific and can also be delivered via injection. (A) Kaplan-Meier plot of male *Lmna*$^{-/-}$ mice fed control (N=12) or rapamycin diet (N=10). Survival is significantly increased in male *Lmna*$^{-/-}$ mice

fed dietary rapamycin (p=0.0068). Control diet=square marker and rapamycin diet=triangle marker. **(B)** Kaplan-Meier plot of female *Lmna*$^{-/-}$ mice fed control (N=11) or rapamycin diet (N=13). Survival is significantly increased in female *Lmna*$^{-/-}$ mice fed dietary rapamycin (p=0.036). Control diet=square marker and rapamycin diet=triangle marker. **(C)** Body weight curve of male *Lmna*$^{-/-}$ mice fed rapamycin diet (dashed black line, white squares) is significantly different than control (solid black line, black squares) (P= 0.048). Error bars are ± s.e.m. **(D)** Body weight curve of female *Lmna*$^{-/-}$ mice fed rapamycin diet (dashed black line, white squares) is significantly different than control (solid black line, black squares) (P=0.0060). Error bars are ± s.e.m. **(E)** Representative western blots of heart tissue lysates from *Lmna*$^{-/-}$ mice (C57BL/6 background) injected with vehicle (N=6) and *Lmna*$^{-/-}$ mice injected with rapamycin (N=5). Phosphorylated S6 kinase$^{(T389)}$ (P= 0.017) and rpS6$^{(S235/S236)}$ (P=0.016) are decreased in *Lmna*$^{-/-}$ mice injected with rapamycin compared to *Lmna*$^{-/-}$ mice injected with vehicle. **(F)** Body weight analysis of *Lmna*$^{-/-}$ mice (C57BL/6 background) injected with vehicle (initial N=11) or rapamycin (initial N=11). The body weight of *Lmna*$^{-/-}$ mice injected with rapamycin is not significantly different than control *Lmna*$^{-/-}$ mice (P=0.88). Solid black line, black squares=vehicle; dashed black line, white squares=8mg/kg rapamycin. For all figures, error bars are ± s.e.m. **(G)** Myofiber cross-sectional area of rapamycin treated *Lmna*$^{-/-}$ mice is similar to control fed *Lmna*$^{-/-}$ mice (P= 0.071). Error bars are ± s.e.m.

Chapter 3

Phosphorylation of Connexin43 on S279/282 May Contribute to Laminopathy-associated Conduction Defects

Having established that A-type lamins are essential for maintaining normal heart function and the role of the mTOR pathway in the cardiac and skeletal muscle phenotype of *Lmna*$^{-/-}$ mice, I became interested in investigating dilated cardiomyopathy with conduction system disease (DCM-CD) as it is the ultimate cause of death in the majority of laminopathy patients. As described in the introduction, cardiac conduction and intercellular communication is mediated by gap junctions, formed by the connexin family of proteins. Regulation of cellular communication through the gap junction is achieved by phosphorylation of connexin proteins on their cytoplasmic C-terminal domain. Phosphorylation of the most widely-expressed connexin, connexin43 (Cx43), by kinases such as MAPK, PKC and Src, have been shown to decrease gap junctional communication. As we established increased pERK1/2 activity in *Lmna*$^{-/-}$ mice, as well as being described in the *Lmna*$^{H222P/H222P}$ mouse, I hypothesized that aberrant pERK1/2 activation and signaling was inhibiting gap junction function and contributing to the cardiac conduction defects observed in laminopathy patients. In my experiments, I utilized both *Lmna*$^{-/-}$ mice and fibroblasts derived from them, showing increased phosphorylation of Cx43 on S279/282, an identified MAPK phosphorylation site, in the absence of A-type lamins. I then

demonstrate that this results in decreased functionality of the gap junction by dye transfer assays in fibroblasts and ECG recordings on Langendorff-perfused mouse hearts.

These experiments were conceived and conducted solely by myself, under the supervision of Dr. Paul Lampe. The results are presented here in manuscript form, currently in preparation for submission.

Phosphorylation of connexin43 on S279/282 may contribute to laminopathy-associated conduction defects

Steven C. Chen[1,2], Brian K. Kennedy[2,3], Paul D. Lampe[1]

[1]Fred Hutchinson Cancer Research Center (FHCRC) Public Health Sciences Division, Seattle, WA; [2]University of Washington Department of Biochemistry, Seattle, WA; [3]Buck Institute for Research on Aging, Novato, CA

Abstract

Despite the prevalence of dilated cardiomyopathy with conduction system disease (DCM-CD) among disease-associated mutations in *LMNA* (termed laminopathies), the molecular mechanism behind the terminal arrhythmic events has remained unclear. A-type lamins have been shown to interact with activated pERK1/2, localizing and sequestering them to the nucleus. Connexin43 (Cx43), which forms gap junctions throughout the heart, can be phosphorylated by pERK1/2 on S279/282, inhibiting gap junctional communication. We hypothesized that without A-type lamins, the fraction of phospho-S279/282 Cx43 is increased due to inappropriate pERK1/2 phosphorylation, ultimately resulting in decreased gap junction function.

We observed that levels of phospho-S279/282 Cx43, which inhibit gap junction conductance and function, are increased by 1.6-fold in *Lmna*$^{-/-}$ MEFs compared to *Lmna*$^{+/+}$. In addition, we measured a 1.8-fold enrichment of pERK1/2, the kinase responsible for S279/282 phosphorylation, in *Lmna*$^{-/-}$ MEFs after immunoprecipitation with Cx43 antibodies. Despite no significant change in total pERK1/2 levels as assayed by Western, we observe a 3-fold increase in the fraction of non-nuclear pERK1/2 and a concomitant 2-fold increase in the fraction of phospho-S279/282 in *Lmna*$^{-/-}$ MEFs by immunofluorescence. Function of gap junctions is also inhibited, as assayed by the calcein/DiI dye transfer assay; *Lmna*$^{-/-}$ MEFs transfer dye to 60% fewer partners compared to *Lmna*$^{+/+}$ controls. We have previously described a 2-fold increase in pERK1/2 levels of *Lmna*$^{-/-}$ mice and here we observe a 1.7-fold increase in phospho-S279/282 Cx43 in *Lmna*$^{-/-}$ mice compared to their *Lmna*$^{+/+}$ littermates at 5-6 weeks of age. In addition, we detect phospho-S279/282 Cx43 is in the gap junctions of *Lmna*$^{-/-}$ mice, but not in *Lmna*$^{+/+}$ mice.

Introduction

Nuclear lamins are intermediate filament proteins associated with the inner nuclear membrane and are the primary component of the nuclear lamina where they perform a variety of functions, providing structure to the nucleus [264,265,266], binding chromatin [267,268], acting as a scaffold for other nuclear proteins (reviewed in [269,270,271]) and positioning the nucleus (reviewed in [209]). Likely due to this spectrum of functions, point mutations in the lamin A/C (*LMNA*) gene can cause a spectrum of diseases collectively termed laminopathies, which include muscular dystrophies, lipodystrophies, dilated cardiomyopathy, restrictive dermopathy, peripheral neuropathy and progeroid syndromes (reviewed in [272]). One pathology of particular interest in laminopathies is dilated cardiomyopathy with conduction system disease (DCM-CD) which can develop in conjunction with muscular dystrophies such as Emery-Dreifuss muscular dystrophy (EDMD) and limb-girdle muscular dystrophy (LGMD), or independently.

LMNA mutations are the top genetic cause of DCM-CD [68] and it has been found that many patients with DCM-CD ultimately have an undiagnosed laminopathy [69,70]. Ultimately, most laminopathy patients that develop DCM-CD die of sudden cardiac death, causing death by ventricular fibrillation, which in certain cases can be delayed by the implantation of pacemakers [71,72,73,74]. It is currently unclear the role A-type lamins have on heart conduction, but it is clear that understanding this relationship will improve our understanding of laminopathies and their treatment.

There are hundreds of mutations in lamin A that result in some form of cardiomyopathy and mouse models for laminopathy also reflect this pathology. The *Lmna*$^{-/-}$ knockout mouse

suffers from severe muscular dystrophy and dilated cardiomyopathy with conduction defect, dying prematurely at 5-7 weeks of age [94,96]. Also of interest is the *Lmna*$^{+/-}$ mouse which develops dilated cardiomyopathy [98], as most mouse laminopathy models are recessive, in contrast with the autosomal dominant inheritance in human laminopathies. The *Lmna*$^{H222P/H222P}$ knock-in mouse, also encodes a mutation associated with EDMD, and results in a much milder phenotype with mice dying at 7-10 months of age while exhibiting classic signs of dilated cardiomyopathy such as decreased fractional shortening, ventricular dilation, degeneration of myocytes and replacement with fibrotic tissue [99]. In later studies, they detected increased activity of the ERK1/2 and JNK1/2 pathways; and treatment with PD98059, the pharmacological inhibitor of MEK1 (the upstream kinase of ERK1/2), was able to improve heart function, though lifespan extension was not measured [100,104]. Recent studies have found a link between the lamin A protein and ERK1/2 showing that lamin A protein serves as a scaffold for activated ERK1/2, anchoring it to the nucleus and presumably keeping it in close proximity with the transcription factors it normally activates [197,211]. In addition to the increased ERK activity observed in the *Lmna*$^{H222P/H222P}$ knock-in mouse, other disease mutations have resulted in increased ERK activity *in vitro* [210,273].

Gap junctions are specialized channels that serve as the intercellular junction that allowing ions to flow freely from the cytoplasm of one cell to another (reviewed in [139]). They play an especially important role in the heart, being responsible for conducting the electrical signal from one cardiomyocyte to the other, allowing for the coordinated and regular contractions that we interpret as heartbeats. Connexin43 (Cx43) is the primary connexin protein in the heart, expressed in all cardiomyocytes and the major connexin in the working

ventricular myocardium [161], and is also found in a multitude of other tissues and cells throughout the body. Cx43 has a very short half-life ranging from 1-3 hours [151,152,274] which suggests extensive post-translational regulation, likely occurring at the C-terminal region of Cx43 [275]. There are at least 14 serines and 2 tyrosines in the cytoplasmic C-terminal region that can be phosphorylated by a variety of kinases [276]. Of particular interest are the three phosphorylation sites that have been identified to be MAPK consensus recognition sites, S255, S279 and S282 [186]. It has been shown that the phosphorylation of these residues can result in decreased conductivity of the gap junction and that ERK1/2 is responsible for these effects [188,277].

As both *Lmna*$^{-/-}$ mice and human laminopathy patients appear to suffer from dilated cardiomyopathy with conduction defects, we have investigated the regulation of the gap junction protein, Cx43 in the *Lmna*$^{-/-}$ context. In the present study, we hypothesize that the loss of lamin A in the *Lmna*$^{-/-}$ mouse results in a loss of its normal sequestration of pERK1/2, resulting in inappropriate localization throughout the cell. Here we show that loss of *Lmna* both *in vitro* and *in vivo* results in inappropriate ERK1/2 signaling, affecting phosphorylation of Cx43 on S279/282, ultimately affecting cellular communication.

Results

Using immortalized MEFs isolated from *Lmna*$^{+/+}$ and *Lmna*$^{-/-}$ mice as previously described [94], we studied whether the regulation and function of Cx43 was perturbed by ERK1/2 activation due to loss of normal lamin A activity. We observe a significant 1.6-fold increase in levels of Cx43 phosphorylated on serines 279 and 282 using a phosphospecific

antibody (phospho-S279/282) when normalized to total Cx43 in *Lmna*$^{-/-}$ cells compared to *Lmna*$^{+/+}$ control cells (n=3, $p < 0.01$) (**Figure 1A**). Treatment of these samples with alkaline phosphatase collapse the Cx43-associated bands to the P0 isoform, confirming that the bands detected with phospho-S279/282 are indeed phospho-Cx43 (**Figure 1B**). As S279/282 have been identified as consensus ERK1/2 phosphorylation sites [186], we expected to find concomitant increased ERK1/2 activity. Surprisingly, we observe no significant increase in the total levels of phospho-ERK1/2 (pERK1/2) normalized to total ERK1/2 by Western blot in whole cell lysate. With the observation that phospho-S279/282 levels are increased in *Lmna*$^{-/-}$ cells, we expected an increased interaction between Cx43 and pERK1/2. Using the IF1 and CT1 Cx43 antibodies to immunoprecipitate total Cx43, we blotted for pERK1/2 to establish whether there is an increased physical interaction between pERK1/2 and Cx43 in the cytoplasm. We observe a 1.8-fold enrichment in pERK1/2 association with Cx43 in *Lmna*$^{-/-}$ cells compared to *Lmna*$^{+/+}$ (**Figure 1C**).

As it has been previously shown that pERK1/2 associates with the nuclear envelope via lamin A [197], we then hypothesized that the loss of normal A-type lamin activity would result in a loss of the sequestration of pERK1/2 to the nuclear envelope and abnormal ERK1/2 activity in the cytoplasm. This would explain why total levels of pERK1/2 were unchanged by SDS-PAGE, while phospho-S279/282 was increased. By immunofluorescence, we observe an increased presence of punctate pERK1/2 foci in the cytoplasm and potentially at the plasma membrane of *Lmna*$^{-/-}$ cells (**Figure 2A**). Utilizing the colocalization feature in Metamorph, we measured the fraction of pERK1/2 signal that lay outside the nucleus as defined by DAPI staining. After quantitation, we see a 3-fold increase in the levels of cytoplasmic pERK1/2 in *Lmna*$^{-/-}$ cells ($p <$

0.001) (**Figure 2B**). We also observe an increase in the amount of phospho-S279/282 Cx43 staining in *Lmna*$^{-/-}$ cells, excluding the cross-reactive staining observed in the nucleus as Cx43 is not found in the nucleus (**Figure 2C**). In order to address the cross reactivity of the phospho-S279/282 Cx43 antibody in immunofluorescence, we utilized Metamorph to both exclude the nuclear staining and quantitate the fraction of Cx43 that was phosphorylated on S279/282. Using the arithmetic function of Metamorph, we utilized the AND logic gate between the IF1 Cx43 images and the phospho-S279/282 Cx43 images to eliminate any phospho-S279/282 Cx43 staining that is not recognized by the IF1 Cx43 antibody. Using this signal, we followed it up with the colocalization feature to determine what fraction of total IF1 Cx43 signal, which represents gap junctional Cx43, was phosphorylated on S279/282. We observe a 2-fold increase in the levels of phospho-S279/282 Cx43 in *Lmna*$^{-/-}$ cells ($p<0.001$), which agrees with our 1.6-fold increase as measured by Western (**Figure 2D**).

After establishing that Cx43 regulation was affected by the loss of lamin A activity, we sought to determine whether gap junction function and cell communication were affected. In order to measure gap junction assembly, we performed a calcein/DiI transfer assay with *Lmna*$^{+/+}$ and *Lmna*$^{-/-}$ MEFs. The calcein/DiI transfer assay utilizes calcein (a cell-permeable fluorescein complex) and DiI (a cell-impermeable lipophilic cyanine dye) in order to distinguish donor cells, which are calcein-positive, from acceptor cells, which are both calcein-positive and DiI-positive. We observe that levels of cell communication are dampened by 60% in *Lmna*$^{-/-}$ cells compared to *Lmna*$^{+/+}$ cells (cells scored≥500/experiment, n=3, $p<0.001$) (**Figure 3A and 3B**). To determine whether the defect was specific to the *Lmna*$^{-/-}$ cells serving as either donor or acceptor, we mixed the communication-deficient *Lmna*$^{-/-}$ cells either as donor or acceptor with

Lmna$^{+/+}$ cells. We observed no difference in either case of *Lmna*$^{-/-}$ cells mixed with *Lmna*$^{+/+}$ compared to results with *Lmna*$^{-/-}$ alone and saw no improvement towards the levels exhibited by *Lmna*$^{+/+}$ cells alone (**Figure 3C**).

Using the *Lmna*$^{-/-}$ mouse strain, we performed Western blotting for phospho-S279/282 Cx43 on whole heart lysates from *Lmna*$^{-/-}$ mice and wild-type littermate controls. We observe a 1.7-fold increase in levels of phospho-S279/282 connexin43 normalized to total connexin43 in 6-week old *Lmna*$^{-/-}$ mice compared to their wild-type littermates (*Lmna*$^{+/+}$ n = 5, *Lmna*$^{-/-}$ n=7, $p<0.01$) (**Figure 4A and 4B**). We also detect increased pERK1/2 in *Lmna*$^{-/-}$ mice, as we have previously described. Immunofluorescence staining of heart cryosections reveals the presence of phospho-S279/282 Cx43 at the gap junction as demarcated with the IF1 Cx43 antibody in *Lmna*$^{-/-}$ mice but not in their *Lmna*$^{+/+}$ littermates (**Figure 4C**).

Discussion

In the course of these studies, we have established a pathway that may explain how loss of A-type lamin activity results in cardiac conduction defects. We have demonstrated that in *Lmna*$^{-/-}$ cells, pERK1/2 is not properly anchored and sequestered to the nuclear envelope, allowing a significant increase in the fraction of cytoplasmic pERK1/2 when compared to *Lmna*$^{+/+}$ cells. This causes increased phosphorylation on S279/282 of Cx43 and decreased cell communication. Consistently, in *Lmna*$^{-/-}$ mice we observe increased pERK1/2 levels and phospho-S279/282 Cx43. As the S279/282 Cx43 phosphorylation event has been previously identified to cause decreased conductance and channel open time, we believe that this likely

contributes to the decreased conduction velocity previously measured by ECG in *Lmna*$^{-/-}$ mice and other mouse models for laminopathies.

Further studies are in progress to determine whether we can rescue the defects described by breeding the *Lmna*$^{-/-}$ with a knock-in mouse expressing Cx43 with four MAPK-associated sites (S255, S262, S279, S282) mutated to alanine (MK4/MK4). The MK4/MK4 mouse appears normal, with no gross developmental defects or noticeable health problems, but is incapable of phosphorylating Cx43 on S279/282. If phosphorylation of S279/282 in the *Lmna*$^{-/-}$ mouse is lifespan-limiting, we believe we should see significant improvement in lifespan and potentially health of *Lmna*$^{-/-}$; MK4/MK4 mice. We plan to utilize hanging Langendorff perfusion to measure ECG parameters of these mice, which will hopefully show significant improvement in P duration and PR interval, both of which are increased in *Lmna*$^{-/-}$ mice indirectly indicating a slowed conduction velocity or conduction defects.

It has already been shown that lamins and ERK1/2 interact at the nuclear envelope [197,211], and ERK1/2 activity is perturbed as a result of different EDMD-causing *LMNA* mutations in a mouse model, myoblasts and patient-derived fibroblasts. [100,210,273]. One of the unanswered questions that remains is how loss of or mutation in A-type lamins could result in inappropriate ERK1/2 signaling. Recently a crystal structure of the Coil2B domain of lamin, the most C-terminal of the four α-helical segments in the central rod domain, encoding either the R335W or E347K mutation causing EDMD has been described [75]. They demonstrate no difference in the ability of these mutations to form the parallel coiled coil dimer indicating that these disease causing residues do not significantly interfere with the structure or polymerization of lamin. Instead, they show that these residues are exposed at the surface of

the coiled coil dimer, hypothesizing that the mutation of these highly conserved residues affect the binding of other components of the nuclear lamina or other binding partners of lamin A.

Mutations in other genes such as emerin, another nuclear membrane protein that causes X-linked EDMD, and desmin, a type III intermediate filament, are also associated with the development of cardiomyopathy. Increased ERK1/2 activity has been shown in both emerin-null *Emd*$^{-/y}$ mice as well as in cells treated with *Emd* siRNA [106,205]. We speculate that emerin, which interacts with A-type lamins and helps anchor the nuclear membrane to the cytoskeleton, may also play some yet undefined role in maintaining normal organization and regulating normal interaction between lamins and ERK1/2. Increased ERK1/2 activity has also been described in airway smooth muscle cells of desmin-null mice resulting in increased *miR-26a* and hypertrophy [278]. Desmin aggregation in *Lmna*$^{-/-}$ cardiac tissue has been previously described [96] (Frock et al. *in review*) and a similar phenotype has been described in mice with a cardiac-specific expression of a 7-amino acid deletion of desmin (D7-des) [214]. D7-des mice exhibit desmin aggregation, loss of Cx43 from the intercalated disk, and decreased conduction velocity. However, analysis of desmin in human patients with EDMD did not reveal any change in desmin localization or expression implying that although desmin aggregation appears to be a downstream effect due to loss of A-type lamin function in mice, desmin may not play a part in the human development of laminopathies [279]. Ultimately, these interesting results from emerin or desmin-deficient mice illustrate the need for analysis of ERK1/2 activity in human patients to clarify its role in the development of laminopathies.

In conclusion, these data demonstrate a pathway by which loss of A-type lamins at the nuclear envelope result in a change in cell communication through phosphorylation of

S279/282 on Cx43 by pERK1/2. We propose a mechanism in which the loss of normal A-type lamin decreases the normal interaction of pERK1/2 with the nuclear envelope and affects cellular function through Cx43. As ERK1/2 signaling has now been demonstrated to be increased in two separate mouse models, it provides a promising target for further investigation of the development of laminopathies in humans.

Materials and Methods

Cell culture

Mouse embryonic fibroblasts from littermate-matched control and *Lmna*$^{-/-}$ were derived and immortalized as previously described [94]. Cells were cultured and maintained in Dulbecco's Modified Eagle Medium (Cellgro) supplemented with 10% fetal bovine serum (SAFC Biosciences), 2mM L-glutamine (Gibco) and penicillin/streptomycin (Gibco). The MEK1 inhibitor PD98059 (EMD) was diluted in DMSO and used at a 50 µM concentration.

Animal husbandry and care

Lmna$^{+/-}$ mice were originally generated and obtained from Dr. Colin Stewart [94] and were backcrossed on C57BL/6 for 20 additional generations. The resulting *Lmna*$^{+/-}$ progeny were interbred to produce *Lmna*$^{+/+}$ and *Lmna*$^{-/-}$ progeny.

All mice were bred and maintained under specific pathogen-free conditions. All experiments were performed in compliance with either the University of Washington Institutional Animal Care and Use Committee (protocol #: 2174-23) or the Fred Hutchinson Cancer Research Center Institutional Animal Care and Use Committee (protocol #: 1673). Euthanasia of mice for analysis were accomplished by either CO_2 or isoflurane exposure followed by cervical dislocation.

Genotyping on ear clip samples was performed using the Extract-N-Amp Tissue PCR Kit (Sigma Aldrich). Primers for the detection of *Lmna* and its knockout allele [94]: 5'-wild-type – TGCTGATGCCATGGATACTC; 5'-knockout – GCACGAGACTAGTGAGACGTG; 3'-common – GAGAAGGCAGAGGTGTGAGCAGC yielding ~1 kb and 700 bp fragments respectively.

SDS-PAGE and Western blotting

Mouse hearts were lysed by sonication on ice in 500uL of lysis buffer consisting of 3X Laemmli buffer supplemented with 5% beta-mercaptoethanol, 10mM NaF, 0.5mM $NaVO_3$, 2 mM PMSF and cOmplete mini protease inhibitor cocktail (Roche). MEF lysates were collected in the same lysis buffer by using a cell scraper followed by sonication on ice.

Lysates were submitted to SDS-PAGE separation using 10% Tris-Glycine PAGEr Gold precast gels (Lonza). Proteins were transferred to nitrocellulose and blocked in 1% milk supplemented with 10mM NaF.

Nitrocellulose membranes were incubated with one or more of the following antibodies overnight at 4°C: lamin A/C (Cell Signaling 2032; 1:500), pERK1/2 (Cell Signaling 9101; 1:500), ERK1/2 (Santa Cruz sc-94; 1:5000), α-tubulin (Cell Signaling 2125; 1:1000), N-terminus connexin43 (NT1) (FHCRC; 1:1000), and pS279/282 connexin43 (FHCRC; 1:1000). Appropriate secondary antibodies were then applied for 60 minutes at room temperature at 1:10000 dilution: AlexaFluor680 goat anti-rabbit (Invitrogen) or AlexaFluor800 donkey anti-mouse (Invitrogen). Blots were scanned using an Odyssey infrared imager (Li-Cor, Omaha, NE). Quantitation was performed with Odyssey software.

Immunofluorescence

Heart tissue was frozen in Tissue-Tek O.C.T compound, cryosectioned at 8µm in thickness on a Leica CM3050S and mounted on Superfrost Plus glass slides (Fisher). Sections were fixed in -20°C acetone for 20 minutes and air dried. Blocking was performed in PBS with 1% BSA (PBSB) supplemented with 0.3% TritonX-100 for 15 minutes. Primary antibodies were diluted in PBSB and applied to slides for 60 minutes at room temperature. Appropriate secondary antibodies were then applied for 60 minutes at 1:200 in PBSB. Following secondary antibody exposure, DAPI staining was performed with 5 ug/ml DAPI in PBS. Sections were then mounted in Fluoromount-G (SouthernBiotech).

MEFs were grown in a 24-well dish on round coverslips and fixed in 2% formalin in PBS for 15 minutes. Cells were then permeabilized with PBS supplemented with 0.5% TritonX-100 for 10 minutes. Blocking was performed by incubating with PBS with 0.2% Tween-20 (PBST) supplemented with 5% goat serum and 0.2% fish skin gelatin (referred to as “blocking buffer”) at 37°C for 15 minutes. Primary and secondary antibodies were diluted in blocking buffer and incubated with coverslips at 37°C for 60 minutes. DAPI staining was performed and coverslips were mounted in Fluoromount-G. Images were collected using NIS-Elements (Nikon) and analyzed using Metamorph (Molecular Devices).

Primary antibodies included: lamin A/C (Cell Signaling 4777; 1:500), pERK1/2 (Cell Signaling 4370; 1:200), connexin43 IF1 (FHCRC; 1:1000), connexin43 CT1 (FHCRC; 1:2000), and pS279/282 connexin43 (FHCRC; 1:500). Secondary antibodies used include: AlexaFluor488 goat anti-mouse, AlexaFluor594 goat anti-rabbit, AlexaFluor488 goat anti-rabbit and AlexaFluor594 goat anti-mouse (Invitrogen).

Co-immunoprecipitation

Recombinant protein A agarose (Pierce) was incubated with PBS containing 10% SDS and 1% BSA then rinsed thoroughly in PBS to remove any unbound protein A. The rinsed beads were then mixed with either pERK1/2 (Cell Signaling) or connexin43 IF1 and CT1 (FHCRC). Cells were lysed in PBS supplemented with 0.5% Triton X-100, 0.25% deoxycholate, 10mM NaF, 0.5mM $NaVO_3$, 2 mM PMSF and cOmplete mini protease inhibitor cocktail. Cell lysates were added to beads and inverted on a rotator at 4°C for 90 minutes then thoroughly rinsed with PBS. Before loading for SDS-PAGE, 3X Laemmli sample buffer supplemented with 5% beta-mercaptoethanol was added and boiled briefly.

Calcein/DiI transfer assay

For each calcein/DiI transfer assay, one 60-mm dish of cells were incubated with 2.5ng/uL calcein in PBS for 10 minutes and one 10-cm dish of cells were incubated with 5nM DiI in PBS for 5 minutes. After thorough rinsing, the two dishes of cells were then trypsinized and plated together in a single well of a 6-well plate. The cells were then allowed to recover and were incubated at 37°C for 2 hours. Imaging was then immediately performed to determine total ratio of donor cells (calcein-labeled only) to acceptor cells (calcein and DiI-labeled) as a measure of cell communication.

Langendorff perfusion and ECG

6-week old *Lmna*$^{-/-}$ mice and littermate wild-type controls were injected with 200U heparin and allowed to rest for 5 minutes prior to euthanization. Following euthanization, heart and lung assembly were rapidly excised and placed in ice-cold modified Krebs-Henseleit buffer consisting of 118mM NaCl, 5.3mM KCl, 1.2mM $MgSO_4$, 25mM $NaHCO_3$, 0.5mM EDTA, 10mM glucose, 2.5mM $CaCl_2$, and 0.5mM sodium pyruvate [280,281]. Lungs were dissected away from heart

under a dissecting scope and ascending aortic arch was identified and maneuvered onto either a 20 or 22 gauge cannula (Radnoti) and tied on with silk thread. Ensuring no introduction of air into the left atria, the cannulated heart was hung on an UP-100 Universal Perfusion System (Harvard Apparatus) and flow of pre-warmed Krebs-Henseleit buffer at 37°C was initiated. Flow rate was set to 3mL/minute with a constant pressure of 60mmHg. After 5 minute recovery, heart was assessed for successful cannulation and general health by observing color and heart rate. ECG leads were then placed on right atria and apex of the heart. ECG recording and analysis was performed using LabChart7 Pro with ECG module installed (ADInstruments).

Acknowledgements

The authors would like to extend thanks to the Comparative Medicine Departments of both the University of Washington and Fred Hutchinson Cancer Research Center for general animal husbandry. S.C.C. is supported by the cardiovascular and pathology training grant NIH T32 HL007312. This study has been supported by NIH grant R01 AG024287 to B.K.K and R01 GM55632 to P.D.L.

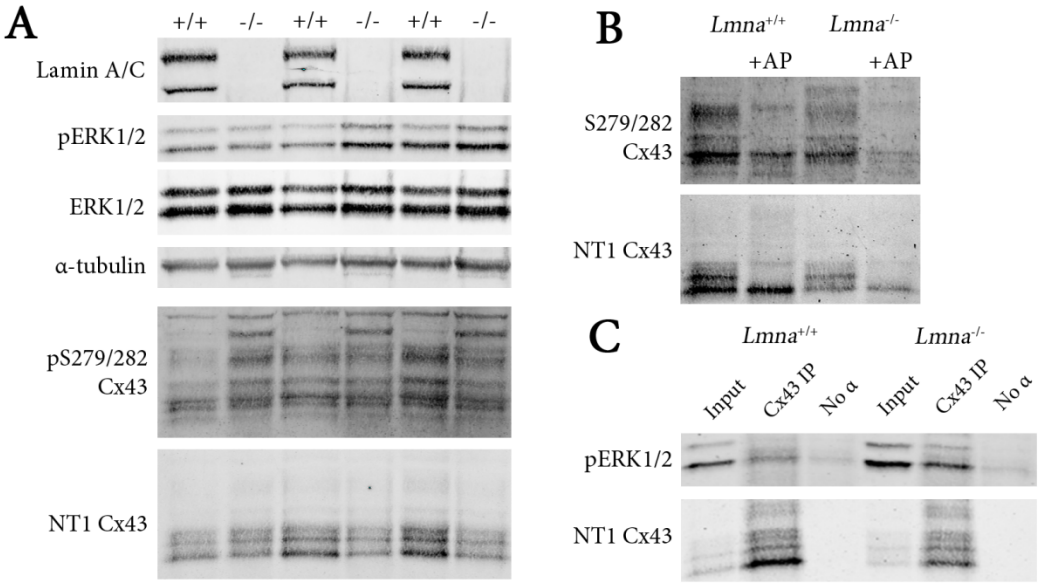

Figure 1 - phospho-S279/282 Cx43 increased in *Lmna*$^{-/-}$ MEFs. (A) Western blot analysis of *Lmna*$^{+/+}$ (+/+) and *Lmna*$^{-/-}$ (-/-) MEFs show increased levels and appearance of high-molecular weight isoform of phospho-S279/282 Cx43 relative to total Cx43 (NT1) in cells deficient for lamin A/C. Levels of pERK1/2 normalized to total ERK1/2 are not significantly changed. α-tubulin is shown as a loading control. **(B)** *Lmna*$^{+/+}$ and *Lmna*$^{-/-}$ lysates treated with alkaline phosphatase (+AP) collapse and reduce phospho-S279/282 Cx43 bands. **(C)** Co-immunoprecipitation of *Lmna*$^{+/+}$ and *Lmna*$^{-/-}$ MEFs using the IF1 and CT1 Cx43 antibodies to precipitate total Cx43 and probed with pERK1/2 show an increased amount of pERK1/2 interacting with Cx43.

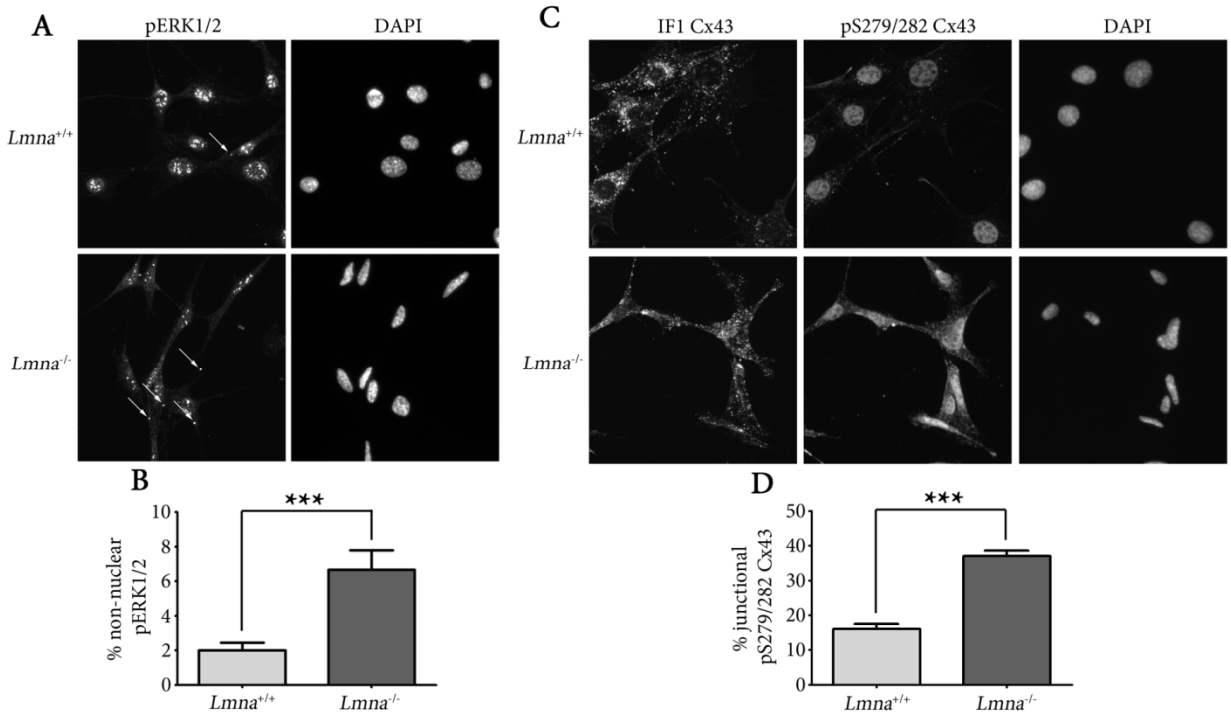

Figure 2. Localization of pERK1/2 shifts towards cytoplasm and affects phospho-S279/282 Cx43. (A) Immunofluorescence staining of *Lmna*$^{+/+}$ and *Lmna*$^{-/-}$ MEFs with CT1 Cx43 and pERK1/2 antibody show an increased presence of pERK1/2 staining in the cytoplasm of *Lmna*$^{-/-}$ MEFs as indicated by white arrows. **(B)** Scoring of cytoplasmic pERK1/2 staining in immunofluorescence images of *Lmna*$^{+/+}$ and *Lmna*$^{-/-}$ cells show a significant increase in frequency of cytoplasmic pERK1/2 in *Lmna*$^{-/-}$ cells compared to *Lmna*$^{+/+}$ ($p < 0.001$) ($n \geq 400$ cells). **(C)** Immunofluorescence staining of *Lmna*$^{+/+}$ and *Lmna*$^{-/-}$ MEFs with IF1 Cx43 and phospho-S279/282 Cx43 show no significant change in Cx43 staining by IF1, but increased levels of phospho-S279/282 Cx43, with a cross-reactive signal in the nucleus. **(D)** Quantitation of phospho-S279/282 Cx43 by excluding non-IF1 Cx43 signal shows a significant 2-fold increase of phospho-S279/282 Cx43 in *Lmna*$^{-/-}$ cells ($p < 0.0001$) ($n \geq 250$ cells).

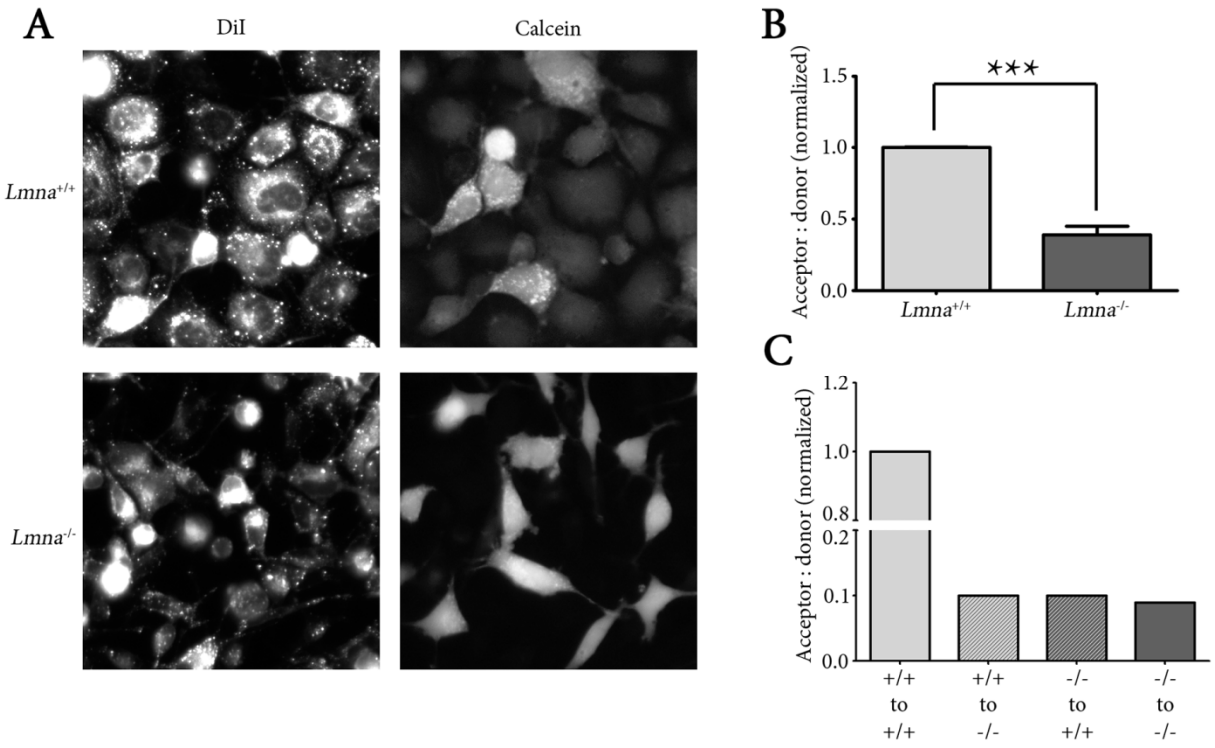

Figure 3 - Cell communication is deficient in *Lmna*$^{-/-}$ MEFs as measured by calcein/DiI transfer assay. (A) *Lmna*$^{-/-}$ cells transfer significantly less dye than *Lmna*$^{+/+}$ cells as illustrated by representative images of calcein/DiI transfer assay showing potential acceptor cells (DiI-positive) and donor cells (calcein-positive). **(B)** Scoring of calcein/DiI images from *Lmna*$^{+/+}$ or *Lmna*$^{-/-}$ cells either stimulated with serum or treated with PD98059. *Lmna*-/- cells had significantly less cell communication compared to *Lmna*+/+ in all cases ($p < 0.001$) ($n \geq 1500$ cells). **(C)** Calcein/DiI transfer was not improved in using *Lmna*$^{+/+}$ cells as donor cells and *Lmna*$^{-/-}$ acceptors (+/+ to -/-) or using *Lmna*$^{+/+}$ cells as acceptor cells with *Lmna*$^{-/-}$ donors (-/- to +/+) ($n \geq 500$ cells).

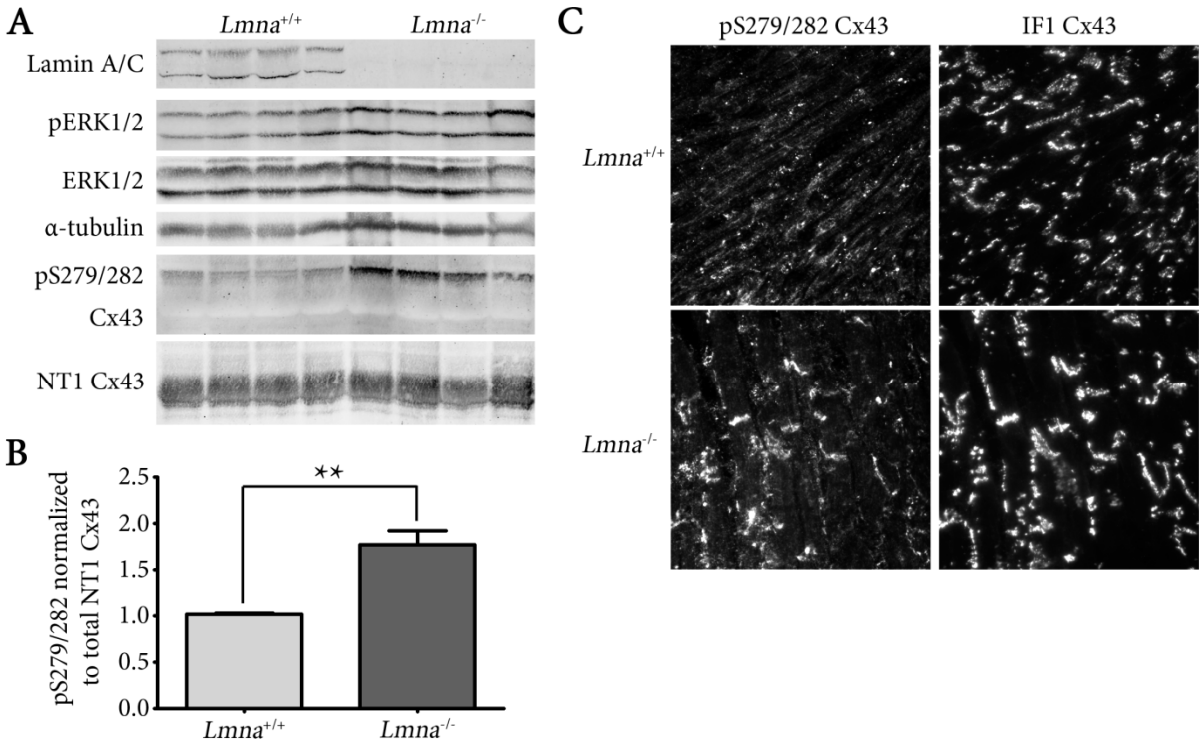

Figure 4 - phospho-S279/282 Cx43 is increased in *Lmna*$^{-/-}$ mouse heart. (A) Representative Western blot analysis of heart lysates from either *Lmna*$^{+/+}$ or *Lmna*$^{-/-}$ mice demonstrating increased pERK1/2 relative to total ERK1/2 and increased phospho-S279/282 Cx43 relative to total NT1 Cx43 signal. α-tubulin is shown as a loading control. **(B)** Quantification of phospho-S279/282 signal normalized to NT1 Cx43 reveals a significant 1.7-fold increase in *Lmna*$^{-/-}$ mice (*Lmna*$^{+/+}$ n = 5, *Lmna*$^{-/-}$ n=7, $p<0.01$). **(C)** Immunofluorescence of ventricle sections from *Lmna*$^{+/+}$ and *Lmna*$^{-/-}$ mice stained with phospho-S279/282 Cx43 and IF1 Cx43, which predominantly recognizes functional gap junctions at the intercalated disk, show localization and increased presence of phospho-S279/282 at the intercalated disk in *Lmna*$^{-/-}$ heart.

Conclusions and Future Directions

In my work, I have further demonstrated the essential role that A-type lamins play in maintaining normal cardiac function. Mutations in this non-essential intermediate filament that forms the nuclear lamina primarily result in the development of muscular dystrophies and cardiomyopathy [272]. Mice deficient in A-type lamins exhibit a similar phenotype and multiple other mouse models for specific disease-causing mutations also appear to have characteristics of the human disease [94,99,107,282]. My research has shown that, although non-essential, loss of A-type lamin in the heart severely compromised cardiac function and begins to dissect the potential molecular mechanisms underlying these defects.

In chapter 1, I illustrate that the loss of A-type lamins in *Lmna*$^{-/-}$ mice is lifespan limiting as partial restoration of normal lamin activity with a human *LMNA* transgene (Tg) in cardiomyocytes significantly extended lifespan by 12%. With my co-author Richard Frock, I observed that aggregation of the cytoskeletal intermediate filament desmin was increased in *Lmna*$^{-/-}$ cardiomyocytes and was rescued on a cell-by-cell basis, depending on whether the transgene was expressed. Echocardiograms revealed that efficiency of heart contraction was significantly decreased in *Lmna*$^{-/-}$ mice, with significant improvement in *Lmna*$^{-/-}$; Tg mice. As desmin is required for proper muscular contraction, I partially attribute the improvement in heart contractility as measured by echocardiogram to the restoration of the normal desmin network. I also investigated the activation of ERK1/2 in *Lmna*$^{-/-}$ mice, as *Lmna*$^{H222P/H222P}$ mice exhibit increased levels of pERK1/2 and activation of the MAPK pathway, observing that *Lmna*$^{-/-}$ mice also have elevated pERK1/2 which is partially corrected in *Lmna*$^{-/-}$; Tg mice. Analysis of the

state of connexin43 (Cx43), the primary gap junction protein responsible for cardiac conduction, showed an increased fraction of Cx43 recognized by the CT1 antibody in *Lmna*$^{-/-}$ mice, which is indicative of increased cytoplasmic and non-functional Cx43. This was coupled with my observation of less Cx43 found at the intercalated disk region by immunofluorescence in *Lmna*$^{-/-}$ mice and another partial rescue in *Lmna*$^{-/-}$; Tg mice. I believe this resulted in functional consequences in the *Lmna*$^{-/-}$ mice, as they exhibited slowed conduction velocity as measured by PR interval on ECG and increased incidence of arrhythmia. These effects cumulatively resulted in a significant, although minor, lifespan extension in *Lmna*$^{-/-}$; Tg mice.

Ultimately, these experiments were greatly affected by the mosaic expression of the transgene as *Lmna*$^{-/-}$; Tg mice only expressed *LMNA* in approximately 1 out of 3 cardiomyocytes. This had the unfortunate effect of confounding much of our data as we only achieved partial rescue of many of the cardiac phenotypes rather than a full restoration. I would expect that expression of *LMNA* in >95% of cardiomyocytes would yield much more significant effects on the molecular phenotypes, the functional aspects and ultimately lifespan. Despite this unforeseen hurdle, I believe these mice are still valuable and could be used for some further experiments to determine whether the observed effects are cell-autonomous or non-cell-autonomous. I believe that isolated cardiomyocytes from these mice would be an ideal approach to tackle some of these questions. In terms of cell-autonomous effects, we have already observed that formation of a normal desmin network occurs in cardiomyocytes expressing the *LMNA* transgene, so we could reasonably assume that would continue to hold true. That said, with the isolated cardiomyocyte, we could then measure the contractile force of individual cardiomyocytes, potentially observing two distinct populations of cardiomyocytes in

the *Lmna*$^{-/-}$; Tg mouse. I would expect that cardiomyocytes expressing the *LMNA* transgene would exhibit strong contraction, while those lacking it to exhibit poor contraction. On the other hand, I believe that cardiac conduction would be a non-cell-autonomous effect, as it relies on proper gap junctional communication between multiple cells. I believe if we visualized cardiac conduction using optical mapping with voltage-sensitive dye, we would observe inhomogeneous wave front propagation in *Lmna*-/-; Tg mice, as there would be a mixed population of intercalated disks some with proper gap junctions and some without. In contrast, *Lmna*$^{+/+}$ and potentially *Lmna*$^{-/-}$ mice would show a smooth wavefront, although much slower in *Lmna*$^{-/-}$ mice. Finally, the mosaic expression of *LMNA* transgene in *Lmna*$^{-/-}$; Tg mice would potentially allow us to answer the question whether activation of ERK1/2 is a direct effect of lamin deficiency in the cardiomyocyte, or if it is an effect of generalized stress in the mouse and external secreted circulating factors. With isolated cardiomyocytes, we could determine the effects of lamin on individual cells. If we observe no difference between cells lacking transgene expression and those with transgene expression, it may indicate that ERK1/2 activation is the result of external factors. However, if there is a difference between these cells, then ERK1/2 activation would be a cell-autonomous defect associated with loss of A-type lamins.

In chapter 2, I reveal that activation of the mTOR pathway in *Lmna*$^{-/-}$ mice significantly contributes to their dystrophic and cardiomyopathic phenotype as treatment with the TORC1 inhibitor rapamycin improved many of their symptoms and resulted in an extension in their median lifespan by up to 55%. In collaboration with Fresnida Ramos and Dr. Matt Kaeberlein, we showed activation of many of the downstream targets of the mTOR pathway such as p70 S6K, rpS6, and 4E-BP1 in skeletal muscle and cardiac tissue of *Lmna*$^{-/-}$ mice. Treatment of these

mice with dietary rapamycin dramatically decreased activity of mTORC1 in *Lmna*$^{-/-}$ mice. Rapamycin-treated *Lmna*$^{-/-}$ mice showed significant improvement in their cardiac contractility, as measured by echocardiogram, though did not achieve the same levels as their wild-type littermates. In addition, treatment of *Lmna*$^{-/-}$ mice with rapamycin ameliorated some of the dystrophic phenotypes as desmin aggregation was decreased and cross-sectional area of myofibers was increased in gastrocnemius muscle. We believe that the improvement in cardiac output and muscle function resulted in the improved performance of rapamycin-treated *Lmna*$^{-/-}$ mice on the rotarod test, demonstrating that rapamycin improved fitness of these mice. Survival was also significantly improved, with a 35% increase in median lifespan of rapamycin-fed *Lmna*$^{-/-}$ mice and a 55% increase in median lifespan if administered by intraperitoneal injection. We finally observe that LC3-I levels are significantly decreased in rapamycin-treated *Lmna*$^{-/-}$ mice, indicating an increase in productive autophagy which we speculate to play a role in the skeletal and cardiac muscle phenotype of these mice.

The mTOR and MAPK pathways appear to intersect at various points, regulating the activity of each other as well as sharing common downstream targets. ERK1/2, as well as its downstream target RSK, have been shown to phosphorylate and inactivate TSC2, one of the two proteins in the TSC complex that inhibit mTORC1 activity through Rheb [283,284,285]. Conversely, inhibition of mTORC1 can result in ERK1/2 activation through a S6K1/PI3K-dependent negative feedback loop [286,287]. In addition to regulating each other, the mTOR and MAPK pathways are both able to phosphorylate eIF4B on Ser422 and promote translation initiation through S6K or RSK, respectively [288]. Deregulation of either the mTOR or MAPK pathways are commonly found in cancer, and given the apparent amount of crosstalk between

mTOR and MAPK, there has been interest in utilizing rapamycin and MAPK inhibitors in the treatment of cancer. It has been shown in cell culture, and more recently in human patients, that co-activation of the mTOR and MAPK pathways exist in cancers and that combinatorial treatment with rapamycin and MAPK inhibitors effectively suppresses tumor growth or can even result in tumor regression [289,290]. With that in mind, I would find it very interesting to attempt similar combinatorial treatment of *Lmna*$^{-/-}$ mice with rapamycin and the MEK1 inhibitor PD98059. Treatment of the *Lmna*$^{H222P/H222P}$ mouse with PD98059 resulted in significant reduction of the cardiomyopathic phenotype [104]. It seems possible that administering PD98059 in combination with rapamycin to *Lmna*$^{-/-}$ mice would provide further improvement to defects not fully rescued by rapamycin alone, in particular the functional aspect of cardiac contraction as measured by echocardiogram.

In chapter 3, I establish a potential pathway to explain the conduction system disease associated with dilated cardiomyopathy in laminopathy patients. I detect that phosphorylation of Cx43 on S279/282, which inhibits gap junction function by decreasing conductance, is increased in *Lmna*$^{-/-}$ MEFs and heart tissue. I then demonstrate a decreased association of pERK1/2, the kinase responsible for this phosphorylation event, with the nuclear envelope of *Lmna*$^{-/-}$ cells and an increased association with Cx43 which likely results in increased phosphorylation of S279/282. I finally show that cell communication through the gap junction is decreased in *Lmna*$^{-/-}$ cells compared to *Lmna*$^{+/+}$ by the calcein/DiI dye transfer assay. These results suggest a mechanism in which the loss of A-type lamins eliminates the normal binding of pERK1/2 to the nuclear envelope, allowing it to inappropriately phosphorylate Cx43 on S279/282 and ultimately inhibiting cellular communication. This may have a more significant

effect in the heart, as Cx43 forms the gap junctions responsible for electrical coupling of cardiomyocytes and normal cardiac conduction.

If this pathway holds true in *Lmna*$^{-/-}$ mice, then I would expect that blocking phosphorylation of Cx43 on S279/282 would decrease the frequency of arrhythmic events and potentially increase lifespan. Crossing the *Lmna*$^{-/-}$ mouse with a knock-in mouse strain expressing Cx43 with the serines associated with MAPK phosphorylation mutated to alanine (MK4), would yield the *Lmna*$^{-/-}$; MK4/MK4 mouse and presumably be resistant to the effects of ERK1/2 phosphorylation. With this mouse, I would demonstrate a complete loss of S279/282 phosphorylation and then determine its functionality by ECG. Utilizing a hanging Langendorff system, I would be able to isolate and measure ECG parameters such as P duration, PR interval and QRS duration, giving an indirect measurement of conduction velocity. Without any phosphorylation of Cx43 on S279/282, I expect to see improved cardiac conduction in *Lmna*$^{-/-}$; MK4/MK4 mice compared to *Lmna*$^{-/-}$. It would also be interesting to investigate how much of a role Cx40 or Cx45, the other connexins expressed in heart, have in the cardiac conduction defect. As these connexins are specific to cells critical for conduction, namely the pacemaker cells and Purkinje fibers, it seems very possible that the function of these proteins would be similarly impaired.

One final question that begs an answer and continues to confound me is why do diseases caused by A-type lamins primarily affect skeletal and cardiac muscle? A-type lamins are found in the majority of differentiated tissues, yet appears not to have any effect on any major organs. The most widely proposed explanation is that skeletal and cardiac muscle are

subject to repeated physical strain, and in combination with an increased fragility of the nucleus from the lack of lamins, results in apoptosis and cell death [291]. However, this does not explain why adipose tissue, which is arguably not subject to significant strain, can be affected by mutations in lamin; or why other tissues that are subject to repeated strain such as the lung, stomach and small intestine, are left unaffected. There has been speculation that the endoplasmic reticulum, which shares a continuous membrane with the inner and outer nuclear membrane, plays a particularly significant role in the affected tissues and may be affected by changes in the nuclear lamina [292]. Another explanation offered hinges on the observation that lamin B1 is not detected in skeletal muscle or cardiomyocyte nuclei affecting binding of proteins associated with B-type lamins [293], though the mechanism by which this results in a dystrophic or cardiomyopathic phenotype is unclear.

In the end, I have shown that A-type lamin function is essential for normal cardiac function and have uncovered some molecular pathways and mechanisms that potentially contribute to dilated cardiomyopathy with conduction system disease in mice. Whether these promising leads will translate to human patients is unknown, but regardless I have made an incremental amount of progress towards unraveling the complex network surrounding A-type lamins.

Appendix I

Decreased Proliferation Kinetics of Mouse Myoblasts Overexpressing FRG1

This manuscript, published May 2011 in *PLoS ONE*, describes my efforts into establishing a role for the protein FRG1 in the development of the muscular dystrophy FSHD. In it, I establish a proliferation defect associated with overexpression of FRG1 in both primary and immortalized myoblast cultures.

Decreased Proliferation Kinetics of Mouse Myoblasts Overexpressing *FRG1*

Steven C. Chen[1], Ellie Frett[1,2], Joseph Marx[1], Darko Bosnakovski[3], Xylena Reed[1,4], Michael Kyba[3], and Brian K. Kennedy[1,5]

[1] Department of Biochemistry, University of Washington, Seattle, Washington, USA

[2] Current address: Department of Pharmacology and Physiology, University of Rochester Medical Center, Rochester, New York, USA

[3] Lillehei Heart Institute and Department of Pediatrics, University of Minnesota, Minneapolis, Minnesota, USA

[4] Current address: McKusick-Nathans Institute of Genetic Medicine, Johns Hopkins University School of Medicine, Baltimore, Maryland, USA

[5] Buck Institute for Age Research, Novato, California, USA

Correspondence to:
Brian K. Kennedy, PhD
Buck Institute for Age Research
Novato, CA 94945.
Phone: 415-209-2039
Fax: 415-493-2248
Email: bkennedy@buckinstitute.org

Abstract

Although recent publications have linked the molecular events driving facioscapulohumeral muscular dystrophy (FSHD) to expression of the double homeobox transcription factor *DUX4*, overexpression of *FRG1* has been proposed as one alternative causal agent as mice overexpressing *FRG1* present with muscular dystrophy. Here, we characterize proliferative defects in two independent myoblast lines overexpressing *FRG1*. Myoblasts isolated from thigh muscle of *FRG1* transgenic mice, an affected dystrophic muscle, exhibit delayed proliferation as measured by decreased clone size, whereas myoblasts isolated from the unaffected diaphragm muscle proliferated normally. To confirm the observation that overexpression of *FRG1* could impair myoblast proliferation, we examined C2C12 myoblasts with inducible overexpression of *FRG1*, finding increased doubling time and G1-phase cells in mass culture after induction of *FRG1* and decreased levels of pRb phosphorylation. We propose that depressed myoblast proliferation may contribute to the pathology of mice overexpressing *FRG1* and may play a part in FSHD.

Keywords: FSHD, myoblast, proliferation, *FRG1*, cell cycle

Introduction

Facioscapulohumeral muscular dystrophy, or FSHD, primarily affects muscles of the face, shoulders and upper arms. It is the third most common muscular dystrophy, following Duchenne muscular dystrophy and myotonic muscular dystrophy, affecting 1 in 20,000 individuals [294]. Onset of muscle weakness in FSHD patients most commonly occurs between puberty and the second decade of life, ultimately leading to patients becoming wheelchair-bound [295,296,297]. Compared to the majority of muscular dystrophies, FSHD is unique in its very low rate of any respiratory or cardiac muscle involvement, which is often the eventual cause of death for patients with other forms of muscular dystrophy [298]. As such, patients with FSHD typically live a normal lifespan, but suffer a severely decreased quality of life.

The molecular basis of FSHD is still under debate, although the genetic event linked with FSHD has been identified to be in the subtelomeric region on the long arm of chromosome 4 [299,300]. This region, denoted as 4q35, contains a series of 3.3kb tandem repeat elements, which have been termed D4Z4 repeats [301]. Unaffected individuals have 11 to 150 D4Z4 repeats, but patients with FSHD have had this region truncated to 10 or less [302]. Efforts to identify the molecular basis of this disease have been hampered, however, because the truncation associated with FSHD is not within a well-characterized gene coding or promoter region.

Multiple models have been proposed to explain how a D4Z4 repeat truncation is linked to FSHD, reviewed in [303]. The primary model is that the loss of D4Z4 repeats increases expression of a double homeobox transcription factor *DUX4c*, a putative gene centromeric to

the D4Z4 repeats and highly homologous to *DUX4* [304,305,306]. *DUX4c* has been shown to be up-regulated in FSHD biopsies and primary myoblasts, possibly leading to induction of the *MYF5* myogenic regulator, which serves to inhibit differentiation and activate proliferation [307,308]. In addition, overexpression of *DUX4* in other cell lines has been shown to cause apoptosis and impair myogenesis in both cell culture models and zebrafish development [309,310,311]. A recent chromosomal analysis of affected and unaffected 4q35 alleles has determined that FSHD is linked to a single nucleotide polymorphism located distal to the last D4Z4 repeat [312], which stabilizes the *DUX4* transcript through polyadenylation and may result in elevated protein levels and cytotoxicity via still unknown mechanisms.

A second model proposes that the loss of D4Z4 repeats may increase the available pool of a repressive complex comprised of YY1, HMG2B and nucleolin that is normally bound to D4Z4 repeats. YY1 interacts with Ezh2, a histone lysine methyltransferase, playing a key role in expression of muscle genes during embryonic development [313,314] and MeCP2, a methyl CpG binding protein involved in Rett syndrome [315]. In addition, YY1 may also be able to interact with the chromatin insulator CTCF [316]. HMGB2 may affect the maintenance of heterochromatic regions by interacting with SP100B and subsequently HP1, establishing higher-order chromatin structures [317,318]. In contrast, nucleolin may have an opposite effect on heterochromatin formation as it serves to decondense chromatin through displacement of histone H1 [319]. Perturbations in any of these proteins due to loss of D4Z4 repeats resulting in increased chromatin accessibility may cause gene deregulation *in trans* and play a role in the pathogenesis of FSHD.

A third model suggests that D4Z4 may serve as nucleating sites for local transcriptional repression involving the previously mentioned YY1 complex. Loss of D4Z4 may lift repression *in cis* of the 4q35 region and thus the nearby genes *FRG1, FRG2* and *ANT1* [320,321]. Additionally, the identification of a nuclear matrix attachment site (S/MAR) and its disassociation from the nuclear matrix in FSHD patients may change the arrangement of DNA loop domains, causing increased transcription of *FRG1* and *FRG2* [322,323,324]. Presently, it is unclear as to which or how many of these many non-exclusive mechanisms play a causal role in the pathogenesis of FSHD.

Previously, it has been observed that there may be increased transcriptional activation of *FRG1, FRG2* and *ANT1,* the three genes upstream of the D4Z4 tandem repeat elements, in muscle of human FSHD patients [321]; however, these results were not observed in another patient study [325]. Unfortunately, generating a relevant mouse model to study FSHD has been exceptionally difficult because mice do not have D4Z4 repeats in an analogous chromosomal setting. Acting under the assumption that overexpression of *FRG1, FRG2* or *ANT1* plays a causative role in the development of FSHD, transgenic mice were generated expressing each of these individual genes under the human skeletal actin promoter, specific for expression in muscle, which resulted in the identification of a potential mouse model for FSHD. In contrast to transgenic mice overexpressing *FRG2* or *ANT1*, only transgenic mice overexpressing *FRG1* appear to have symptoms characteristic of muscular dystrophy [326]. It should be noted, however, that the *FRG1* transgenic mouse model that resulted in dystrophic phenotypes had FRG1 skeletal muscle protein levels considerably higher than that observed in FSHD patients.

Facioscapulohumeral muscular dystrophy region gene-1 (*FRG1*) is an actin-bundling protein associated with muscle-attachment sites, specifically located to the Z-disc in mature muscle tissue [327,328]. *FRG1* has been shown to play a crucial and specific role in muscle development of *Xenopus laevis*, further implicating its importance in muscle development and maintenance [329,330]. Recently, Bodega et al. showed that the *FRG1* gene was prematurely expressed during FSHD myoblast differentiation, thereby suggesting that the number of D4Z4 repeats in the array may affect the correct timing of *FRG1* expression [320].

Based on this work, we hypothesized that the dystrophic phenotype in *FRG1* transgenic mice is caused, at least in part, by decreased proliferation in the muscle satellite cell population, which are the cells responsible for maintaining proper muscle regenerative potential. Satellite cells are often thought of as muscle stem cells, proliferating when there is a need for either muscle repair or growth and then differentiating into skeletal muscle. We have observed that increased levels of FRG1 impair normal satellite cell proliferation and may contribute to disease progression by limiting the pool of cells to repair damaged muscle and/or delaying the kinetics of repair.

Results

Expression of FRG1 in skeletal muscle of mice causes dystrophic characteristics

Mice overexpressing *FRG1* have been previously described [326]. In that study, three lines of transgenic mice overexpressing *FRG1* specifically in muscle were generated by using the human skeletal actin promoter to drive transcription of the human *FRG1* cDNA. These mice develop spinal kyphosis and characteristics of muscular dystrophy, including increased fibrosis in muscles, lower body weight, lower muscle weight and decreased cross-sectional area, reduced tolerance to exercise and mis-splicing of specific transcripts associated with myotonic dystrophy. Mice used in the Gabellini et al. study [326] were kindly provided by Dr. Rossella Tupler. After establishing an independent colony with continual back-crossing to C57BL/6 mice, we performed a limited characterization of the *in vivo* phenotypes in their highest *FRG1* expressing line (H-*FRG1*^{TG}) as a confirmation of their reported findings. As expected, these mice begin to show mild spinal kyphosis and reduced body weight by 4 weeks of age, both of which become progressively more severe over time.

To verify that *FRG1* expression was increased specifically in skeletal muscle, we performed Western blot analysis on lysates generated from a variety of tissues from 10-week old mice using a specific α-FRG1 antibody. Equivalent amounts of total protein were loaded and increased FRG1 protein was detected in all tested skeletal muscles of H-*FRG1*^{TG} mice compared to wild-type littermate controls (**Figure 1A**). We observed a specific increase in the expression of *FRG1* in skeletal muscles such as quadriceps, gastrocnemius and diaphragm muscle, and no increase of *FRG1* in cardiac muscle or other tissues, confirming the skeletal muscle-specific

expression of *FRG1*. Endogenous expression of *FRG1* was detected in the lung, but there was no significant difference in expression between H-*FRG1*^{TG} mice and wild-type littermate controls.

Muscle weights of collected tissues were measured at different ages and normalized to body weight, to account for runted phenotype of H-*FRG1*^{TG} mice. Quadriceps and gastrocnemius wet muscle weight comprised a smaller percentage of total body weight in H-*FRG1*^{TG} mice compared to wild-type mice, but diaphragm weight showed no significant change (data not shown). This observation agrees with previous observations demonstrating that despite *FRG1* expression in all skeletal muscle tissue, only specific muscles may exhibit a dystrophic phenotype [326,331].

To examine the histology of specific muscles, we collected and cryosectioned muscle tissue from 13-week old H-*FRG1*^{TG} mice and wild-type littermate controls. Hemotoxylin and eosin staining of these sections showed an increased incidence of centrally located nuclei and increased fiber size variability in affected muscle tissues, namely the quadriceps, but this was not noted in internal muscles such as the diaphragm (**Figure 1B**). From these experiments we find that overexpression of *FRG1* only causes a dystrophic phenotype in a subset of skeletal muscles. We also noted that H-*FRG1*^{TG} mice were able to survive past 1 year of age (data not shown) despite the worsening of their muscular dystrophy and other associated phenotypes. The apparent sparing of the diaphragm muscle of any measurable defect may possibly replicate the muscle specificity of FSHD in human patients, which similarly does not appear to affect internal muscles. All of these observations confirm the muscular dystrophy phenotype in H-*FRG1*^{TG} mice as originally characterized.

Effects of FRG1 expression in mouse-derived myoblasts

In principle, dystrophic phenotypes in muscle can arise from enhanced degeneration, defective regeneration, or both. For instance, myoblasts from mice lacking A-type lamins that exhibit signs of muscular dystrophy plate with high viability and proliferate normally, but ultimately have impaired differentiation [95]. Thus, muscular dystrophies associated with mutations in the A-type lamin gene, *LMNA*, may be associated with decreased satellite cell differentiation , causing depressed regeneration in addition to reduced myofiber stability. As a test for potential regeneration defects in satellite cells of H-*FRG1*^{TG} mice, we sought to determine whether myoblasts from these mice had altered proliferation or differentiation potential in cell culture. Myoblast cultures were isolated and cultured by standard techniques [332], which, if treated appropriately, are comprised predominantly of proliferating myoblasts and can provide an accurate readout of the regenerative potential of muscle from the H-*FRG1*^{TG} mice. We speculated that myoblasts from H-*FRG1*^{TG} mice may have similar defects to those from *Lmna*$^{-/-}$ mice.

We isolated and cultured the satellite cell population from affected quadriceps and unaffected diaphragm muscle of 18-week old H-*FRG1*^{TG} mice and wild-type littermate controls. Since the quadriceps muscle, but not the diaphragm, exhibited characteristics of muscular dystrophy, we speculated that there is a specific defect in satellite cells derived from the thigh. We thus performed a clonal assay on primary isolated myoblasts in order to measure the proliferation rates of the isolated satellite cells.

We quantified transcript levels of *FRG1* in our isolated satellite cells by qPCR, and observed increased levels of *FRG1* transcript in both proliferating and differentiated cultures from H-*FRG1*^{TG} mice (**Figure S1A**). This was somewhat surprising as the promoter driving *FRG1* expression, the human skeletal actin promoter, is reported to be active only after differentiation. We also performed Western analysis on cell lysates generated from the same satellite cells to observe protein levels of FRG1. Levels of FRG1 protein are increased in both proliferating and differentiated cultures of satellite cells from of H-*FRG1*^{TG} mice (**Figure S1B**). In addition, FRG1 is detected in satellite cell cultures derived from either diaphragm or thigh muscle (**Figure S1C**).

For clonal analysis, the tissue-derived satellite cells were plated at a very low density, 1000 cells per 10 cm dish, and allowed to grow for a predefined amount of time. At regular intervals, plates were fixed and nuclei were visualized by staining with methylene blue. We also stained for myosin heavy chain (MyHC) as a control to verify that cells did not prematurely differentiate over the course of the clonal assay, in which bFGF and high serum levels were maintained. After fixation and staining, the total number of cells per clone was determined and binned for comparison in a histogram format. Thigh-derived satellite cells from an 18-week old H-*FRG1*^{TG} mouse show a marked decrease in average clone size compared to those derived from a wild-type littermate control (**Figure 2A)**. A significant fraction of these cells show arrest in a 2-cell clone size skewing the distribution compared to the wild-type thigh-derived satellite cells. This effect may be even more dramatic considering that single cell clones were not scored in this assay, as we consider single cell clones may potentially be new clones arising from detached satellite cells floating away from the original clone during mitosis. We replicated

these observations with an independent satellite cell culture isolated from 20-week old mouse limbs obtained directly from Dr. Rossella Tupler which were comparable to our 18-week old thigh-derived satellite cells at a similar time point (**Figure S2**). The proliferative defect was not replicated in the diaphragm-derived satellite cells, which show a very similar clone size distribution between the H-*FRG1*^{TG} and wild-type C57BL/6 littermates. These findings indicate that *FRG1* overexpression leads to a muscle-type specific defect in proliferation, and correlates with the dystrophic phenotype.

To determine whether there is an age-dependent increase in severity of the observed proliferation defect, we isolated and performed a clonal assay on both thigh- and diaphragm-derived satellite cells isolated from 4-week old mice, which appear asymptomatic, to compare to the aforementioned data from more severely symptomatic 18-week old mice. For each of these populations, we scored multiple time points of a clonal assay, to more thoroughly assay the proliferative defect. The clone size distributions of myoblasts from asymptomatic 4-week old mice did not show any significant proliferative defect when compared to their 18-week old counterparts at a similar clone size (**Figure 2B**). To more easily compare the data from these clone size distributions, we obtained the average clone size for each of these populations and calculated the average doubling time of each of these lines. The data show that the proliferative defects associated with *FRG1* overexpression appear to be age-specific, as myoblasts obtained from quadriceps muscle of 4-week old H-*FRG1*^{TG} mice are indistinguishable from those derived from littermate controls, whereas satellite cells from 18-week old mice H-*FRG1*^{TG} mice have a severe defect (**Table 1**). These effects are further reflected in the general health of the mice and severity of muscle dystrophy at later ages. It is interesting to observe

that by 52-weeks of age, we were unable to successfully culture satellite cells from the thigh muscle of H-*FRG1*^{TG} mice, possibly due to either extremely depressed proliferation rates or exhaustion of the satellite cell population. It should also be noted that we never observed any significant differentiation defect in any of our satellite cell cultures (data not shown). We conclude that the overexpression of *FRG1* in muscle tissue causes muscle-type-specific and age-dependent impairment in the ability of satellite cells to proliferate when isolated in cell culture.

Inducible FRG1 expression in C2C12 myoblasts

In addition to experiments performed in mouse-derived satellite cell culture, we sought to establish an independent cell culture model system that would be free of any potential artifacts introduced during generation of the H-*FRG1*^{TG} mice. Initially, we performed viral transduction of *FRG1* under the CMV promoter in the pMXIH vector as previously described [333]. Findings in early passages after selection indicated a proliferative defect associated with *FRG1* overexpression. Unfortunately, we observed a loss of the proliferative defect over time as measured by BrdU-positive cells (**Figure S3**). The loss of defects in proliferation was accompanied by an increase in cells staining negative for FRG1, suggesting either that expression was being actively silenced or, more likely, high *FRG1* expressing cells were being outcompeted over time by lower expressing cells with a faster rate of proliferation. Given this complication, we adopted another strategy to drive *FRG1* overexpression.

We chose to employ an inducible system to control expression of *FRG1* that would allow us to turn on expression when needed. We utilized C2C12 myoblasts that have an integrated

cassette expressing FLAG-tagged *FRG1* under a tetracycline-responsive promoter (iC2C12-FRG1) generated as previously described and kindly provided to us by Dr. Michael Kyba [310]. *FRG1* expression is induced in iC2C12-*FRG1* myoblasts by the addition of doxycycline and levels of induction can be modulated by adjusting levels of the drug. There is no detectable expression of *FRG1* in uninduced cells as assayed by Western blot of whole cell lysates using an α-FLAG antibody. In comparison, robust expression of *FRG1* was observed under a variety of induction conditions ranging from 250 to 1000 ng/mL doxycycline (**Figure 3A**).

FRG1 is believed to play a role in post-transcriptional mRNA processing and localizes to nuclear Cajal bodies [334], therefore we performed immunofluorescence to investigate whether FRG1 was properly localized in iC2C12-FRG1 myoblasts after induction. iC2C12-FRG1 myoblasts were cultured on glass coverslips and cells were grown for 24 hours in the presence or absence of doxycycline followed by fixation and staining. Staining with DAPI and an α-FLAG antibody revealed nuclear localization of FRG1-FLAG following induction (**Figure 3B**). There was some variation in magnitude of expression of FRG1-FLAG on a cell-to-cell basis, but we observed robust partially punctuate staining in the nucleus, consistent with possible localization to Cajal bodies.

Interestingly, we observed in our initial characterization of induced iC2C12-*FRG1* myoblasts a similar phenomenon as the virally transduced C2C12 cells in that after numerous passages in the presence of doxycycline, induced cells showed much lower expression levels of FRG1-FLAG (**Figure S4**) and likely a loss of any proliferative defect. A similar explanation is likely

that lower *FRG1* expressing cells in this non-clonal population ultimately outcompete higher expressing cells and take over the culture.

Characterizing defects in proliferation following FRG1 expression in iC2C12-FRG1 myoblasts

To investigate the proliferation defect caused by *FRG1* overexpression, we conducted a number of assays in iC2C12-FRG1 myoblasts. We first assayed the proliferation rates of cells in mass culture in the presence or absence of doxycycline. In order to determine growth rates, identical numbers of cells were plated in wells of a 24-well plate and at regular time intervals the total number of cells per well were counted using a hemocytometer. We determined that induction of FRG1-FLAG in iC2C12-FRG1 myoblasts has a negative effect on their proliferation rate, as shown by the increased doubling time when grown in doxycycline (**Figure 4A**). Naïve C2C12 myoblasts were not affected by exposure to doxycycline (data not shown), demonstrating that the phenotype is likely specific to *FRG1* overexpression.

To further investigate the proliferative defect of iC2C12-FRG1 myoblasts expressing *FRG1*, we utilized flow cytometry to determine the fraction of cycling cells in specific phases of the cell cycle. Actively proliferating iC2C12-FRG1 myoblasts grown in either the presence or absence of doxycycline were fixed and stained with DAPI. Subsequent flow cytometry analysis of the cells for DNA content indicated an increased fraction of FRG1 overexpressing iC2C12-FRG1 myoblasts in G1-phase, coupled with a corresponding decrease in the fraction of cells in S-phase (**Figure 4A**). These findings suggest that cells overexpressing FRG1 are delayed in transit

through G1. We believe that this shift in cell cycle profile may at least in part explain the gross proliferation defect that we have observed.

One potential weakness of just looking at a cell cycle phase distribution is that absolute cell cycle length is indeterminate in a mass culture cell cycle profile. To address this issue, we performed a mitotic shakeoff assay to synchronize proliferating iC2C12-FRG1 myoblasts so that transit through specific cell cycle phases could be measured. Since cells progressing through mitosis are less adherent to culture dishes, this technique provides a way to synchronize cells in the absence of any drugs to mediate cell cycle arrest. After being plated in the presence or absence of doxycycline for a period of 24 hours, mitotic cells were isolated by mild shaking and rocking for a period of 20 minutes to generate synchronized cultures. Fixation at 2-hour intervals followed by subsequent analysis by flow cytometry for DNA content was performed to track cells as they progressed through the cell cycle. We observed that FRG1 overexpressing cells exhibited a consistent 1-2 hour delay in exit from G1 and entry into S-phase (**Figure 4B & Table 2**). This finding is consistent with the FACS analysis of asynchronous cells, which indicated that a higher percentage of FRG1 overexpressing cells were in G1 phase. It should be noted that it is difficult to monitor progression beyond one cell cycle in this assay since the iC2C12-FRG1 myoblasts rapidly lose synchronicity.

Cell cycle specific factors are affected by FRG1 expression

The retinoblastoma protein (pRb) is one of the primary regulators of the mammalian cell cycle, inhibiting E2F-dependent transcription and maintaining cells in G1-phase when

hypophosphorylated. Phosphorylation by cyclin-dependent kinases interferes with the capacity of pRb to repress E2F-dependent transcription, permitting S-phase entry [335,336]. Since *FRG1* overexpression led to increased G1 phase occupancy, we examined the phosphorylation state of pRb as an indicator of these altered cell cycle kinetics. We observe via Western blot that compared to naïve C1C12 or uninduced iC2C12-FRG1 myoblasts, levels of 807/811 phosphorylated pRb are lower in induced iC2C12-FRG1 myoblasts (**Figure 5A**). Total levels of pRb appear lower, however this is likely an artifact of the antibody used, since it is known to have somewhat greater affinity for hyperphosphorylated pRb. Decreased pRb phosphorylation is consistent with a decreased proliferation rate and increased G1 phase occupancy.

Discussion

In this study, we demonstrate decreased proliferation rates of myoblasts expressing *FRG1*, an attribute that could contribute to the long term reduction in muscle regenerative potential and muscular dystrophy observed in transgenic mice overexpressing *FRG1*. We have verified expression and muscular dystrophy in the H-*FRG1*^{TG} mouse and seen that thigh-derived myoblasts, but not diaphragm-derived myoblasts, from these animals demonstrate a proliferative defect by clonal analysis. We also find that induction of *FRG1* in myoblasts by a tetracycline-responsive system negatively affects proliferation as determined in cell cycle profiles measured by flow cytometry and hypophosphorylation of pRb.

Reduced myoblast proliferation is not commonly linked to muscular dystrophy, which is more classically attributed to death of muscle fibers, such as in Duchenne muscular dystrophy

[337], or a combination of enhanced fiber degeneration and defective differentiation kinetics such as in *Lmna*$^{-/-}$ mouse models [95,338]. However, there have been reports of depressed proliferation kinetics in Duchenne muscular dystrophy myoblasts, compounding the existing mechanisms of muscular dystrophy [339]. Since the proliferation defect gets more severe in myoblasts isolated from H-*FRG1*^{TG} mice of increasing age, it is difficult to differentiate between two models: (1) that the proliferation defect precedes onset of the dystrophic phenotype or (2) that the defect derives from reduced satellite potential with age resulting from increasing strain on satellite cells to repair damage.

Our findings in C2C12 cells may indicate that a cell cycle defect can occur as a primary result of *FRG1* overexpression. However, it ultimately remains unclear precisely how FRG1 impacts cell cycle progression. FRG1 has been shown to localize to Cajal bodies in the nucleus, where it is reported to regulate RNA processing [334,340]. Misprocessing of RNA transcripts has also been linked to myotonic dystrophy [341,342]. One possible hypothesis for induction of G1 arrest by FRG1 involves altered splicing of transcripts encoding cell cycle components. For instance, altered processing of the cyclin E RNA produced different isoforms of the protein with different affinities for Cdk2 [343,344,345].

One contentious observation regarding overexpression of *FRG1* in patients with FSHD is that other research groups have been unable to replicate the results published showing increased *FRG1* transcript in affected muscle [321]. Some studies of myoblasts subjected to microarray analysis or measuring RNA transcription of *FRG1* have not yielded any results showing an increase of *FRG1* transcript [346,347], while similar experiments with qRT-PCR done

in other groups have shown an increased trend [320]. Recently, however, Bodega et al. reported that overexpression of *FRG1* in muscle biopsies is not a uniform finding and may depend on the composition and age of the muscle biopsy, as *FRG1* is only upregulated during an early state of differentiation into myotubes. Regardless of whether the levels of *FRG1* are increased or not in FSHD patients, the H-*FRG1*^{TG} mouse is a valuable tool for studying the mechanics of muscular dystrophy, though it is important to note that *FRG1* expression in these mice is many fold higher than observed in any human patients. Ultimately, FRG1 remains relatively poorly characterized and our findings may help to further elucidate its function.

It has been reported that myoblasts isolated from human muscle biopsies exhibit a morphological difference upon differentiation [348]. The authors observed that, compared to differentiated wild-type myotubes, FSHD myotubes were thinner, less branched, more disorganized and were comprised of fewer myoblasts as measured by total number of nuclei per myotube. Converse to our findings, they did not note any proliferation defects in their myoblast cultures, which may be attributed to differences in their isolation technique, sample sources and/or assay techniques. Regardless of the caveats, this raises the possibility of a compound defect in both proliferation and differentiation as a mechanism for the development of FSHD.

One disparity in our data may be the difference observed between the proliferative defect described in mass culture (Figure 4A) and that seen by mitotic shakeoff analyzed by flow cytometry (Figure 4B). Although the difference seen by mitotic shakeoff is less severe than that observed by mass culture doubling time, it is worth noting that the cells are kept under

different conditions in each of these assays. In mass culture, myoblasts find themselves in much denser conditions with self-conditioned media. In the mitotic shakeoff, myoblasts are in a much less dense environment and exposed to fresh media and growth factors. It is possible that, given enough time, the cell cycle profiles of myoblasts isolated by mitotic shakeoff would exhibit a more severe defect with increased cell density, but it is impossible to determine this within the time frame whereby cells remain synchronized.

In summary, our experiments have demonstrated the expression of *FRG1* in mouse muscle causes a tissue-specific and age-dependent proliferative defect in the satellite cell population, possibly playing a part in the development of muscular dystrophies and FSHD in humans.

Materials and Methods

Animal care and genotyping

High-expressing *FRG1* transgenic mice (H-*FRG1*^{TG}) were kindly provided by Dr. R. Tupler [326]. DNA was extracted from tail samples by digestion with TENS solution (50 mM Tris pH 7.5, 100 mM EDTA pH 8.0, 400 mM NaCl, 0.4% SDS, proteinase K 0.5 mg/mL) followed by ethanol precipitation of genomic DNA. PCR genotyping of FRG1 mice was performed with the following primers: HSA-FRG1-5' 5'-GAT CTA GCG GCC GCC ATG GCC GAG TAC TCC TAT GTG AAG TCT-3' and HSA-FRG1-3' 5'-GCG CGC TTA ATT AAT CAC TTG CAG TAT CTG TCG GCT TTC A-3'. Mice were bred and maintained under specific pathogen-free conditions. All experiments were performed

in compliance with the University of Washington Institutional Animal Care and Use Committee protocol #2362-04.

Analysis of FRG1 expression

Tissue lysates were generated from quadriceps, gastrocnemius, diaphragm, heart, liver, lung and brain tissue isolated from H-*FRG1*^{TG} mice and wild-type littermate controls. Homogenization was done in 5 mL of ice-cold RIPA buffer supplemented with protease inhibitors (50 mM Tris-HCl pH 7.4, 150 mM NaCl, 1% NP-40, 0.25% deoxycholate, 1 mM Na3VO4, 1mM NaF, 1mM PMSF, 1 µg/mL aprotinin, 1 µg/mL leupeptin) per gram of tissue for 30 seconds using the Omni-Tip system (OMNI International). Samples were incubated on ice for 30 minutes, spun down at 16,500 rcf for 15 minutes at 4°C, followed by transferring of supernatant and recentrifugation for an additional 10 minutes to generate tissue lysates.

RNA was isolated from both proliferating and differentiated mouse muscle satellite cell cultures using the RNAqueous kit (Ambion Inc). qPCR was performed using primers as previously described [326]. Cell lysates were also generated from the aforementioned muscle satellite cell cultures by homogenization in RIPA buffer as described above.

Histological analysis of muscle

Quadriceps, gastrocnemius, soleus and diaphragm were isolated from H-*FRG1*^{TG} mice and wild-type littermate controls, blotted briefly on filter paper and weighed on an analytical balance. Tissues were mounted in Tissue-Tek OCT compound (Sakura Finetek), frozen in a liquid nitrogen-cooled bath of isopentane and stored at -80°C. Cryosections were collected using a

Leica CM1850 for hemotoxylin and eosin staining. Stained sections were viewed and photographed under 100x magnification on a Zeiss Axiovert 200M. Analysis of images was performed using AxioVision v4.3.

Isolation of mouse muscle satellite cells and cell culture

To isolate satellite cells, 4-week and 18-week old FRG1 or wild-type mouse thigh or diaphragm muscle tissue was dissected away and placed in chilled Growth Media (GM) consisting of Ham's F10C + 15% horse serum (Atlanta Biologicals Lot D0195) + 50 µg/ml gentamicin with the addition of 0.25 µg/ml Fungizone. Connective tissue and fat were dissected away from muscle tissue under a dissecting microscope and muscle was weighed on an analytical balance. Isolation of the myoblastic population was performed as previously described [332], with the following modifications and details. Diced muscle was minced for 2 minutes using curved-tip scissors and treated with 50 µL of 0.05% trypsin-EDTA (Gibco) diluted in Hank's saline per mg of tissue. The tissue/trypsin mixture was incubated at 37°C and pipetted thoroughly every 5 minutes for 20 minutes total. The trypsinized tissue mixture was then passed through a 70 µm cell strainer (BD Falcon) to reduce fibroblast contamination and the strainer was rinsed with an additional 100 µL of F10C per mg of tissue. The flowthrough was then centrifuged at 800 rpm (Sorvall Legend T) for 5 minutes and plated on gelatin-coated dishes in GM + 6 ng/ml basic fibroblast growth factor (bFGF) + 0.25 µg/ml Fungizone [332]. The satellite cell cultures were observed carefully and differentially passaged to eliminate any fibroblast contamination over 5 passages. To differential passage, satellite cells were treated to a mild trypsinization and observed under a microscope until the round satellite cells were seen

detaching from the plate. Because of their morphological differences, satellite cells will detach from the dish before the flattened and larger fibroblasts. Once the satellite cells were observed detaching, the trypsin solution was immediately removed and plated to isolate the satellite cell population.

The established mouse-derived satellite cell cultures were cultured on 10 cm collagen-coated tissue culture plates in GM with 4 ng/ml bFGF. Cells were supplemented with fresh bFGF every 12 hours to inhibit differentiation of satellite cells into myocytes. Passaging occurred when cells reached 5 x 10^5 cells in a 10 cm dish by rinsing with Saline A (10 mM dextrose, 30 mM HEPES, 3 mM KCl, 130 mM NaCl, 1 mM Na_2HPO_4-$7H_2O$), trypsinization and replating at 5 x 10^4 in a new 10 cm dish.

iC2C12-FRG1 myoblasts were generated as described and generously provided by Dr. Michael Kyba at the University of Texas Southwestern [349]. iC2C12-FRG1 myoblasts were maintained in DMEM (Hyclone) + 10% FBS (Atlanta Biologicals Lot A0087) taking care to passage before confluency to avoid loss of the myoblastic population. Induction of FRG1-FLAG in iC2C12-FRG1 myoblasts was achieved by incubating cells with 500 ng/mL doxycycline for 24 hours.

Clonal analysis of proliferation

To perform clonal assays, proliferating satellite cells were trypsinized and plated at 1000 cells per 10 cm dish in GM with 6 ng/mL bFGF to prevent premature differentiation. Cells were left undisturbed to minimize the formation of satellite clones and fixed with AFA (50% ethanol, 5% formalin, 5% acetic acid) at regular intervals. Myoblast clones were then immunostained for

myosin heavy-chain (MyHC) using mouse monoclonal MF-20, biotinylated rabbit anti-mouse IgG, streptavidin and biotinylated horseradish peroxidase (Vector Labs, Inc.), followed by counterstaining with 1% methylene blue as previously described [95]. Clones were then scored by visualization at 25X/50X magnification on a dissecting microscope for both number and percent differentiation. Doubling times were calculated with the formula "Doubling Time = [Time post-plating * Ln(2)] / Ln(average clone size)".

Viral transduction of C2C12 myoblasts

Expression vectors for *FRG1* were generated in the pMXIH vector as described previously [333]. 293T cells were transfected with either pMXIH or pMXIH-FRG1 in combination with the ϕ-ampho packaging plasmid using calcium phosphate. Virus-containing media were filtered through a 0.45 μm filter and applied to C2C12 myoblasts to generate C2C12-pMXIH vector control myoblasts and C2C12-FRG1 myoblasts which should stably express FRG1 protein.

Flow cytometry and other proliferation assays

To assay doubling time of iC2C12-FRG1 myoblasts, proliferating cells were grown in the presence or absence of doxycycline to induce expression of *FRG1*. 2000 cells were plated per well of a 24-well dish. One well of cells plated in this dish per condition was trypsinized every 24 hours over 120 hours and total cell number was counted in triplicate on an improved Neubauer hemocytometer. Cell number was graphed and exponential curve fit was performed using Microsoft Excel to determine the growth constant and calculate the doubling time.

For BrdU staining of virally-transduced C2C12 myoblasts, after viral transduction, cells were plated on glass coverslips and pulsed with BrdU cell proliferation reagent (Amersham) for 60 minutes. Cells were then fixed in 4% formalin, permeabilized with 0.5% Triton X-100 in PBS and blocked in 5% goat serum, 5% horse serum, 0.2% Tween-20, 0.2% fish skin gelatin in PBS. α-BrdU mouse antibody (BD Biosciences) was diluted 1:350 in PBS and incubated for 1 hour at 37°C followed by goat α-mouse antibody conjugated to AlexaFluor488 diluted 1:400. Coverslips were mounted using Vectashield (Vector Labs).

For flow cytometry assays, proliferating iC2C12-FRG1 myoblasts were also plated in 10 cm dishes for cell cycle profile analysis. After trypsinization, cell pellets were resuspended in DAPI solution (2 mM $CaCl_2$, 22 mM $MgCl_2$ 0.1 mg/mL BSA, 0.1% Nonidet P-40, 10 μg/mL DAPI, 10% DMSO) and run on an InFlux flow cytometer (Cytopeia). 20,000 cells were run through the flow cytometer measuring DNA content. Analysis was done using WinCycle (Phoenix Flow Systems) to determine cell cycle phase distributions as previously described [350].

For determining initial effects of FRG1 expression in synchronized cells, proliferating iC2C12-FRG1 myoblasts either exposed to doxycycline for 24 hours previously or grown in the absence of doxycycline were synchronized by mitotic shakeoff as described [351]. Three 10-cm dishes were tapped vigorously against a hard surface to shake off mitotic cells, incubated with gentle rocking for 20 minutes to prevent reattachment, then tapped vigorously again to further dislodge mitotic cells, and finally the medium containing mitotic cells was centrifuged and plated in a single 60-mm dish. Twelve 60-mm dishes of synchronized cells were collected and placed either in the presence or absence of doxycycline. Every 2 hours after the initial plating,

cells were trypsinized and pellets were fixed and resuspended in the same DAPI solution used for flow cytometry to cover a total period of 24 hours. DNA content was measure as previously mentioned using flow cytometry, with 20,000 cells being analyzed.

Immunofluorescence and immunoblotting

iC2C12-FRG1 myoblasts with or without the induction of FRG1-FLAG were grown on round glass coverslips, fixed in a 4% formalin solution and stained with mouse monoclonal α-FLAG antibody (Sigma) at 1:10,000 dilution. For cell lysates, proliferating satellite cells or iC2C12-FRG1 myoblasts were lysed in RIPA buffer at 4°C, incubated on ice for 30 minutes, and centrifuged at 16,500 rcf for 10 minutes to remove cell debris. Cell lysates were run on a 10% SDS-PAGE gel, transferred to nitrocellulose overnight at 4°C in a Tris-glycine buffer and incubated overnight at 4°C with one of the following primary antibodies. Monoclonal α-FRG1 at 1:1000 (Abnova clone 4A5), mouse monoclonal pRb at 1:1000 (BD Pharmingen clone 14001A), rabbit anti-mouse α-pRb Ser795 at 1:1000 (Cell Signaling), rabbit anti-mouse α-pRb Ser807/811 at 1:1000 (Cell Signaling), or mouse monoclonal α-β-actin at 1:10000 (Abcam). Western blotting was completed the next day using the corresponding secondary antibody of donkey anti-rabbit HRP at 1:10000 (Amersham Biosciences) or rabbit anti-mouse HRP at 1:10000 (Amersham Biosciences). Blots were visualized using ECL substrate (PerkinElmer) on Kodak Biomax Light (Sigma) film.

Acknowledgements

This work was supported by a grant from the Pacific Northwest Friends of FSHD. S.C.C. is supported by the cardiovascular pathology training grant NIH T32 HL007312. The authors would like to thank Rubysue Mangalindan, Ashot Safarli and other members of the Ladiges lab in the Department of Comparative Medicine for handling and maintenance of mouse colonies. Flow cytometry and assistance with analysis was graciously provided by Donna Prunkard in the Rabinovitch lab, Department of Pathology, UW.

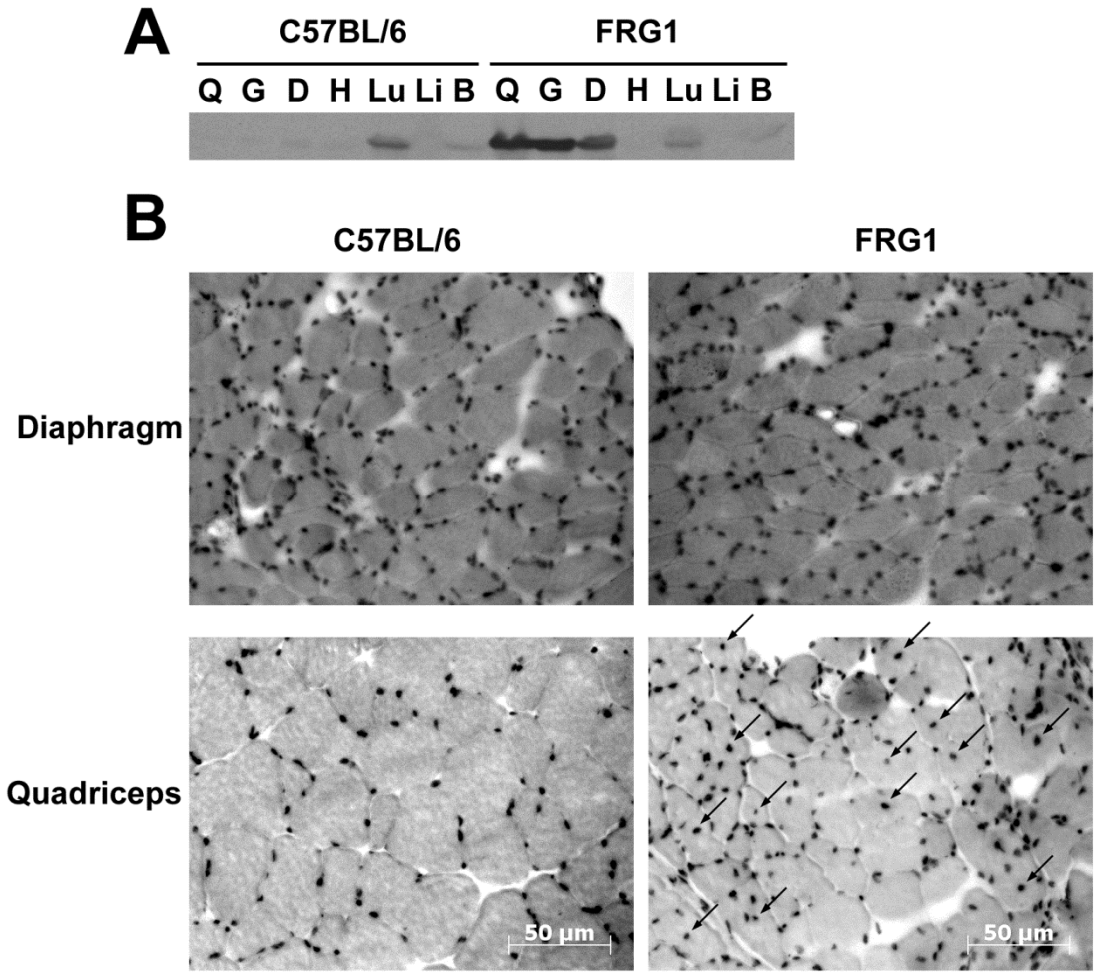

Figure 1. FRG1 expression and dystrophic phenotype of mice. (A) Muscles and tissue from either H-*FRG1*^{TG} transgenic mice (FRG1) or wild-type littermate control (C57BL/6) were collected from 10-week old mice. 300 µg of total protein from tissue lysates isolated from quadriceps muscle (Q), gastrocnemius muscle (G), diaphragm muscle (D), whole heart (H), lung tissue (Lu), liver tissue (Li) and brain tissue (B) were probed with α-FRG1 antibody after SDS-PAGE. **(B)** Diaphragm and quadriceps muscle from 13-week old H-*FRG1*^{TG} mouse (FRG1) or wild-type littermate control (C57BL/6) stained with hemotoxylin/eosin and viewed under 100X

magnification. Arrows note location of centrally located nuclei present in FRG1 cross-section. Scale bar notes 50 µm.

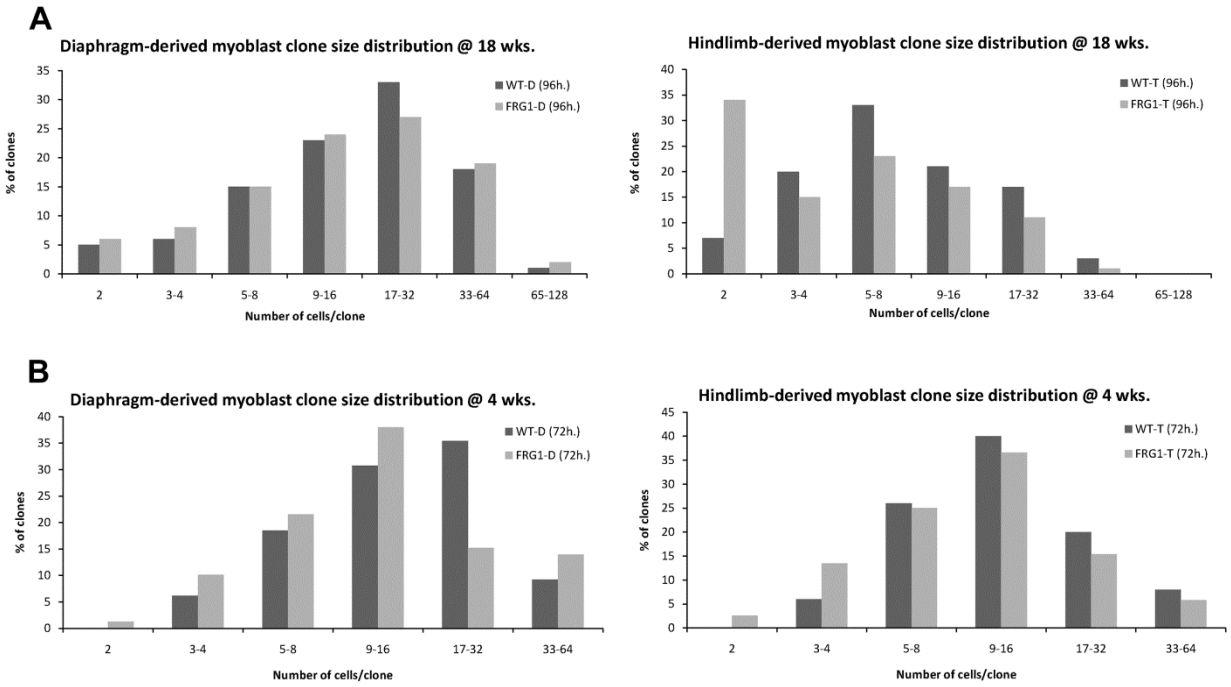

Figure 2. Clonal analysis of mouse-derived myoblasts. (A) Myoblasts isolated from diaphragm (D) or thigh (T) of 18-week old H-*FRG1*^{TG} mice (FRG1) or wild-type littermate controls (WT) were cultured and plated at low density. Cells were fixed at regular time intervals and stained for myosin heavy chain. Total number of nuclei per clone was counted and a representative graph of data from 96-hours post-plating is shown (n = 100). **(B)** Myoblasts isolated from diaphragm (D) or thigh (T) of 4-week old H-*FRG1*^{TG} mice (FRG1) or wild-type littermate controls (WT) were scored for proliferation as above at 72-hours post-plating ($50 < n < 80$).

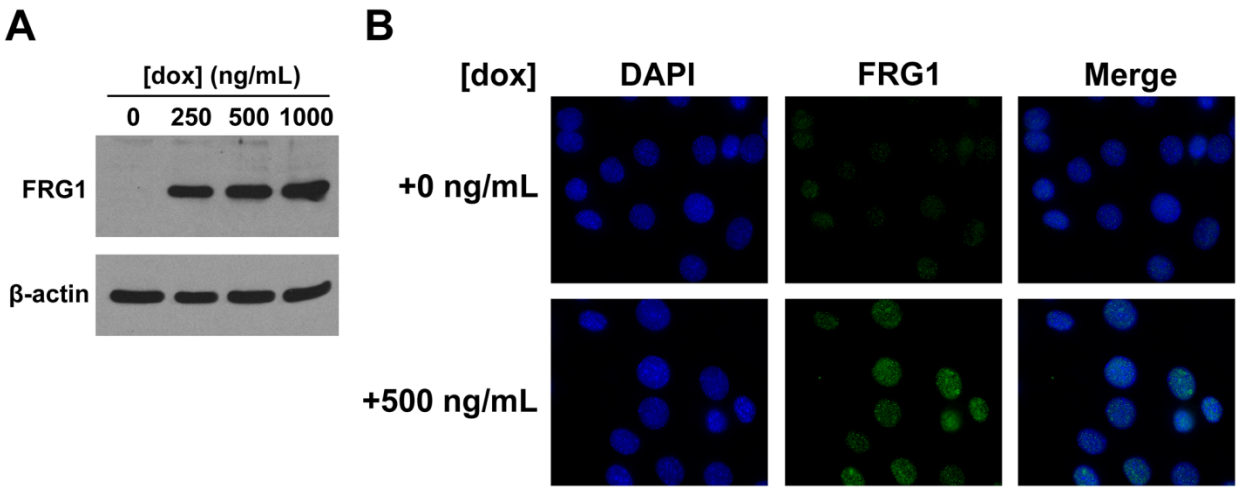

Figure 3. Expression of FRG1 in iC2C12-FRG1 myoblasts. (A) Western blot of lysates from iC2C12-FRG1 myoblasts before induction with doxycycline or after induction for 24 hours with concentrations ranging from 250 ng/mL to 1000 ng/mL using α-FLAG antibody. β-actin loading control shown below. **(B)** Localization of FRG1 by immunofluorescence in iC2C12-FRG1either uninduced or induced with 500 ng/mL doxycycline for 24 hours. DAPI stain is represented in the blue channel and α-FRG1 antibody staining is represented in the green channel.

A

	+0 ng/ml dox	+500 ng/ml dox	
Doubling time	20.2 ± 2.2 h.	**34.4 ± 6.6 h. ***	
	+0 ng/ml dox	**+500 ng/ml dox**	
		24 h. total	**72 h. total**
% G1-phase	45.7 ± 4.4%	**51.8 ± 3.5% ***	**55.8 ± 2.8% ****
% S-phase	37.7 ± 5.4%	**32.6 ± 3.3%**	**29.2 ± 3.6% ***
% G2-phase	16.6 ± 2.5%	15.7 ± 2.6%	15.1 ± 2.0%

* $p < 0.05$ vs 0 ng/ml dox
** $p < 0.005$ vs 0 ng/ml dox

B

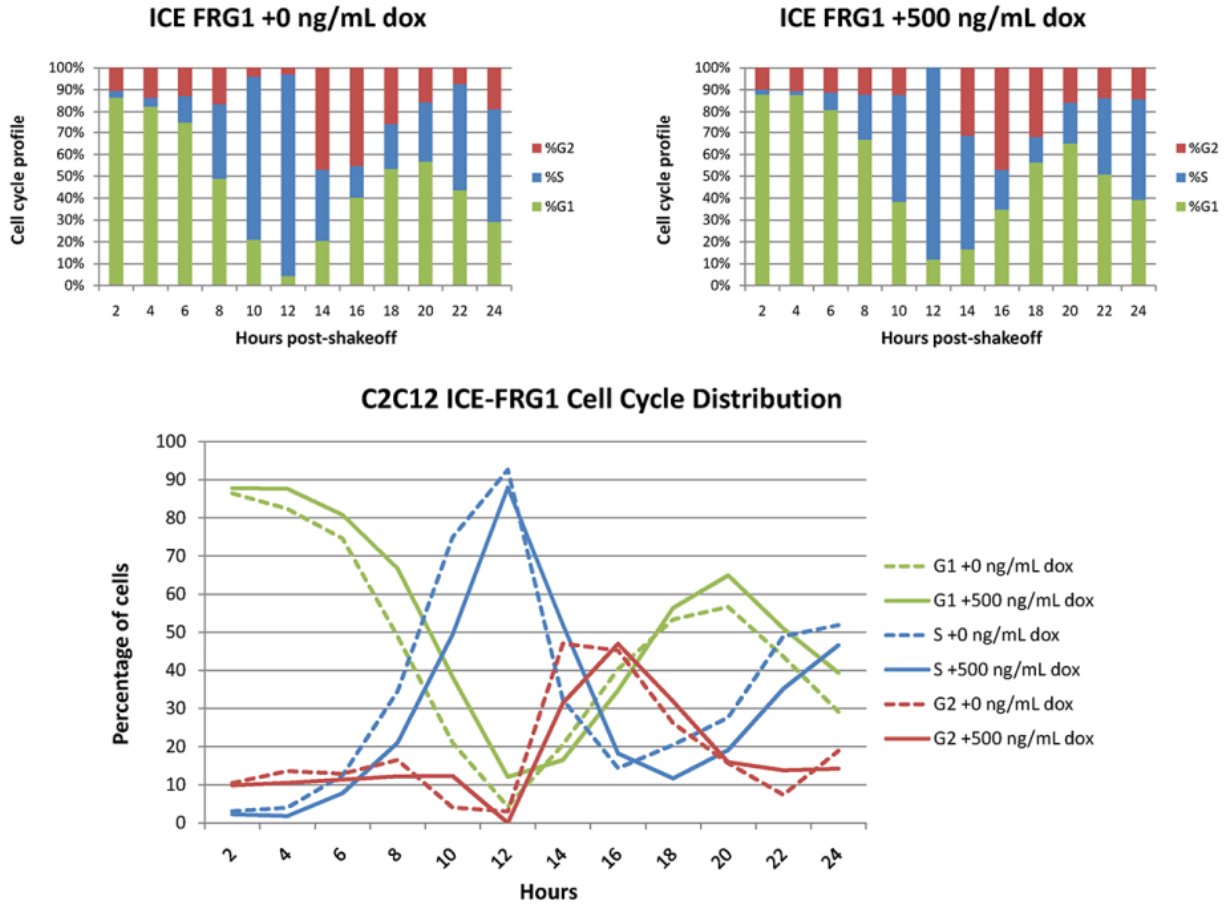

Figure 4. Characterization of proliferation defect in iC2C12-FRG1 myoblasts. (A) Mass culture doubling times calculated from hemocytometer counts of iC2C12-FRG1 myoblasts with or without induction of expression by doxycycline over 120 hours. Below are the cell cycle profiles of uninduced iC2C12-FRG1 myoblasts as well as after 24 hours and 72 hours in the presence of doxycycline. Cell cycle profiles were calculated from DNA content analysis by flow cytometry on proliferating myoblasts that were fixed and DAPI stained. * denotes statistical significance $p<0.05$, ** $p<0.005$. **(B)** Cell cycle profiles of synchronized iC2C12-*FRG1* myoblasts over 24 hours in the absence or presence of doxycycline showing fraction of cells in G1, S or G2-phase. Comparison of data is plotted in a line graph fashion showing G1 in green, S in blue and G2 in red to demonstrate the generalized lag exhibited by iC2C12-*FRG1* myoblasts expressing *FRG1*. Uninduced iC2C12-FRG1 myoblasts are graphed with a dashed line, while iC2C12-*FRG1* myoblasts with doxycycline-induced *FRG1* expression are graphed with a solid line. $n > 20,000$ cells analyzed for each time point.

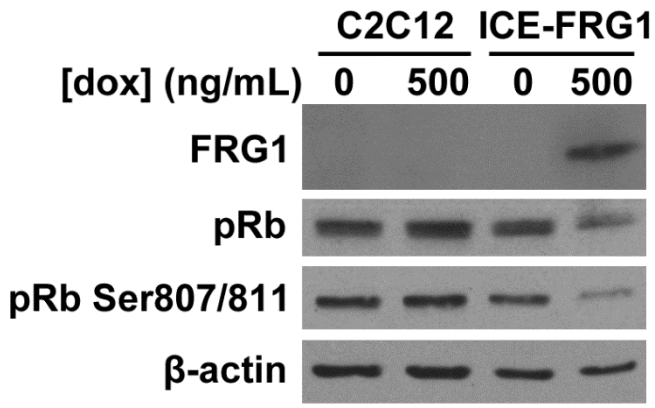

Figure 5. Phosphorylation of pRb is perturbed by FRG1 expression. Western blot analysis for pRb, pRb Ser807/811 and FRG1 in iC2C12-FRG1 cells grown in the presence or absence of doxycycline. β-actin loading control shown below.

	4 wk. old		18 wk. old		
Hours post-plating	**48 h.**	**72 h.**	**48 h.**	**96 h.**	**144 h.**
BL/6-D	18	17.4	19.9	22.2	25.6
FRG1-D	17.4	17.7	25.7	21.9	24.4
BL/6-T	18.6	18.8	23	28.1	26
FRG1-T	18.5	19.4	**31.1**	**33.3**	**28.2**

Average calculated doubling time of myoblasts isolated from 4-week or 18-week old H-*FRG1*^{TG} mice (FRG1) or wild-type littermate control (BL/6) at varying times post-plating. Doubling times were calculated from average clone size with the following formula: [T *Ln(2)]/Ln(average clone size).
doi:10.1371/journal.pone.0019780.t001

Table 1. Doubling times derived from clonal assays.

	2	4	6	8	10	12	14	16	18	20	22	24
ICE FRG1 −dox												
%G1	86.41	82.4	74.58	48.95	21.03	4.31	20.55	40.35	53.35	56.66	43.65	29.16
%S	3.11	4	12.52	34.53	74.94	92.66	32.41	14.43	20.47	27.68	48.95	51.91
%G2	10.48	13.6	12.9	16.52	4.03	3.03	47.04	45.22	26.18	15.66	7.4	18.93
ICE FRG1 +dox												
%G1	87.83	87.67	80.81	66.74	38.25	12.04	16.5	34.75	56.41	64.96	50.97	39.37
%S	2.31	1.82	7.83	21.04	49.45	87.96	52.06	18.24	11.67	19.11	35.2	46.6
%G2	9.86	10.51	11.36	12.22	12.3	0	31.44	47.01	31.92	15.93	13.83	14.23

Values from WinCycle analysis of synchronized ICE-FRG1 myoblasts in the presence or absence of doxycycline-induced FRG1 expression showing fraction of cells in G1, S or G2-phase of the cell cycle plotted in table form to emphasize differences. N>20,000 analyzed for each timepoint.
doi:10.1371/journal.pone.0019780.t002

Table 2. Raw cell cycle profile data

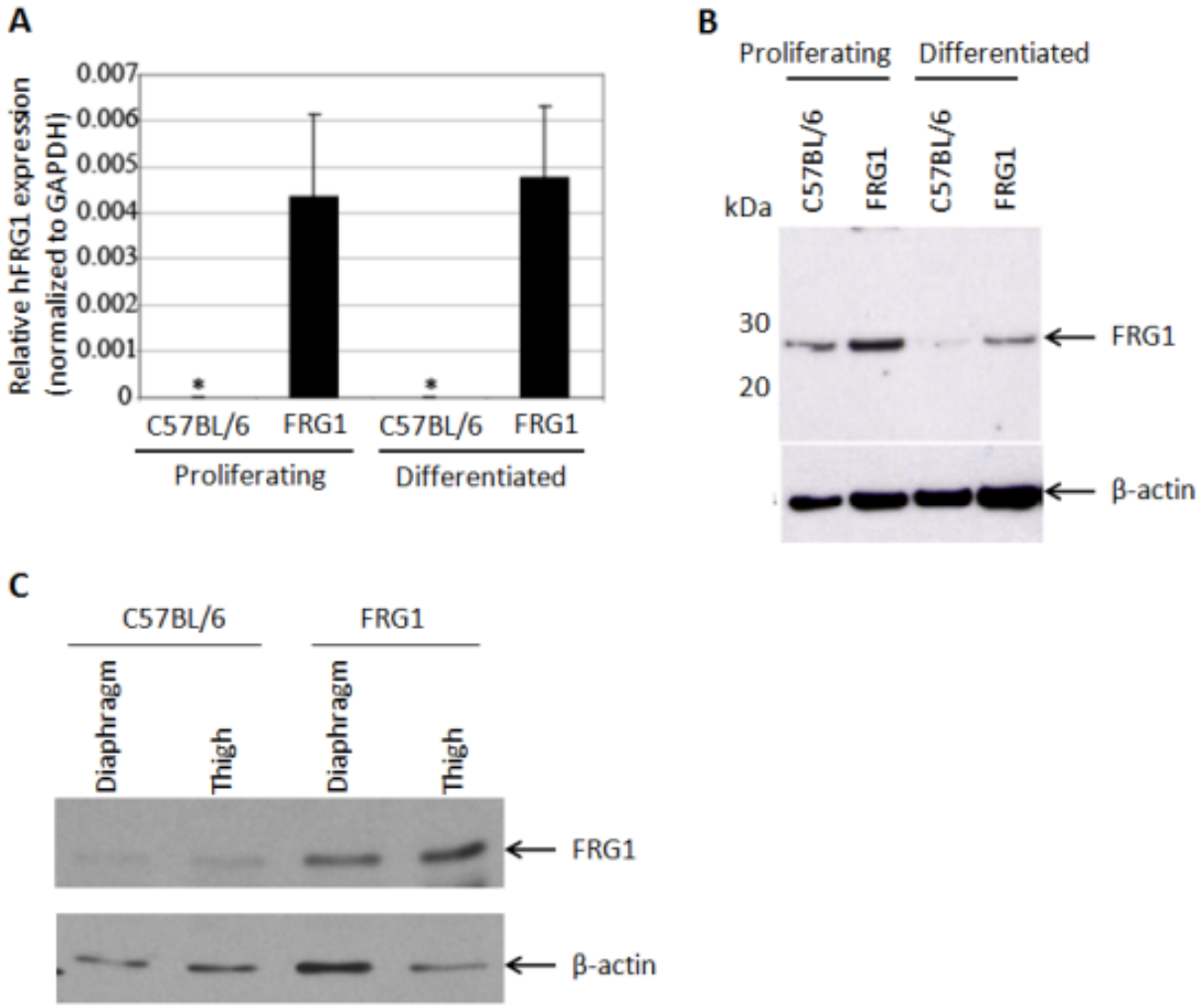

Figure S1. Examination of *FRG1* expression in muscle-derived myoblasts. (A) Levels of *FRG1* in 20-week old diaphragm-derived myoblasts from either H-*FRG1*^{TG} (FRG1) or wild-type littermate control (C57BL/6) as assayed by qPCR normalized to GAPDH. Proliferating cultures were judged to have less than 5% differentiated cells while differentiated cultures exhibited greater than 70% differentiation. * indicates no expression detected. **(B)** Western analysis on proliferating and differentiated diaphragm-derived myoblast cultures from 20-week old mice as described above probing for total FRG1 levels. β-actin loading control shown below. **(C)** Western analysis on proliferating satellite cell cultures from diaphragm or thigh of 4-week old mice probing for total FRG1 protein levels. β-actin loading control shown below.

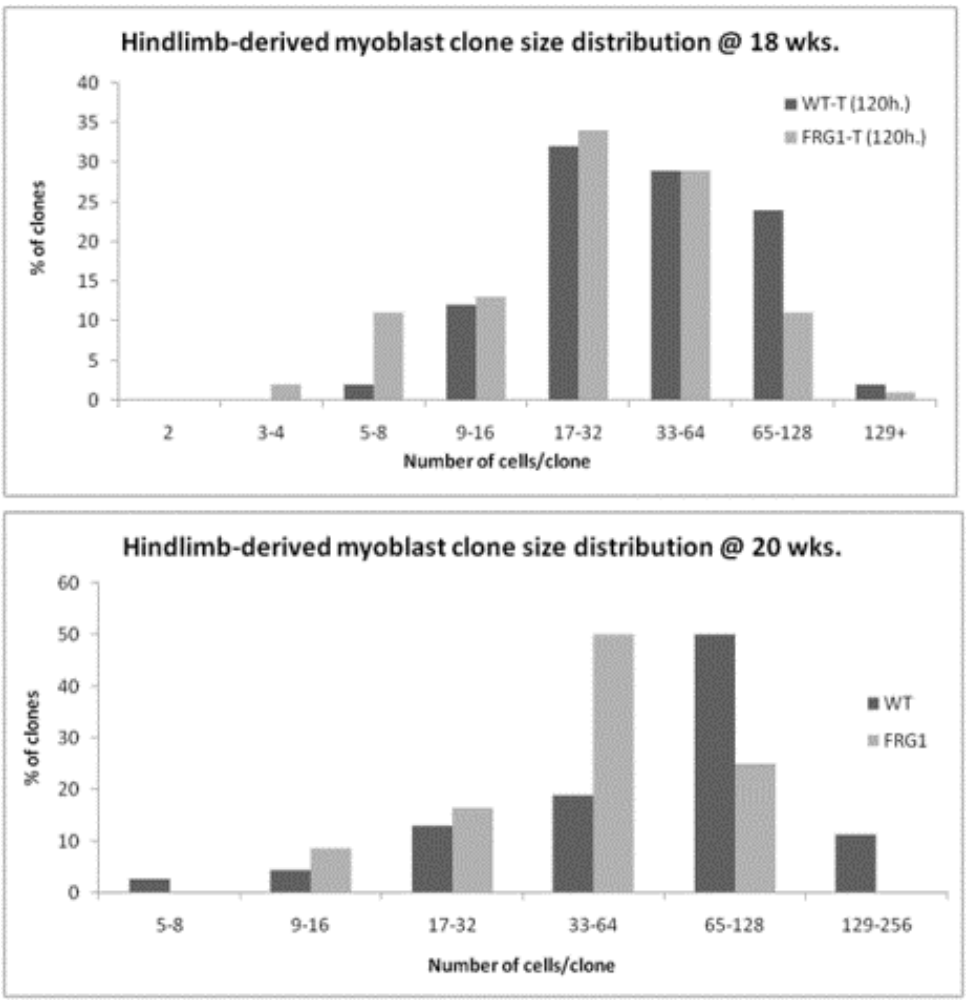

Figure S2. Additional clonal analysis of mouse-derived myoblasts. Myoblasts isolated from hindlimb of 18-week old H-*FRG1*^{TG} (FRG1) or wild-type littermate controls (WT) were cultured and plated at low-density. Total number of nuclei per clone were counted at 120-hours post-plating (n = 100). Similarly myoblasts isolated from dissected hindlimbs of 20-week old H-*FRG1*^{TG} mouse (FRG1) or wild-type littermate controls (WT) were subjected to this procedure in the lower figure showing total number of nuclei per clone at 120-hours post-plating (n = 13 for FRG1 line, n = 73 for WT line).

Cell line/passage	Total cells	BrdU+ cells	% S-phase
C2C12-pMXIH (early)	260	86	33%
C2C12-FRG1 (early)	260	23	9%
C2C12-pMXIH (late)	2575	602	23%
C2C12-FRG1 (late)	2570	672	26%

Figure S3. Loss of proliferative defect in virus-transduced C2C12 myoblasts. C2C12 mouse myoblasts transduced with either vector control (pMXIH) or a *FRG1*-expressing construct (*FRG1*) were scored for incorporation of BrdU after 60-minute pulse to determine % of S-phase cells. Transduced myoblasts show proliferative defect at early passages (passage 8) but lose the phenotype over time.

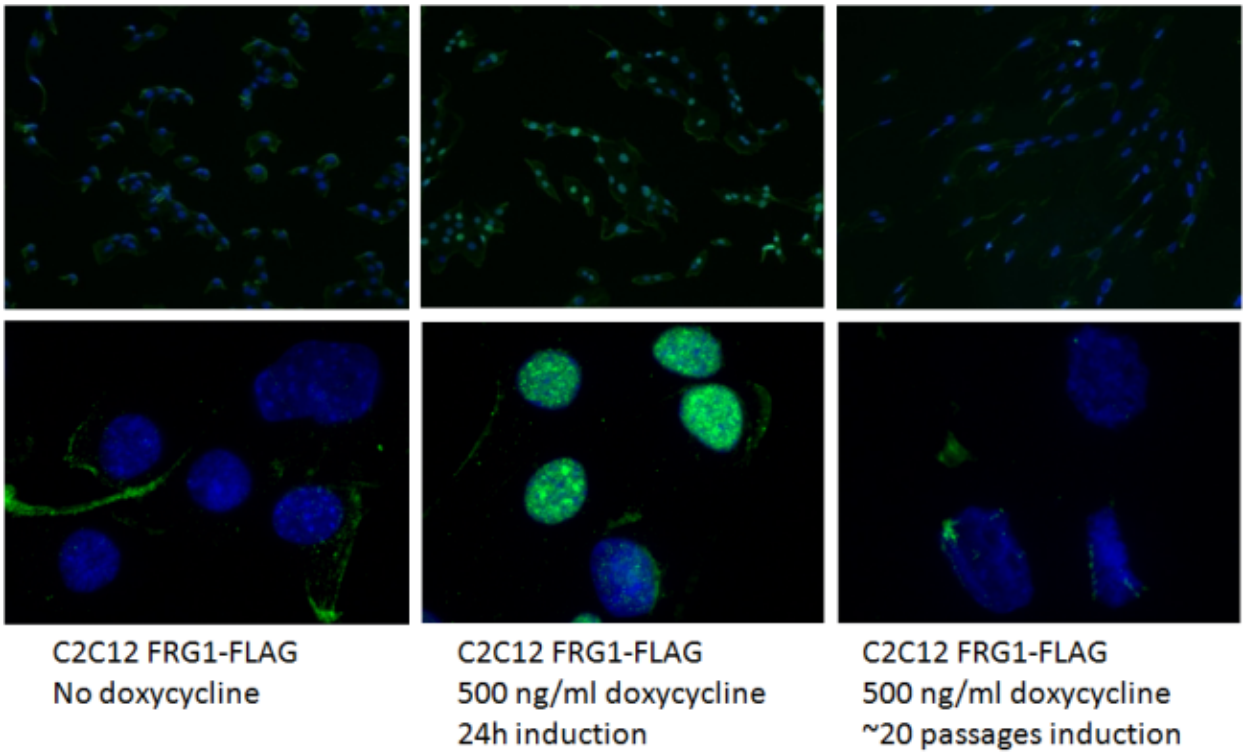

Figure S4. Loss of FRG1 expression in iC2C12-FRG1 myoblasts over time. iC2C12-FRG1 myoblasts were cultured and maintained with or without the presence of 500 ng/mL doxycycline to induce *FRG1* expression. Immunofluorescence with an α-FLAG antibody (green) and DAPI staining (blue) reveals loss of *FRG1* expression after ~20 passages under induction conditions, but robust expression with an acute induction of 24 hours.

References

1. Fawcett DW (1966) On the occurrence of a fibrous lamina on the inner aspect of the nuclear envelope in certain cells of vertebrates. Am J Anat 119: 129-145.
2. Gerace L, Blum A, Blobel G (1978) Immunocytochemical localization of the major polypeptides of the nuclear pore complex-lamina fraction. Interphase and mitotic distribution. J Cell Biol 79: 546-566.
3. McKeon FD, Kirschner MW, Caput D (1986) Homologies in both primary and secondary structure between nuclear envelope and intermediate filament proteins. Nature 319: 463-468.
4. Furukawa K, Inagaki H, Hotta Y (1994) Identification and cloning of an mRNA coding for a germ cell-specific A-type lamin in mice. Exp Cell Res 212: 426-430.
5. Machiels BM, Zorenc AH, Endert JM, Kuijpers HJ, van Eys GJ, et al. (1996) An alternative splicing product of the lamin A/C gene lacks exon 10. J Biol Chem 271: 9249-9253.
6. Furukawa K, Hotta Y (1993) cDNA cloning of a germ cell specific lamin B3 from mouse spermatocytes and analysis of its function by ectopic expression in somatic cells. EMBO J 12: 97-106.
7. Peter M, Kitten GT, Lehner CF, Vorburger K, Bailer SM, et al. (1989) Cloning and sequencing of cDNA clones encoding chicken lamins A and B1 and comparison of the primary structures of vertebrate A- and B-type lamins. J Mol Biol 208: 393-404.
8. Vorburger K, Lehner CF, Kitten GT, Eppenberger HM, Nigg EA (1989) A second higher vertebrate B-type lamin. cDNA sequence determination and in vitro processing of chicken lamin B2. J Mol Biol 208: 405-415.
9. Rober RA, Weber K, Osborn M (1989) Differential timing of nuclear lamin A/C expression in the various organs of the mouse embryo and the young animal: a developmental study. Development 105: 365-378.
10. Alsheimer M, von Glasenapp E, Hock R, Benavente R (1999) Architecture of the nuclear periphery of rat pachytene spermatocytes: distribution of nuclear envelope proteins in relation to synaptonemal complex attachment sites. Mol Biol Cell 10: 1235-1245.
11. Herrmann H, Kreplak L, Aebi U (2004) Isolation, characterization, and in vitro assembly of intermediate filaments. Methods Cell Biol 78: 3-24.
12. Herrmann H, Aebi U (2004) Intermediate filaments: molecular structure, assembly mechanism, and integration into functionally distinct intracellular Scaffolds. Annu Rev Biochem 73: 749-789.
13. Ben-Harush K, Wiesel N, Frenkiel-Krispin D, Moeller D, Soreq E, et al. (2009) The supramolecular organization of the C. elegans nuclear lamin filament. J Mol Biol 386: 1392-1402.
14. Farnsworth CC, Wolda SL, Gelb MH, Glomset JA (1989) Human lamin B contains a farnesylated cysteine residue. J Biol Chem 264: 20422-20429.
15. Sobotka-Briner C, Chelsky D (1992) COOH-terminal methylation of lamin B and inhibition of methylation by farnesylated peptides corresponding to lamin B and other CAAX motif proteins. J Biol Chem 267: 12116-12122.
16. Holtz D, Tanaka RA, Hartwig J, McKeon F (1989) The CaaX motif of lamin A functions in conjunction with the nuclear localization signal to target assembly to the nuclear envelope. Cell 59: 969-977.
17. Kitten GT, Nigg EA (1991) The CaaX motif is required for isoprenylation, carboxyl methylation, and nuclear membrane association of lamin B2. J Cell Biol 113: 13-23.
18. Firmbach-Kraft I, Stick R (1993) The role of CaaX-dependent modifications in membrane association of Xenopus nuclear lamin B3 during meiosis and the fate of B3 in transfected mitotic cells. J Cell Biol 123: 1661-1670.

19. Hofemeister H, Weber K, Stick R (2000) Association of prenylated proteins with the plasma membrane and the inner nuclear membrane is mediated by the same membrane-targeting motifs. Mol Biol Cell 11: 3233-3246.
20. Kudlow BA, Kennedy BK, Monnat RJ, Jr. (2007) Werner and Hutchinson-Gilford progeria syndromes: mechanistic basis of human progeroid diseases. Nat Rev Mol Cell Biol 8: 394-404.
21. D'Angelo MA, Hetzer MW (2006) The role of the nuclear envelope in cellular organization. Cell Mol Life Sci 63: 316-332.
22. Feldherr CM, Kallenbach E, Schultz N (1984) Movement of a karyophilic protein through the nuclear pores of oocytes. J Cell Biol 99: 2216-2222.
23. Burke B, Gerace L (1986) A cell free system to study reassembly of the nuclear envelope at the end of mitosis. Cell 44: 639-652.
24. Ulitzur N, Gruenbaum Y (1989) Nuclear envelope assembly around sperm chromatin in cell-free preparations from Drosophila embryos. FEBS Lett 259: 113-116.
25. Dabauvalle MC, Loos K, Merkert H, Scheer U (1991) Spontaneous assembly of pore complex-containing membranes ("annulate lamellae") in Xenopus egg extract in the absence of chromatin. J Cell Biol 112: 1073-1082.
26. Ulitzur N, Harel A, Feinstein N, Gruenbaum Y (1992) Lamin activity is essential for nuclear envelope assembly in a Drosophila embryo cell-free extract. J Cell Biol 119: 17-25.
27. Ulitzur N, Harel A, Goldberg M, Feinstein N, Gruenbaum Y (1997) Nuclear membrane vesicle targeting to chromatin in a Drosophila embryo cell-free system. Mol Biol Cell 8: 1439-1448.
28. Lenz-Bohme B, Wismar J, Fuchs S, Reifegerste R, Buchner E, et al. (1997) Insertional mutation of the Drosophila nuclear lamin Dm0 gene results in defective nuclear envelopes, clustering of nuclear pore complexes, and accumulation of annulate lamellae. J Cell Biol 137: 1001-1016.
29. Liu J, Rolef Ben-Shahar T, Riemer D, Treinin M, Spann P, et al. (2000) Essential roles for Caenorhabditis elegans lamin gene in nuclear organization, cell cycle progression, and spatial organization of nuclear pore complexes. Mol Biol Cell 11: 3937-3947.
30. Lopez-Soler RI, Moir RD, Spann TP, Stick R, Goldman RD (2001) A role for nuclear lamins in nuclear envelope assembly. J Cell Biol 154: 61-70.
31. Newport JW, Wilson KL, Dunphy WG (1990) A lamin-independent pathway for nuclear envelope assembly. J Cell Biol 111: 2247-2259.
32. Meier J, Campbell KH, Ford CC, Stick R, Hutchison CJ (1991) The role of lamin LIII in nuclear assembly and DNA replication, in cell-free extracts of Xenopus eggs. J Cell Sci 98 (Pt 3): 271-279.
33. Ellis DJ, Jenkins H, Whitfield WG, Hutchison CJ (1997) GST-lamin fusion proteins act as dominant negative mutants in Xenopus egg extract and reveal the function of the lamina in DNA replication. J Cell Sci 110 (Pt 20): 2507-2518.
34. Spann TP, Moir RD, Goldman AE, Stick R, Goldman RD (1997) Disruption of nuclear lamin organization alters the distribution of replication factors and inhibits DNA synthesis. J Cell Biol 136: 1201-1212.
35. Moir RD, Spann TP, Herrmann H, Goldman RD (2000) Disruption of nuclear lamin organization blocks the elongation phase of DNA replication. J Cell Biol 149: 1179-1192.
36. Moir RD, Spann TP, Goldman RD (1995) The dynamic properties and possible functions of nuclear lamins. Int Rev Cytol 162B: 141-182.
37. Walter J, Sun L, Newport J (1998) Regulated chromosomal DNA replication in the absence of a nucleus. Mol Cell 1: 519-529.
38. Venables RS, McLean S, Luny D, Moteleb E, Morley S, et al. (2001) Expression of individual lamins in basal cell carcinomas of the skin. Br J Cancer 84: 512-519.

39. Imai S, Nishibayashi S, Takao K, Tomifuji M, Fujino T, et al. (1997) Dissociation of Oct-1 from the nuclear peripheral structure induces the cellular aging-associated collagenase gene expression. Mol Biol Cell 8: 2407-2419.
40. Mancini MA, Shan B, Nickerson JA, Penman S, Lee WH (1994) The retinoblastoma gene product is a cell cycle-dependent, nuclear matrix-associated protein. Proc Natl Acad Sci U S A 91: 418-422.
41. Ozaki T, Saijo M, Murakami K, Enomoto H, Taya Y, et al. (1994) Complex formation between lamin A and the retinoblastoma gene product: identification of the domain on lamin A required for its interaction. Oncogene 9: 2649-2653.
42. Spann TP, Goldman AE, Wang C, Huang S, Goldman RD (2002) Alteration of nuclear lamin organization inhibits RNA polymerase II-dependent transcription. J Cell Biol 156: 603-608.
43. Dessev G, Goldman R (1988) Meiotic breakdown of nuclear envelope in oocytes of Spisula solidissima involves phosphorylation and release of nuclear lamin. Dev Biol 130: 543-550.
44. Paddy MR, Belmont AS, Saumweber H, Agard DA, Sedat JW (1990) Interphase nuclear envelope lamins form a discontinuous network that interacts with only a fraction of the chromatin in the nuclear periphery. Cell 62: 89-106.
45. Luderus ME, de Graaf A, Mattia E, den Blaauwen JL, Grande MA, et al. (1992) Binding of matrix attachment regions to lamin B1. Cell 70: 949-959.
46. Luderus ME, den Blaauwen JL, de Smit OJ, Compton DA, van Driel R (1994) Binding of matrix attachment regions to lamin polymers involves single-stranded regions and the minor groove. Mol Cell Biol 14: 6297-6305.
47. Zhao K, Harel A, Stuurman N, Guedalia D, Gruenbaum Y (1996) Binding of matrix attachment regions to nuclear lamin is mediated by the rod domain and depends on the lamin polymerization state. FEBS Lett 380: 161-164.
48. Pickersgill H, Kalverda B, de Wit E, Talhout W, Fornerod M, et al. (2006) Characterization of the Drosophila melanogaster genome at the nuclear lamina. Nat Genet 38: 1005-1014.
49. Guelen L, Pagie L, Brasset E, Meuleman W, Faza MB, et al. (2008) Domain organization of human chromosomes revealed by mapping of nuclear lamina interactions. Nature 453: 948-951.
50. Taddei A, Hediger F, Neumann FR, Gasser SM (2004) The function of nuclear architecture: a genetic approach. Annu Rev Genet 38: 305-345.
51. Misteli T (2007) Beyond the sequence: cellular organization of genome function. Cell 128: 787-800.
52. Simon DN, Wilson KL (2011) The nucleoskeleton as a genome-associated dynamic 'network of networks'. Nat Rev Mol Cell Biol 12: 695-708.
53. Lammerding J, Schulze PC, Takahashi T, Kozlov S, Sullivan T, et al. (2004) Lamin A/C deficiency causes defective nuclear mechanics and mechanotransduction. J Clin Invest 113: 370-378.
54. Mellad JA, Warren DT, Shanahan CM (2011) Nesprins LINC the nucleus and cytoskeleton. Curr Opin Cell Biol 23: 47-54.
55. Lombardi ML, Jaalouk DE, Shanahan CM, Burke B, Roux KJ, et al. (2011) The interaction between nesprins and sun proteins at the nuclear envelope is critical for force transmission between the nucleus and cytoskeleton. J Biol Chem 286: 26743-26753.
56. Crisp M, Liu Q, Roux K, Rattner JB, Shanahan C, et al. (2006) Coupling of the nucleus and cytoplasm: role of the LINC complex. J Cell Biol 172: 41-53.
57. Nikolova-Krstevski V, Leimena C, Xiao XH, Kesteven S, Tan JC, et al. (2011) Nesprin-1 and actin contribute to nuclear and cytoskeletal defects in lamin A/C-deficient cardiomyopathy. J Mol Cell Cardiol 50: 479-486.
58. Brosig M, Ferralli J, Gelman L, Chiquet M, Chiquet-Ehrismann R (2010) Interfering with the connection between the nucleus and the cytoskeleton affects nuclear rotation, mechanotransduction and myogenesis. Int J Biochem Cell Biol 42: 1717-1728.

59. Bonne G, Di Barletta MR, Varnous S, Becane HM, Hammouda EH, et al. (1999) Mutations in the gene encoding lamin A/C cause autosomal dominant Emery-Dreifuss muscular dystrophy. Nat Genet 21: 285-288.
60. Worman HJ, Ostlund C, Wang Y (2010) Diseases of the nuclear envelope. Cold Spring Harb Perspect Biol 2: a000760.
61. Muchir A, Worman HJ (2007) Emery-Dreifuss muscular dystrophy. Curr Neurol Neurosci Rep 7: 78-83.
62. Bione S, Maestrini E, Rivella S, Mancini M, Regis S, et al. (1994) Identification of a novel X-linked gene responsible for Emery-Dreifuss muscular dystrophy. Nat Genet 8: 323-327.
63. Muchir A, Bonne G, van der Kooi AJ, van Meegen M, Baas F, et al. (2000) Identification of mutations in the gene encoding lamins A/C in autosomal dominant limb girdle muscular dystrophy with atrioventricular conduction disturbances (LGMD1B). Hum Mol Genet 9: 1453-1459.
64. Fatkin D, MacRae C, Sasaki T, Wolff MR, Porcu M, et al. (1999) Missense mutations in the rod domain of the lamin A/C gene as causes of dilated cardiomyopathy and conduction-system disease. N Engl J Med 341: 1715-1724.
65. Brodsky GL, Muntoni F, Miocic S, Sinagra G, Sewry C, et al. (2000) Lamin A/C gene mutation associated with dilated cardiomyopathy with variable skeletal muscle involvement. Circulation 101: 473-476.
66. Canki-Klain N, Recan D, Milicic D, Llense S, Leturcq F, et al. (2000) Clinical variability and molecular diagnosis in a four-generation family with X-linked Emery-Dreifuss muscular dystrophy. Croat Med J 41: 389-395.
67. Vytopil M, Ricci E, Dello Russo A, Hanisch F, Neudecker S, et al. (2002) Frequent low penetrance mutations in the Lamin A/C gene, causing Emery Dreifuss muscular dystrophy. Neuromuscul Disord 12: 958-963.
68. Malhotra R, Mason PK (2009) Lamin A/C deficiency as a cause of familial dilated cardiomyopathy. Curr Opin Cardiol 24: 203-208.
69. van Tintelen JP, Hofstra RM, Katerberg H, Rossenbacker T, Wiesfeld AC, et al. (2007) High yield of LMNA mutations in patients with dilated cardiomyopathy and/or conduction disease referred to cardiogenetics outpatient clinics. American Heart Journal 154: 1130-1139.
70. Parks SB, Kushner JD, Nauman D, Burgess D, Ludwigsen S, et al. (2008) Lamin A/C mutation analysis in a cohort of 324 unrelated patients with idiopathic or familial dilated cardiomyopathy. American Heart Journal 156: 161-169.
71. van Berlo JH, de Voogt WG, van der Kooi AJ, van Tintelen JP, Bonne G, et al. (2005) Meta-analysis of clinical characteristics of 299 carriers of LMNA gene mutations: do lamin A/C mutations portend a high risk of sudden death? J Mol Med 83: 79-83.
72. van Rijsingen IA, Arbustini E, Elliott PM, Mogensen J, Hermans-van Ast JF, et al. (2012) Risk factors for malignant ventricular arrhythmias in lamin a/c mutation carriers a European cohort study. J Am Coll Cardiol 59: 493-500.
73. Lu JT, Muchir A, Nagy PL, Worman HJ (2011) LMNA cardiomyopathy: cell biology and genetics meet clinical medicine. Dis Model Mech 4: 562-568.
74. Becane HM, Bonne G, Varnous S, Muchir A, Ortega V, et al. (2000) High incidence of sudden death with conduction system and myocardial disease due to lamins A and C gene mutation. Pacing Clin Electrophysiol 23: 1661-1666.
75. Bollati M, Barbiroli A, Favalli V, Arbustini E, Charron P, et al. (2012) Structures of the lamin A/C R335W and E347K mutants: implications for dilated cardiolaminopathies. Biochem Biophys Res Commun 418: 217-221.
76. Cao H, Hegele RA (2000) Nuclear lamin A/C R482Q mutation in canadian kindreds with Dunnigan-type familial partial lipodystrophy. Hum Mol Genet 9: 109-112.

77. Shackleton S, Lloyd DJ, Jackson SN, Evans R, Niermeijer MF, et al. (2000) LMNA, encoding lamin A/C, is mutated in partial lipodystrophy. Nat Genet 24: 153-156.
78. Speckman RA, Garg A, Du F, Bennett L, Veile R, et al. (2000) Mutational and haplotype analyses of families with familial partial lipodystrophy (Dunnigan variety) reveal recurrent missense mutations in the globular C-terminal domain of lamin A/C. Am J Hum Genet 66: 1192-1198.
79. Vigouroux C, Magre J, Vantyghem MC, Bourut C, Lascols O, et al. (2000) Lamin A/C gene: sex-determined expression of mutations in Dunnigan-type familial partial lipodystrophy and absence of coding mutations in congenital and acquired generalized lipoatrophy. Diabetes 49: 1958-1962.
80. Ludtke A, Genschel J, Brabant G, Bauditz J, Taupitz M, et al. (2005) Hepatic steatosis in Dunnigan-type familial partial lipodystrophy. Am J Gastroenterol 100: 2218-2224.
81. Dhe-Paganon S, Werner ED, Chi YI, Shoelson SE (2002) Structure of the globular tail of nuclear lamin. J Biol Chem 277: 17381-17384.
82. Krimm I, Ostlund C, Gilquin B, Couprie J, Hossenlopp P, et al. (2002) The Ig-like structure of the C-terminal domain of lamin A/C, mutated in muscular dystrophies, cardiomyopathy, and partial lipodystrophy. Structure 10: 811-823.
83. Novelli G, Muchir A, Sangiuolo F, Helbling-Leclerc A, D'Apice MR, et al. (2002) Mandibuloacral dysplasia is caused by a mutation in LMNA-encoding lamin A/C. Am J Hum Genet 71: 426-431.
84. De Sandre-Giovannoli A, Chaouch M, Kozlov S, Vallat JM, Tazir M, et al. (2002) Homozygous defects in LMNA, encoding lamin A/C nuclear-envelope proteins, cause autosomal recessive axonal neuropathy in human (Charcot-Marie-Tooth disorder type 2) and mouse. Am J Hum Genet 70: 726-736.
85. Sarkar PK, Shinton RA (2001) Hutchinson-Guilford progeria syndrome. Postgrad Med J 77: 312-317.
86. Merideth MA, Gordon LB, Clauss S, Sachdev V, Smith AC, et al. (2008) Phenotype and course of Hutchinson-Gilford progeria syndrome. N Engl J Med 358: 592-604.
87. Scaffidi P, Misteli T (2005) Reversal of the cellular phenotype in the premature aging disease Hutchinson-Gilford progeria syndrome. Nat Med 11: 440-445.
88. Liu B, Wang J, Chan KM, Tjia WM, Deng W, et al. (2005) Genomic instability in laminopathy-based premature aging. Nat Med 11: 780-785.
89. Liu Y, Wang Y, Rusinol AE, Sinensky MS, Liu J, et al. (2008) Involvement of xeroderma pigmentosum group A (XPA) in progeria arising from defective maturation of prelamin A. FASEB J 22: 603-611.
90. Constantinescu D, Csoka AB, Navara CS, Schatten GP (2010) Defective DSB repair correlates with abnormal nuclear morphology and is improved with FTI treatment in Hutchinson-Gilford progeria syndrome fibroblasts. Exp Cell Res 316: 2747-2759.
91. Liu GH, Barkho BZ, Ruiz S, Diep D, Qu J, et al. (2011) Recapitulation of premature ageing with iPSCs from Hutchinson-Gilford progeria syndrome. Nature 472: 221-225.
92. Scaffidi P, Misteli T (2008) Lamin A-dependent misregulation of adult stem cells associated with accelerated ageing. Nat Cell Biol 10: 452-459.
93. Hernandez L, Roux KJ, Wong ES, Mounkes LC, Mutalif R, et al. (2010) Functional coupling between the extracellular matrix and nuclear lamina by Wnt signaling in progeria. Dev Cell 19: 413-425.
94. Sullivan T, Escalante-Alcalde D, Bhatt H, Anver M, Bhat N, et al. (1999) Loss of A-type lamin expression compromises nuclear envelope integrity leading to muscular dystrophy. J Cell Biol 147: 913-920.
95. Frock RL, Kudlow BA, Evans AM, Jameson SA, Hauschka SD, et al. (2006) Lamin A/C and emerin are critical for skeletal muscle satellite cell differentiation. Genes Dev 20: 486-500.
96. Nikolova V, Leimena C, McMahon AC, Tan JC, Chandar S, et al. (2004) Defects in nuclear structure and function promote dilated cardiomyopathy in lamin A/C-deficient mice. J Clin Invest 113: 357-369.

97. van Engelen BG, Muchir A, Hutchison CJ, van der Kooi AJ, Bonne G, et al. (2005) The lethal phenotype of a homozygous nonsense mutation in the lamin A/C gene. Neurology 64: 374-376.
98. Wolf CM, Wang L, Alcalai R, Pizard A, Burgon PG, et al. (2008) Lamin A/C haploinsufficiency causes dilated cardiomyopathy and apoptosis-triggered cardiac conduction system disease. J Mol Cell Cardiol 44: 293-303.
99. Arimura T, Helbling-Leclerc A, Massart C, Varnous S, Niel F, et al. (2005) Mouse model carrying H222P-Lmna mutation develops muscular dystrophy and dilated cardiomyopathy similar to human striated muscle laminopathies. Hum Mol Genet 14: 155-169.
100. Muchir A, Pavlidis P, Decostre V, Herron AJ, Arimura T, et al. (2007) Activation of MAPK pathways links LMNA mutations to cardiomyopathy in Emery-Dreifuss muscular dystrophy. J Clin Invest 117: 1282-1293.
101. Rose BA, Force T, Wang Y (2010) Mitogen-activated protein kinase signaling in the heart: angels versus demons in a heart-breaking tale. Physiol Rev 90: 1507-1546.
102. Bueno OF, De Windt LJ, Tymitz KM, Witt SA, Kimball TR, et al. (2000) The MEK1-ERK1/2 signaling pathway promotes compensated cardiac hypertrophy in transgenic mice. EMBO J 19: 6341-6350.
103. Lorenz K, Schmitt JP, Schmitteckert EM, Lohse MJ (2009) A new type of ERK1/2 autophosphorylation causes cardiac hypertrophy. Nat Med 15: 75-83.
104. Muchir A, Shan J, Bonne G, Lehnart SE, Worman HJ (2009) Inhibition of extracellular signal-regulated kinase signaling to prevent cardiomyopathy caused by mutation in the gene encoding A-type lamins. Hum Mol Genet 18: 241-247.
105. Wu W, Muchir A, Shan J, Bonne G, Worman HJ (2011) Mitogen-activated protein kinase inhibitors improve heart function and prevent fibrosis in cardiomyopathy caused by mutation in lamin A/C gene. Circulation 123: 53-61.
106. Muchir A, Pavlidis P, Bonne G, Hayashi YK, Worman HJ (2007) Activation of MAPK in hearts of EMD null mice: similarities between mouse models of X-linked and autosomal dominant Emery Dreifuss muscular dystrophy. Hum Mol Genet 16: 1884-1895.
107. Mounkes LC, Kozlov SV, Rottman JN, Stewart CL (2005) Expression of an LMNA-N195K variant of A-type lamins results in cardiac conduction defects and death in mice. Hum Mol Genet 14: 2167-2180.
108. Yang SH, Bergo MO, Toth JI, Qiao X, Hu Y, et al. (2005) Blocking protein farnesyltransferase improves nuclear blebbing in mouse fibroblasts with a targeted Hutchinson-Gilford progeria syndrome mutation. Proc Natl Acad Sci U S A 102: 10291-10296.
109. Yang SH, Meta M, Qiao X, Frost D, Bauch J, et al. (2006) A farnesyltransferase inhibitor improves disease phenotypes in mice with a Hutchinson-Gilford progeria syndrome mutation. J Clin Invest 116: 2115-2121.
110. Pendas AM, Zhou Z, Cadinanos J, Freije JM, Wang J, et al. (2002) Defective prelamin A processing and muscular and adipocyte alterations in Zmpste24 metalloproteinase-deficient mice. Nat Genet 31: 94-99.
111. Bergo MO, Gavino B, Ross J, Schmidt WK, Hong C, et al. (2002) Zmpste24 deficiency in mice causes spontaneous bone fractures, muscle weakness, and a prelamin A processing defect. Proc Natl Acad Sci U S A 99: 13049-13054.
112. Fong LG, Ng JK, Meta M, Cote N, Yang SH, et al. (2004) Heterozygosity for Lmna deficiency eliminates the progeria-like phenotypes in Zmpste24-deficient mice. Proc Natl Acad Sci U S A 101: 18111-18116.
113. Fong LG, Frost D, Meta M, Qiao X, Yang SH, et al. (2006) A protein farnesyltransferase inhibitor ameliorates disease in a mouse model of progeria. Science 311: 1621-1623.

114. Fong LG, Ng JK, Lammerding J, Vickers TA, Meta M, et al. (2006) Prelamin A and lamin A appear to be dispensable in the nuclear lamina. J Clin Invest 116: 743-752.
115. Kunz J, Henriquez R, Schneider U, Deuter-Reinhard M, Movva NR, et al. (1993) Target of rapamycin in yeast, TOR2, is an essential phosphatidylinositol kinase homolog required for G1 progression. Cell 73: 585-596.
116. Loewith R, Jacinto E, Wullschleger S, Lorberg A, Crespo JL, et al. (2002) Two TOR complexes, only one of which is rapamycin sensitive, have distinct roles in cell growth control. Mol Cell 10: 457-468.
117. Yip CK, Murata K, Walz T, Sabatini DM, Kang SA (2010) Structure of the human mTOR complex I and its implications for rapamycin inhibition. Mol Cell 38: 768-774.
118. Yang Q, Inoki K, Kim E, Guan KL (2006) TSC1/TSC2 and Rheb have different effects on TORC1 and TORC2 activity. Proc Natl Acad Sci U S A 103: 6811-6816.
119. Inoki K, Li Y, Zhu T, Wu J, Guan KL (2002) TSC2 is phosphorylated and inhibited by Akt and suppresses mTOR signalling. Nat Cell Biol 4: 648-657.
120. Sancak Y, Thoreen CC, Peterson TR, Lindquist RA, Kang SA, et al. (2007) PRAS40 is an insulin-regulated inhibitor of the mTORC1 protein kinase. Mol Cell 25: 903-915.
121. Kim E, Goraksha-Hicks P, Li L, Neufeld TP, Guan KL (2008) Regulation of TORC1 by Rag GTPases in nutrient response. Nat Cell Biol 10: 935-945.
122. Gwinn DM, Shackelford DB, Egan DF, Mihaylova MM, Mery A, et al. (2008) AMPK phosphorylation of raptor mediates a metabolic checkpoint. Mol Cell 30: 214-226.
123. Ma XM, Blenis J (2009) Molecular mechanisms of mTOR-mediated translational control. Nat Rev Mol Cell Biol 10: 307-318.
124. Fingar DC, Salama S, Tsou C, Harlow E, Blenis J (2002) Mammalian cell size is controlled by mTOR and its downstream targets S6K1 and 4EBP1/eIF4E. Genes Dev 16: 1472-1487.
125. Holz MK, Ballif BA, Gygi SP, Blenis J (2005) mTOR and S6K1 mediate assembly of the translation preinitiation complex through dynamic protein interchange and ordered phosphorylation events. Cell 123: 569-580.
126. Magnuson B, Ekim B, Fingar DC (2012) Regulation and function of ribosomal protein S6 kinase (S6K) within mTOR signalling networks. Biochem J 441: 1-21.
127. Chang YY, Neufeld TP (2009) An Atg1/Atg13 complex with multiple roles in TOR-mediated autophagy regulation. Mol Biol Cell 20: 2004-2014.
128. Harrison DE, Strong R, Sharp ZD, Nelson JF, Astle CM, et al. (2009) Rapamycin fed late in life extends lifespan in genetically heterogeneous mice. Nature 460: 392-395.
129. Cao K, Graziotto JJ, Blair CD, Mazzulli JR, Erdos MR, et al. (2011) Rapamycin reverses cellular phenotypes and enhances mutant protein clearance in Hutchinson-Gilford progeria syndrome cells. Sci Transl Med 3: 89ra58.
130. Barr L, Dewey MM, Berger W (1965) Propagation of Action Potentials and the Structure of the Nexus in Cardiac Muscle. J Gen Physiol 48: 797-823.
131. Orkand RK, Nicholls JG, Kuffler SW (1966) Effect of nerve impulses on the membrane potential of glial cells in the central nervous system of amphibia. J Neurophysiol 29: 788-806.
132. Revel JP, Yee AG, Hudspeth AJ (1971) Gap junctions between electrotonically coupled cells in tissue culture and in brown fat. Proc Natl Acad Sci U S A 68: 2924-2927.
133. Paul DL (1986) Molecular cloning of cDNA for rat liver gap junction protein. J Cell Biol 103: 123-134.
134. Beyer EC, Paul DL, Goodenough DA (1987) Connexin43: a protein from rat heart homologous to a gap junction protein from liver. J Cell Biol 105: 2621-2629.
135. Heynkes R, Kozjek G, Traub O, Willecke K (1986) Identification of a rat liver cDNA and mRNA coding for the 28 kDa gap junction protein. FEBS Lett 205: 56-60.

136. Musil LS, Goodenough DA (1993) Multisubunit assembly of an integral plasma membrane channel protein, gap junction connexin43, occurs after exit from the ER. Cell 74: 1065-1077.
137. Lauf U, Giepmans BN, Lopez P, Braconnot S, Chen SC, et al. (2002) Dynamic trafficking and delivery of connexons to the plasma membrane and accretion to gap junctions in living cells. Proc Natl Acad Sci U S A 99: 10446-10451.
138. Harris AL (2007) Connexin channel permeability to cytoplasmic molecules. Prog Biophys Mol Biol 94: 120-143.
139. Saez JC, Berthoud VM, Branes MC, Martinez AD, Beyer EC (2003) Plasma membrane channels formed by connexins: their regulation and functions. Physiol Rev 83: 1359-1400.
140. Sohl G, Willecke K (2003) An update on connexin genes and their nomenclature in mouse and man. Cell Commun Adhes 10: 173-180.
141. Willecke K, Eiberger J, Degen J, Eckardt D, Romualdi A, et al. (2002) Structural and functional diversity of connexin genes in the mouse and human genome. Biol Chem 383: 725-737.
142. Laird DW (2006) Life cycle of connexins in health and disease. Biochem J 394: 527-543.
143. Das Sarma J, Wang F, Koval M (2002) Targeted gap junction protein constructs reveal connexin-specific differences in oligomerization. J Biol Chem 277: 20911-20918.
144. Berthoud VM, Montegna EA, Atal N, Aithal NH, Brink PR, et al. (2001) Heteromeric connexons formed by the lens connexins, connexin43 and connexin56. Eur J Cell Biol 80: 11-19.
145. Jiang JX, Goodenough DA (1996) Heteromeric connexons in lens gap junction channels. Proc Natl Acad Sci U S A 93: 1287-1291.
146. Martinez AD, Hayrapetyan V, Moreno AP, Beyer EC (2002) Connexin43 and connexin45 form heteromeric gap junction channels in which individual components determine permeability and regulation. Circ Res 90: 1100-1107.
147. Martin PE, Blundell G, Ahmad S, Errington RJ, Evans WH (2001) Multiple pathways in the trafficking and assembly of connexin 26, 32 and 43 into gap junction intercellular communication channels. J Cell Sci 114: 3845-3855.
148. George CH, Kendall JM, Evans WH (1999) Intracellular trafficking pathways in the assembly of connexins into gap junctions. J Biol Chem 274: 8678-8685.
149. Jongen WM, Fitzgerald DJ, Asamoto M, Piccoli C, Slaga TJ, et al. (1991) Regulation of connexin 43-mediated gap junctional intercellular communication by Ca2+ in mouse epidermal cells is controlled by E-cadherin. J Cell Biol 114: 545-555.
150. Wei CJ, Francis R, Xu X, Lo CW (2005) Connexin43 associated with an N-cadherin-containing multiprotein complex is required for gap junction formation in NIH3T3 cells. J Biol Chem 280: 19925-19936.
151. Darrow BJ, Laing JG, Lampe PD, Saffitz JE, Beyer EC (1995) Expression of multiple connexins in cultured neonatal rat ventricular myocytes. Circ Res 76: 381-387.
152. Laird DW, Puranam KL, Revel JP (1991) Turnover and phosphorylation dynamics of connexin43 gap junction protein in cultured cardiac myocytes. Biochem J 273(Pt 1): 67-72.
153. Severs NJ, Shovel KS, Slade AM, Powell T, Twist VW, et al. (1989) Fate of gap junctions in isolated adult mammalian cardiomyocytes. Circ Res 65: 22-42.
154. Naus CC, Hearn S, Zhu D, Nicholson BJ, Shivers RR (1993) Ultrastructural analysis of gap junctions in C6 glioma cells transfected with connexin43 cDNA. Exp Cell Res 206: 72-84.
155. Mazet F, Wittenberg BA, Spray DC (1985) Fate of intercellular junctions in isolated adult rat cardiac cells. Circ Res 56: 195-204.
156. Jordan K, Chodock R, Hand AR, Laird DW (2001) The origin of annular junctions: a mechanism of gap junction internalization. J Cell Sci 114: 763-773.
157. Laing JG, Beyer EC (1995) The gap junction protein connexin43 is degraded via the ubiquitin proteasome pathway. J Biol Chem 270: 26399-26403.

158. Laing JG, Tadros PN, Westphale EM, Beyer EC (1997) Degradation of connexin43 gap junctions involves both the proteasome and the lysosome. Exp Cell Res 236: 482-492.
159. Dunn CA, Su V, Lau AF, Lampe PD (2012) Activation of Akt, not connexin 43 protein ubiquitination, regulates gap junction stability. J Biol Chem 287: 2600-2607.
160. van Kempen MJ, Fromaget C, Gros D, Moorman AF, Lamers WH (1991) Spatial distribution of connexin43, the major cardiac gap junction protein, in the developing and adult rat heart. Circ Res 68: 1638-1651.
161. Davis LM, Rodefeld ME, Green K, Beyer EC, Saffitz JE (1995) Gap junction protein phenotypes of the human heart and conduction system. J Cardiovasc Electrophysiol 6: 813-822.
162. Davis LM, Kanter HL, Beyer EC, Saffitz JE (1994) Distinct gap junction protein phenotypes in cardiac tissues with disparate conduction properties. J Am Coll Cardiol 24: 1124-1132.
163. Gourdie RG, Severs NJ, Green CR, Rothery S, Germroth P, et al. (1993) The spatial distribution and relative abundance of gap-junctional connexin40 and connexin43 correlate to functional properties of components of the cardiac atrioventricular conduction system. J Cell Sci 105 (Pt 4): 985-991.
164. Bastide B, Neyses L, Ganten D, Paul M, Willecke K, et al. (1993) Gap junction protein connexin40 is preferentially expressed in vascular endothelium and conductive bundles of rat myocardium and is increased under hypertensive conditions. Circ Res 73: 1138-1149.
165. Kanter HL, Laing JG, Beau SL, Beyer EC, Saffitz JE (1993) Distinct patterns of connexin expression in canine Purkinje fibers and ventricular muscle. Circ Res 72: 1124-1131.
166. Smith JH, Green CR, Peters NS, Rothery S, Severs NJ (1991) Altered patterns of gap junction distribution in ischemic heart disease. An immunohistochemical study of human myocardium using laser scanning confocal microscopy. Am J Pathol 139: 801-821.
167. Peters NS, Green CR, Poole-Wilson PA, Severs NJ (1993) Reduced content of connexin43 gap junctions in ventricular myocardium from hypertrophied and ischemic human hearts. Circulation 88: 864-875.
168. Kostin S, Rieger M, Dammer S, Hein S, Richter M, et al. (2003) Gap junction remodeling and altered connexin43 expression in the failing human heart. Mol Cell Biochem 242: 135-144.
169. Dupont E, Matsushita T, Kaba RA, Vozzi C, Coppen SR, et al. (2001) Altered connexin expression in human congestive heart failure. J Mol Cell Cardiol 33: 359-371.
170. Chen X, Zhang Y (2006) Myocardial Cx43 expression in the cases of sudden death due to dilated cardiomyopathy. Forensic Sci Int 162: 170-173.
171. Reaume AG, de Sousa PA, Kulkarni S, Langille BL, Zhu D, et al. (1995) Cardiac malformation in neonatal mice lacking connexin43. Science 267: 1831-1834.
172. Guerrero PA, Schuessler RB, Davis LM, Beyer EC, Johnson CM, et al. (1997) Slow ventricular conduction in mice heterozygous for a connexin43 null mutation. J Clin Invest 99: 1991-1998.
173. Gutstein DE, Morley GE, Fishman GI (2001) Conditional gene targeting of connexin43: exploring the consequences of gap junction remodeling in the heart. Cell Commun Adhes 8: 345-348.
174. Gutstein DE, Morley GE, Tamaddon H, Vaidya D, Schneider MD, et al. (2001) Conduction slowing and sudden arrhythmic death in mice with cardiac-restricted inactivation of connexin43. Circ Res 88: 333-339.
175. Danik SB, Liu F, Zhang J, Suk HJ, Morley GE, et al. (2004) Modulation of cardiac gap junction expression and arrhythmic susceptibility. Circ Res 95: 1035-1041.
176. van Rijen HV, Eckardt D, Degen J, Theis M, Ott T, et al. (2004) Slow conduction and enhanced anisotropy increase the propensity for ventricular tachyarrhythmias in adult mice with induced deletion of connexin43. Circulation 109: 1048-1055.

177. Eckardt D, Theis M, Degen J, Ott T, van Rijen HV, et al. (2004) Functional role of connexin43 gap junction channels in adult mouse heart assessed by inducible gene deletion. J Mol Cell Cardiol 36: 101-110.
178. Musil LS, Cunningham BA, Edelman GM, Goodenough DA (1990) Differential phosphorylation of the gap junction protein connexin43 in junctional communication-competent and -deficient cell lines. J Cell Biol 111: 2077-2088.
179. Musil LS, Goodenough DA (1991) Biochemical analysis of connexin43 intracellular transport, phosphorylation, and assembly into gap junctional plaques. J Cell Biol 115: 1357-1374.
180. Sosinsky GE, Solan JL, Gaietta GM, Ngan L, Lee GJ, et al. (2007) The C-terminus of connexin43 adopts different conformations in the Golgi and gap junction as detected with structure-specific antibodies. Biochem J 408: 375-385.
181. Solan JL, Lampe PD (2007) Key connexin 43 phosphorylation events regulate the gap junction life cycle. J Membr Biol 217: 35-41.
182. Solan JL, Marquez-Rosado L, Sorgen PL, Thornton PJ, Gafken PR, et al. (2007) Phosphorylation at S365 is a gatekeeper event that changes the structure of Cx43 and prevents down-regulation by PKC. J Cell Biol 179: 1301-1309.
183. Lampe PD, Cooper CD, King TJ, Burt JM (2006) Analysis of Connexin43 phosphorylated at S325, S328 and S330 in normoxic and ischemic heart. J Cell Sci 119: 3435-3442.
184. Cooper CD, Lampe PD (2002) Casein kinase 1 regulates connexin-43 gap junction assembly. J Biol Chem 277: 44962-44968.
185. Atkinson MM, Lampe PD, Lin HH, Kollander R, Li XR, et al. (1995) Cyclic AMP modifies the cellular distribution of connexin43 and induces a persistent increase in the junctional permeability of mouse mammary tumor cells. J Cell Sci 108 (Pt 9): 3079-3090.
186. Warn-Cramer BJ, Lampe PD, Kurata WE, Kanemitsu MY, Loo LW, et al. (1996) Characterization of the mitogen-activated protein kinase phosphorylation sites on the connexin-43 gap junction protein. J Biol Chem 271: 3779-3786.
187. Cottrell GT, Lin R, Warn-Cramer BJ, Lau AF, Burt JM (2003) Mechanism of v-Src- and mitogen-activated protein kinase-induced reduction of gap junction communication. Am J Physiol Cell Physiol 284: C511-520.
188. Warn-Cramer BJ, Cottrell GT, Burt JM, Lau AF (1998) Regulation of connexin-43 gap junctional intercellular communication by mitogen-activated protein kinase. J Biol Chem 273: 9188-9196.
189. Cameron SJ, Malik S, Akaike M, Lerner-Marmarosh N, Yan C, et al. (2003) Regulation of epidermal growth factor-induced connexin 43 gap junction communication by big mitogen-activated protein kinase1/ERK5 but not ERK1/2 kinase activation. J Biol Chem 278: 18682-18688.
190. Ek-Vitorin JF, King TJ, Heyman NS, Lampe PD, Burt JM (2006) Selectivity of connexin 43 channels is regulated through protein kinase C-dependent phosphorylation. Circ Res 98: 1498-1505.
191. Lampe PD, TenBroek EM, Burt JM, Kurata WE, Johnson RG, et al. (2000) Phosphorylation of connexin43 on serine368 by protein kinase C regulates gap junctional communication. J Cell Biol 149: 1503-1512.
192. Swenson KI, Piwnica-Worms H, McNamee H, Paul DL (1990) Tyrosine phosphorylation of the gap junction protein connexin43 is required for the pp60v-src-induced inhibition of communication. Cell Regul 1: 989-1002.
193. Lin R, Warn-Cramer BJ, Kurata WE, Lau AF (2001) v-Src phosphorylation of connexin 43 on Tyr247 and Tyr265 disrupts gap junctional communication. J Cell Biol 154: 815-827.
194. Solan JL, Lampe PD (2008) Connexin 43 in LA-25 cells with active v-src is phosphorylated on Y247, Y265, S262, S279/282, and S368 via multiple signaling pathways. Cell Commun Adhes 15: 75-84.
195. Hwang SK, Kim HH (2011) The functions of mTOR in ischemic diseases. BMB Rep 44: 506-511.

196. Goodman CA, Mayhew DL, Hornberger TA (2011) Recent progress toward understanding the molecular mechanisms that regulate skeletal muscle mass. Cell Signal 23: 1896-1906.
197. Rodriguez J, Calvo F, Gonzalez JM, Casar B, Andres V, et al. (2010) ERK1/2 MAP kinases promote cell cycle entry by rapid, kinase-independent disruption of retinoblastoma-lamin A complexes. J Cell Biol 191: 967-979.
198. Wang Y, Herron AJ, Worman HJ (2006) Pathology and nuclear abnormalities in hearts of transgenic mice expressing M371K lamin A encoded by an LMNA mutation causing Emery-Dreifuss muscular dystrophy. Hum Mol Genet 15: 2479-2489.
199. Lee DC, Welton KL, Smith ED, Kennedy BK (2009) A-type nuclear lamins act as transcriptional repressors when targeted to promoters. Exp Cell Res 315: 996-1007.
200. Shumaker DK, Solimando L, Sengupta K, Shimi T, Adam SA, et al. (2008) The highly conserved nuclear lamin Ig-fold binds to PCNA: its role in DNA replication. J Cell Biol 181: 269-280.
201. Burtner CR, Kennedy BK (2010) Progeria syndromes and ageing: what is the connection? Nat Rev Mol Cell Biol 11: 567-578.
202. Davies BS, Barnes RH, 2nd, Tu Y, Ren S, Andres DA, et al. (2010) An accumulation of non-farnesylated prelamin A causes cardiomyopathy but not progeria. Hum Mol Genet 19: 2682-2694.
203. Bonne G, Mercuri E, Muchir A, Urtizberea A, Becane HM, et al. (2000) Clinical and molecular genetic spectrum of autosomal dominant Emery-Dreifuss muscular dystrophy due to mutations of the lamin A/C gene. Ann Neurol 48: 170-180.
204. Dai DF, Santana LF, Vermulst M, Tomazela DM, Emond MJ, et al. (2009) Overexpression of catalase targeted to mitochondria attenuates murine cardiac aging. Circulation 119: 2789-2797.
205. Muchir A, Wu W, Worman HJ (2009) Reduced expression of A-type lamins and emerin activates extracellular signal-regulated kinase in cultured cells. Biochim Biophys Acta 1792: 75-81.
206. Ruch RJ, Trosko JE, Madhukar BV (2001) Inhibition of connexin43 gap junctional intercellular communication by TPA requires ERK activation. J Cell Biochem 83: 163-169.
207. Gary-Bobo G, Parlakian A, Escoubet B, Franco CA, Clement S, et al. (2008) Mosaic inactivation of the serum response factor gene in the myocardium induces focal lesions and heart failure. Eur J Heart Fail 10: 635-645.
208. Gonzalez S, Aguilera S, Urzua U, Quest AF, Molina C, et al. (2011) Mechanotransduction and epigenetic control in autoimmune diseases. Autoimmun Rev 10: 175-179.
209. Dahl KN, Ribeiro AJ, Lammerding J (2008) Nuclear shape, mechanics, and mechanotransduction. Circ Res 102: 1307-1318.
210. Favreau C, Delbarre E, Courvalin JC, Buendia B (2008) Differentiation of C2C12 myoblasts expressing lamin A mutated at a site responsible for Emery-Dreifuss muscular dystrophy is improved by inhibition of the MEK-ERK pathway and stimulation of the PI3-kinase pathway. Exp Cell Res 314: 1392-1405.
211. Gonzalez JM, Navarro-Puche A, Casar B, Crespo P, Andres V (2008) Fast regulation of AP-1 activity through interaction of lamin A/C, ERK1/2, and c-Fos at the nuclear envelope. J Cell Biol 183: 653-666.
212. Kodama H, Fukuda K, Pan J, Sano M, Takahashi T, et al. (2000) Significance of ERK cascade compared with JAK/STAT and PI3-K pathway in gp130-mediated cardiac hypertrophy. Am J Physiol Heart Circ Physiol 279: H1635-1644.
213. Gutstein DE, Danik SB, Lewitton S, France D, Liu F, et al. (2005) Focal gap junction uncoupling and spontaneous ventricular ectopy. Am J Physiol Heart Circ Physiol 289: H1091-1098.
214. Gard JJ, Yamada K, Green KG, Eloff BC, Rosenbaum DS, et al. (2005) Remodeling of gap junctions and slow conduction in a mouse model of desmin-related cardiomyopathy. Cardiovasc Res 67: 539-547.

215. Aplin M, Christensen GL, Schneider M, Heydorn A, Gammeltoft S, et al. (2007) Differential extracellular signal-regulated kinases 1 and 2 activation by the angiotensin type 1 receptor supports distinct phenotypes of cardiac myocytes. Basic Clin Pharmacol Toxicol 100: 296-301.
216. Ivorra C, Kubicek M, Gonzalez JM, Sanz-Gonzalez SM, Alvarez-Barrientos A, et al. (2006) A mechanism of AP-1 suppression through interaction of c-Fos with lamin A/C. Genes Dev 20: 307-320.
217. Polontchouk L, Ebelt B, Jackels M, Dhein S (2002) Chronic effects of endothelin 1 and angiotensin II on gap junctions and intercellular communication in cardiac cells. Faseb J 16: 87-89.
218. Lu G, Haider H, Porollo A, Ashraf M (2010) Mitochondria-specific transgenic overexpression of connexin-43 simulates preconditioning-induced cytoprotection of stem cells. Cardiovasc Res 88: 277-286.
219. Rottlaender D, Boengler K, Wolny M, Michels G, Endres-Becker J, et al. (2010) Connexin 43 acts as a cytoprotective mediator of signal transduction by stimulating mitochondrial KATP channels in mouse cardiomyocytes. J Clin Invest 120: 1441-1453.
220. Roth DM, Swaney JS, Dalton ND, Gilpin EA, Ross J, Jr. (2002) Impact of anesthesia on cardiac function during echocardiography in mice. Am J Physiol Heart Circ Physiol 282: H2134-2140.
221. Allegra S, Bouazza L, Benetollo C, Li JY, Langlois D (2005) A 7.1 kbp beta-myosin heavy chain promoter, efficient for green fluorescent protein expression, probably induces lethality when overexpressing a mutated transforming growth factor-beta type II receptor in transgenic mice. Transgenic Res 14: 69-80.
222. Taimen P, Pfleghaar K, Shimi T, Moller D, Ben-Harush K, et al. (2009) A progeria mutation reveals functions for lamin A in nuclear assembly, architecture, and chromosome organization. Proc Natl Acad Sci U S A 106: 20788-20793.
223. Lattanzi G, Columbaro M, Mattioli E, Cenni V, Camozzi D, et al. (2007) Pre-Lamin A processing is linked to heterochromatin organization. J Cell Biochem 102: 1149-1159.
224. Kumaran RI, Muralikrishna B, Parnaik VK (2002) Lamin A/C speckles mediate spatial organization of splicing factor compartments and RNA polymerase II transcription. J Cell Biol 159: 783-793.
225. De Sandre-Giovannoli A, Bernard R, Cau P, Navarro C, Amiel J, et al. (2003) Lamin a truncation in Hutchinson-Gilford progeria. Science 300: 2055.
226. Pasotti M, Klersy C, Pilotto A, Marziliano N, Rapezzi C, et al. (2008) Long-term outcome and risk stratification in dilated cardiolaminopathies. J Am Coll Cardiol 52: 1250-1260.
227. Chandar S, Yeo LS, Leimena C, Tan JC, Xiao XH, et al. (2010) Effects of mechanical stress and carvedilol in lamin A/C-deficient dilated cardiomyopathy. Circ Res 106: 573-582.
228. Hara K, Maruki Y, Long X, Yoshino K, Oshiro N, et al. (2002) Raptor, a binding partner of target of rapamycin (TOR), mediates TOR action. Cell 110: 177-189.
229. Kim DH, Sarbassov DD, Ali SM, King JE, Latek RR, et al. (2002) mTOR interacts with raptor to form a nutrient-sensitive complex that signals to the cell growth machinery. Cell 110: 163-175.
230. Kim DH, Sarbassov DD, Ali SM, Latek RR, Guntur KV, et al. (2003) GbetaL, a positive regulator of the rapamycin-sensitive pathway required for the nutrient-sensitive interaction between raptor and mTOR. Mol Cell 11: 895-904.
231. Hara K, Yonezawa K, Kozlowski MT, Sugimoto T, Andrabi K, et al. (1997) Regulation of eIF-4E BP1 phosphorylation by mTOR. J Biol Chem 272: 26457-26463.
232. Burnett PE, Barrow RK, Cohen NA, Snyder SH, Sabatini DM (1998) RAFT1 phosphorylation of the translational regulators p70 S6 kinase and 4E-BP1. Proc Natl Acad Sci U S A 95: 1432-1437.
233. Ono Y, Ito H, Tamamori M, Nozato T, Adachi S, et al. (2000) Role and relation of p70 S6 and extracellular signal-regulated kinases in the phenotypic changes of hypertrophy of cardiac myocytes. Jpn Circ J 64: 695-700.

234. Rommel C, Bodine SC, Clarke BA, Rossman R, Nunez L, et al. (2001) Mediation of IGF-1-induced skeletal myotube hypertrophy by PI(3)K/Akt/mTOR and PI(3)K/Akt/GSK3 pathways. Nat Cell Biol 3: 1009-1013.
235. Bodine SC, Stitt TN, Gonzalez M, Kline WO, Stover GL, et al. (2001) Akt/mTOR pathway is a crucial regulator of skeletal muscle hypertrophy and can prevent muscle atrophy in vivo. Nat Cell Biol 3: 1014-1019.
236. McMullen JR, Sherwood MC, Tarnavski O, Zhang L, Dorfman AL, et al. (2004) Inhibition of mTOR signaling with rapamycin regresses established cardiac hypertrophy induced by pressure overload. Circulation 109: 3050-3055.
237. Sasai N, Agata N, Inoue-Miyazu M, Kawakami K, Kobayashi K, et al. (2010) Involvement of PI3K/Akt/TOR pathway in stretch-induced hypertrophy of myotubes. Muscle Nerve 41: 100-106.
238. Zoncu R, Efeyan A, Sabatini DM (2011) mTOR: from growth signal integration to cancer, diabetes and ageing. Nat Rev Mol Cell Biol 12: 21-35.
239. Hosokawa N, Hara T, Kaizuka T, Kishi C, Takamura A, et al. (2009) Nutrient-dependent mTORC1 association with the ULK1-Atg13-FIP200 complex required for autophagy. Mol Biol Cell 20: 1981-1991.
240. Ogura Y, Iemitsu M, Naito H, Kakigi R, Kakehashi C, et al. (2011) Single bout of running exercise changes LC3-II expression in rat cardiac muscle. Biochem Biophys Res Commun 414: 756-760.
241. Grumati P, Coletto L, Sabatelli P, Cescon M, Angelin A, et al. (2010) Autophagy is defective in collagen VI muscular dystrophies, and its reactivation rescues myofiber degeneration. Nat Med 16: 1313-1320.
242. Kassiotis C, Ballal K, Wellnitz K, Vela D, Gong M, et al. (2009) Markers of autophagy are downregulated in failing human heart after mechanical unloading. Circulation 120: S191-197.
243. Kim YA, Kim YS, Song W (2011) Autophagic response to a single bout of moderate exercise in murine skeletal muscle. J Physiol Biochem.
244. Cupesi M, Yoshioka J, Gannon J, Kudinova A, Stewart CL, et al. (2010) Attenuated hypertrophic response to pressure overload in a lamin A/C haploinsufficiency mouse. J Mol Cell Cardiol 48: 1290-1297.
245. Giordano A (2010) Molecular basis of different outcomes for drug-eluting stents that release sirolimus or tacrolimus. Curr Opin Drug Discov Devel 13: 159-168.
246. Borders EB, Bivona C, Medina PJ (2010) Mammalian target of rapamycin: biological function and target for novel anticancer agents. Am J Health Syst Pharm 67: 2095-2106.
247. Stanfel MN, Shamieh LS, Kaeberlein M, Kennedy BK (2009) The TOR pathway comes of age. Biochim Biophys Acta 1790: 1067-1074.
248. Weir MR, Diekmann F, Flechner SM, Lebranchu Y, Mandelbrot DA, et al. (2010) mTOR inhibition: the learning curve in kidney transplantation. Transpl Int 23: 447-460.
249. Miller RA, Harrison DE, Astle CM, Baur JA, Boyd AR, et al. (2011) Rapamycin, but not resveratrol or simvastatin, extends life span of genetically heterogeneous mice. J Gerontol A Biol Sci Med Sci 66: 191-201.
250. Feldman ME, Apsel B, Uotila A, Loewith R, Knight ZA, et al. (2009) Active-site inhibitors of mTOR target rapamycin-resistant outputs of mTORC1 and mTORC2. PLoS Biol 7: e38.
251. Bogdanovich S, McNally EM, Khurana TS (2008) Myostatin blockade improves function but not histopathology in a murine model of limb-girdle muscular dystrophy 2C. Muscle Nerve 37: 308-316.
252. Nevo Y, Halevy O, Genin O, Moshe I, Turgeman T, et al. (2010) Fibrosis inhibition and muscle histopathology improvement in laminin-alpha2-deficient mice. Muscle Nerve 42: 218-229.
253. Zheng Q, Su H, Ranek MJ, Wang X (2011) Autophagy and p62 in cardiac proteinopathy. Circ Res 109: 296-308.

254. Pattingre S, Espert L, Biard-Piechaczyk M, Codogno P (2008) Regulation of macroautophagy by mTOR and Beclin 1 complexes. Biochimie 90: 313-323.
255. Klionsky DJ, Abeliovich H, Agostinis P, Agrawal DK, Aliev G, et al. (2008) Guidelines for the use and interpretation of assays for monitoring autophagy in higher eukaryotes. Autophagy 4: 151-175.
256. Shiojima I, Sato K, Izumiya Y, Schiekofer S, Ito M, et al. (2005) Disruption of coordinated cardiac hypertrophy and angiogenesis contributes to the transition to heart failure. J Clin Invest 115: 2108-2118.
257. Marin TM, Keith K, Davies B, Conner DA, Guha P, et al. (2011) Rapamycin reverses hypertrophic cardiomyopathy in a mouse model of LEOPARD syndrome-associated PTPN11 mutation. J Clin Invest 121: 1026-1043.
258. Hein S, Kostin S, Heling A, Maeno Y, Schaper J (2000) The role of the cytoskeleton in heart failure. Cardiovasc Res 45: 273-278.
259. McLendon PM, Robbins J (2011) Desmin-related cardiomyopathy: an unfolding story. Am J Physiol Heart Circ Physiol 301: H1220-1228.
260. Taylor MR, Slavov D, Ku L, Di Lenarda A, Sinagra G, et al. (2007) Prevalence of desmin mutations in dilated cardiomyopathy. Circulation 115: 1244-1251.
261. Di Somma S, Marotta M, Salvatore G, Cudemo G, Cuda G, et al. (2000) Changes in myocardial cytoskeletal intermediate filaments and myocyte contractile dysfunction in dilated cardiomyopathy: an in vivo study in humans. Heart 84: 659-667.
262. Hermans MC, Pinto YM, Merkies IS, de Die-Smulders CE, Crijns HJ, et al. (2010) Hereditary muscular dystrophies and the heart. Neuromuscul Disord 20: 479-492.
263. Zomzely CE, Roberts S, Gruber CP, Brown DM (1968) Cerebral protein synthesis. II. Instability of cerebral messenger ribonucleic acid-ribosome complexes. J Biol Chem 243: 5396-5409.
264. Broers JL, Kuijpers HJ, Ostlund C, Worman HJ, Endert J, et al. (2005) Both lamin A and lamin C mutations cause lamina instability as well as loss of internal nuclear lamin organization. Exp Cell Res 304: 582-592.
265. Lammerding J, Fong LG, Ji JY, Reue K, Stewart CL, et al. (2006) Lamins A and C but not lamin B1 regulate nuclear mechanics. J Biol Chem 281: 25768-25780.
266. Stuurman N, Heins S, Aebi U (1998) Nuclear lamins: their structure, assembly, and interactions. J Struct Biol 122: 42-66.
267. Stierle V, Couprie J, Ostlund C, Krimm I, Zinn-Justin S, et al. (2003) The carboxyl-terminal region common to lamins A and C contains a DNA binding domain. Biochemistry 42: 4819-4828.
268. Worman HJ, Courvalin JC (2000) The inner nuclear membrane. J Membr Biol 177: 1-11.
269. Stewart CL, Roux KJ, Burke B (2007) Blurring the boundary: the nuclear envelope extends its reach. Science 318: 1408-1412.
270. Goldman RD, Gruenbaum Y, Moir RD, Shumaker DK, Spann TP (2002) Nuclear lamins: building blocks of nuclear architecture. Genes Dev 16: 533-547.
271. Cohen TV, Hernandez L, Stewart CL (2008) Functions of the nuclear envelope and lamina in development and disease. Biochem Soc Trans 36: 1329-1334.
272. Worman HJ (2012) Nuclear lamins and laminopathies. J Pathol 226: 316-325.
273. Emerson LJ, Holt MR, Wheeler MA, Wehnert M, Parsons M, et al. (2009) Defects in cell spreading and ERK1/2 activation in fibroblasts with lamin A/C mutations. Biochim Biophys Acta 1792: 810-821.
274. Beardslee MA, Laing JG, Beyer EC, Saffitz JE (1998) Rapid turnover of connexin43 in the adult rat heart. Circ Res 83: 629-635.
275. Solan JL, Lampe PD (2009) Connexin43 phosphorylation: structural changes and biological effects. Biochem J 419: 261-272.

276. Marquez-Rosado L, Solan JL, Dunn CA, Norris RP, Lampe PD (2011) Connexin43 phosphorylation in brain, cardiac, endothelial and epithelial tissues. Biochim Biophys Acta.
277. Rivedal E, Opsahl H (2001) Role of PKC and MAP kinase in EGF- and TPA-induced connexin43 phosphorylation and inhibition of gap junction intercellular communication in rat liver epithelial cells. Carcinogenesis 22: 1543-1550.
278. Mohamed JS, Hajira A, Li Z, Paulin D, Boriek AM (2011) Desmin regulates airway smooth muscle hypertrophy through early growth-responsive protein-1 and microRNA-26a. J Biol Chem 286: 43394-43404.
279. Piercy RJ, Zhou H, Feng L, Pombo A, Muntoni F, et al. (2007) Desmin immunolocalisation in autosomal dominant Emery-Dreifuss muscular dystrophy. Neuromuscul Disord 17: 297-305.
280. Sutherland FJ, Hearse DJ (2000) The isolated blood and perfusion fluid perfused heart. Pharmacol Res 41: 613-627.
281. Skrzypiec-Spring M, Grotthus B, Szelag A, Schulz R (2007) Isolated heart perfusion according to Langendorff---still viable in the new millennium. J Pharmacol Toxicol Methods 55: 113-126.
282. Stewart CL, Kozlov S, Fong LG, Young SG (2007) Mouse models of the laminopathies. Exp Cell Res 313: 2144-2156.
283. Ma L, Chen Z, Erdjument-Bromage H, Tempst P, Pandolfi PP (2005) Phosphorylation and functional inactivation of TSC2 by Erk implications for tuberous sclerosis and cancer pathogenesis. Cell 121: 179-193.
284. Ballif BA, Roux PP, Gerber SA, MacKeigan JP, Blenis J, et al. (2005) Quantitative phosphorylation profiling of the ERK/p90 ribosomal S6 kinase-signaling cassette and its targets, the tuberous sclerosis tumor suppressors. Proc Natl Acad Sci U S A 102: 667-672.
285. Roux PP, Ballif BA, Anjum R, Gygi SP, Blenis J (2004) Tumor-promoting phorbol esters and activated Ras inactivate the tuberous sclerosis tumor suppressor complex via p90 ribosomal S6 kinase. Proc Natl Acad Sci U S A 101: 13489-13494.
286. Carracedo A, Ma L, Teruya-Feldstein J, Rojo F, Salmena L, et al. (2008) Inhibition of mTORC1 leads to MAPK pathway activation through a PI3K-dependent feedback loop in human cancer. J Clin Invest 118: 3065-3074.
287. Sunayama J, Matsuda K, Sato A, Tachibana K, Suzuki K, et al. (2010) Crosstalk between the PI3K/mTOR and MEK/ERK pathways involved in the maintenance of self-renewal and tumorigenicity of glioblastoma stem-like cells. Stem Cells 28: 1930-1939.
288. Shahbazian D, Roux PP, Mieulet V, Cohen MS, Raught B, et al. (2006) The mTOR/PI3K and MAPK pathways converge on eIF4B to control its phosphorylation and activity. Embo Journal 25: 2781-2791.
289. Kinkade CW, Castillo-Martin M, Puzio-Kuter A, Yan J, Foster TH, et al. (2008) Targeting AKT/mTOR and ERK MAPK signaling inhibits hormone-refractory prostate cancer in a preclinical mouse model. J Clin Invest 118: 3051-3064.
290. Shimizu T, Tolcher AW, Papadopoulos KP, Beeram M, Rasco DW, et al. (2012) The Clinical Effect of the Dual-Targeting Strategy Involving PI3K/AKT/mTOR and RAS/MEK/ERK Pathways in Patients with Advanced Cancer. Clin Cancer Res 18: 2316-2325.
291. Morris GE, Manilal S (1999) Heart to heart: from nuclear proteins to Emery-Dreifuss muscular dystrophy. Hum Mol Genet 8: 1847-1851.
292. Mounkes LC, Burke B, Stewart CL (2001) The A-type lamins: nuclear structural proteins as a focus for muscular dystrophy and cardiovascular diseases. Trends Cardiovasc Med 11: 280-285.
293. Manilal S, Sewry CA, Pereboev A, Man N, Gobbi P, et al. (1999) Distribution of emerin and lamins in the heart and implications for Emery-Dreifuss muscular dystrophy. Hum Mol Genet 8: 353-359.
294. van der Maarel SM, Frants RR, Padberg GW (2007) Facioscapulohumeral muscular dystrophy. Biochim Biophys Acta 1772: 186-194.

295. Lunt PW, Jardine PE, Koch MC, Maynard J, Osborn M, et al. (1995) Correlation between fragment size at D4F104S1 and age at onset or at wheelchair use, with a possible generational effect, accounts for much phenotypic variation in 4q35-facioscapulohumeral muscular dystrophy (FSHD). Hum Mol Genet 4: 951-958.
296. Tawil R, Forrester J, Griggs RC, Mendell J, Kissel J, et al. (1996) Evidence for anticipation and association of deletion size with severity in facioscapulohumeral muscular dystrophy. The FSH-DY Group. Ann Neurol 39: 744-748.
297. Ricci E, Galluzzi G, Deidda G, Cacurri S, Colantoni L, et al. (1999) Progress in the molecular diagnosis of facioscapulohumeral muscular dystrophy and correlation between the number of KpnI repeats at the 4q35 locus and clinical phenotype. Ann Neurol 45: 751-757.
298. Tawil R, Van Der Maarel SM (2006) Facioscapulohumeral muscular dystrophy. Muscle Nerve 34: 1-15.
299. Sarfarazi M, Wijmenga C, Upadhyaya M, Weiffenbach B, Hyser C, et al. (1992) Regional mapping of facioscapulohumeral muscular dystrophy gene on 4q35: combined analysis of an international consortium. Am J Hum Genet 51: 396-403.
300. Wijmenga C, Frants RR, Brouwer OF, Moerer P, Weber JL, et al. (1990) Location of facioscapulohumeral muscular dystrophy gene on chromosome 4. Lancet 336: 651-653.
301. Wijmenga C, Hewitt JE, Sandkuijl LA, Clark LN, Wright TJ, et al. (1992) Chromosome 4q DNA rearrangements associated with facioscapulohumeral muscular dystrophy. Nat Genet 2: 26-30.
302. van Deutekom JC, Wijmenga C, van Tienhoven EA, Gruter AM, Hewitt JE, et al. (1993) FSHD associated DNA rearrangements are due to deletions of integral copies of a 3.2 kb tandemly repeated unit. Hum Mol Genet 2: 2037-2042.
303. de Greef JC, Frants RR, van der Maarel SM (2008) Epigenetic mechanisms of facioscapulohumeral muscular dystrophy. Mutat Res 647: 94-102.
304. Gabriels J, Beckers MC, Ding H, De Vriese A, Plaisance S, et al. (1999) Nucleotide sequence of the partially deleted D4Z4 locus in a patient with FSHD identifies a putative gene within each 3.3 kb element. Gene 236: 25-32.
305. Beckers M, Gabriels J, van der Maarel S, De Vriese A, Frants RR, et al. (2001) Active genes in junk DNA? Characterization of DUX genes embedded within 3.3 kb repeated elements. Gene 264: 51-57.
306. Clapp J, Mitchell LM, Bolland DJ, Fantes J, Corcoran AE, et al. (2007) Evolutionary conservation of a coding function for D4Z4, the tandem DNA repeat mutated in facioscapulohumeral muscular dystrophy. Am J Hum Genet 81: 264-279.
307. Ansseau E, Laoudj-Chenivesse D, Marcowycz A, Tassin A, Vanderplanck C, et al. (2009) DUX4c is up-regulated in FSHD. It induces the MYF5 protein and human myoblast proliferation. PLoS One 4: e7482.
308. Snider L, Geng LN, Lemmers RJ, Kyba M, Ware CB, et al. (2010) Facioscapulohumeral dystrophy: incomplete suppression of a retrotransposed gene. PLoS Genet 6: e1001181.
309. Kowaljow V, Marcowycz A, Ansseau E, Conde CB, Sauvage S, et al. (2007) The DUX4 gene at the FSHD1A locus encodes a pro-apoptotic protein. Neuromuscul Disord 17: 611-623.
310. Bosnakovski D, Xu Z, Gang EJ, Galindo CL, Liu M, et al. (2008) An isogenetic myoblast expression screen identifies DUX4-mediated FSHD-associated molecular pathologies. Embo J 27: 2766-2779.
311. Snider L, Asawachaicharn A, Tyler AE, Geng LN, Petek LM, et al. (2009) RNA transcripts, miRNA-sized fragments and proteins produced from D4Z4 units: new candidates for the pathophysiology of facioscapulohumeral dystrophy. Hum Mol Genet 18: 2414-2430.
312. Lemmers RJ, van der Vliet PJ, Klooster R, Sacconi S, Camano P, et al. A unifying genetic model for facioscapulohumeral muscular dystrophy. Science 329: 1650-1653.

313. Caretti G, Di Padova M, Micales B, Lyons GE, Sartorelli V (2004) The Polycomb Ezh2 methyltransferase regulates muscle gene expression and skeletal muscle differentiation. Genes Dev 18: 2627-2638.
314. Laible G, Wolf A, Dorn R, Reuter G, Nislow C, et al. (1997) Mammalian homologues of the Polycomb-group gene Enhancer of zeste mediate gene silencing in Drosophila heterochromatin and at S. cerevisiae telomeres. Embo J 16: 3219-3232.
315. Forlani G, Giarda E, Ala U, Di Cunto F, Salani M, et al. The MeCP2/YY1 interaction regulates ANT1 expression at 4q35: novel hints for Rett syndrome pathogenesis. Hum Mol Genet 19: 3114-3123.
316. Donohoe ME, Zhang LF, Xu N, Shi Y, Lee JT (2007) Identification of a Ctcf cofactor, Yy1, for the X chromosome binary switch. Mol Cell 25: 43-56.
317. Lehming N, Le Saux A, Schuller J, Ptashne M (1998) Chromatin components as part of a putative transcriptional repressing complex. Proc Natl Acad Sci U S A 95: 7322-7326.
318. Lomberk G, Wallrath L, Urrutia R (2006) The Heterochromatin Protein 1 family. Genome Biol 7: 228.
319. Erard MS, Belenguer P, Caizergues-Ferrer M, Pantaloni A, Amalric F (1988) A major nucleolar protein, nucleolin, induces chromatin decondensation by binding to histone H1. Eur J Biochem 175: 525-530.
320. Bodega B, Ramirez GD, Grasser F, Cheli S, Brunelli S, et al. (2009) Remodeling of the chromatin structure of the facioscapulohumeral muscular dystrophy (FSHD) locus and upregulation of FSHD-related gene 1 (FRG1) expression during human myogenic differentiation. BMC Biol 7: 41.
321. Gabellini D, Green MR, Tupler R (2002) Inappropriate gene activation in FSHD: a repressor complex binds a chromosomal repeat deleted in dystrophic muscle. Cell 110: 339-348.
322. Petrov A, Allinne J, Pirozhkova I, Laoudj D, Lipinski M, et al. (2008) A nuclear matrix attachment site in the 4q35 locus has an enhancer-blocking activity in vivo: implications for the facio-scapulo-humeral dystrophy. Genome Res 18: 39-45.
323. Petrov A, Pirozhkova I, Carnac G, Laoudj D, Lipinski M, et al. (2006) Chromatin loop domain organization within the 4q35 locus in facioscapulohumeral dystrophy patients versus normal human myoblasts. Proc Natl Acad Sci U S A 103: 6982-6987.
324. Pirozhkova I, Petrov A, Dmitriev P, Laoudj D, Lipinski M, et al. (2008) A functional role for 4qA/B in the structural rearrangement of the 4q35 region and in the regulation of FRG1 and ANT1 in facioscapulohumeral dystrophy. PLoS One 3: e3389.
325. Osborne RJ, Welle S, Venance SL, Thornton CA, Tawil R (2007) Expression profile of FSHD supports a link between retinal vasculopathy and muscular dystrophy. Neurology 68: 569-577.
326. Gabellini D, D'Antona G, Moggio M, Prelle A, Zecca C, et al. (2006) Facioscapulohumeral muscular dystrophy in mice overexpressing FRG1. Nature 439: 973-977.
327. Liu Q, Jones TI, Tang VW, Brieher WM, Jones PL Facioscapulohumeral muscular dystrophy region gene-1 (FRG-1) is an actin-bundling protein associated with muscle-attachment sites. J Cell Sci 123: 1116-1123.
328. Hanel ML, Sun CY, Jones TI, Long SW, Zanotti S, et al. Facioscapulohumeral muscular dystrophy (FSHD) region gene 1 (FRG1) is a dynamic nuclear and sarcomeric protein. Differentiation.
329. Hanel ML, Wuebbles RD, Jones PL (2009) Muscular dystrophy candidate gene FRG1 is critical for muscle development. Dev Dyn 238: 1502-1512.
330. Wuebbles RD, Long SW, Hanel ML, Jones PL (2010) Testing the effects of FSHD candidate gene expression in vertebrate muscle development. Int J Clin Exp Pathol 3: 386-400.
331. D'Antona G, Brocca L, Pansarasa O, Rinaldi C, Tupler R, et al. (2007) Structural and functional alterations of muscle fibres in the novel mouse model of facioscapulohumeral muscular dystrophy. J Physiol 584: 997-1009.
332. Neville C, Rosenthal N, McGrew M, Bogdanova N, Hauschka S (1997) Skeletal muscle cultures. Methods Cell Biol 52: 85-116.

333. Kudlow BA, Jameson SA, Kennedy BK (2005) HIV protease inhibitors block adipocyte differentiation independently of lamin A/C. Aids 19: 1565-1573.
334. van Koningsbruggen S, Dirks RW, Mommaas AM, Onderwater JJ, Deidda G, et al. (2004) FRG1P is localised in the nucleolus, Cajal bodies, and speckles. J Med Genet 41: e46.
335. Frolov MV, Dyson NJ (2004) Molecular mechanisms of E2F-dependent activation and pRB-mediated repression. J Cell Sci 117: 2173-2181.
336. Trimarchi JM, Lees JA (2002) Sibling rivalry in the E2F family. Nat Rev Mol Cell Biol 3: 11-20.
337. Watchko JF, O'Day TL, Hoffman EP (2002) Functional characteristics of dystrophic skeletal muscle: insights from animal models. J Appl Physiol 93: 407-417.
338. Mittelbronn M, Sullivan T, Stewart CL, Bornemann A (2008) Myonuclear degeneration in LMNA null mice. Brain Pathol 18: 338-343.
339. Melone MA, Peluso G, Petillo O, Galderisi U, Cotrufo R (1999) Defective growth in vitro of Duchenne Muscular Dystrophy myoblasts: the molecular and biochemical basis. J Cell Biochem 76: 118-132.
340. van Koningsbruggen S, Straasheijm KR, Sterrenburg E, de Graaf N, Dauwerse HG, et al. (2007) FRG1P-mediated aggregation of proteins involved in pre-mRNA processing. Chromosoma 116: 53-64.
341. Day JW, Ranum LP (2005) RNA pathogenesis of the myotonic dystrophies. Neuromuscul Disord 15: 5-16.
342. Ranum LP, Day JW (2004) Myotonic dystrophy: RNA pathogenesis comes into focus. Am J Hum Genet 74: 793-804.
343. Mumberg D, Wick M, Burger C, Haas K, Funk M, et al. (1997) Cyclin ET, a new splice variant of human cyclin E with a unique expression pattern during cell cycle progression and differentiation. Nucleic Acids Res 25: 2098-2105.
344. Sewing A, Ronicke V, Burger C, Funk M, Muller R (1994) Alternative splicing of human cyclin E. J Cell Sci 107 (Pt 2): 581-588.
345. Porter DC, Keyomarsi K (2000) Novel splice variants of cyclin E with altered substrate specificity. Nucleic Acids Res 28: E101.
346. Klooster R, Straasheijm K, Shah B, Sowden J, Frants R, et al. (2009) Comprehensive expression analysis of FSHD candidate genes at the mRNA and protein level. Eur J Hum Genet 17: 1615-1624.
347. Masny PS, Chan OY, de Greef JC, Bengtsson U, Ehrlich M, et al. (2009) Analysis of allele-specific RNA transcription in FSHD by RNA-DNA FISH in single myonuclei. Eur J Hum Genet.
348. Barro M, Carnac G, Flavier S, Mercier J, Vassetzky Y, et al. (2008) Myoblasts from affected and non affected FSHD muscles exhibit morphological differentiation defects. J Cell Mol Med.
349. Kyba M, Perlingeiro RC, Daley GQ (2002) HoxB4 confers definitive lymphoid-myeloid engraftment potential on embryonic stem cell and yolk sac hematopoietic progenitors. Cell 109: 29-37.
350. Rabinovitch PS (1994) DNA content histogram and cell-cycle analysis. Methods Cell Biol 41: 263-296.
351. Schorl C, Sedivy JM (2007) Analysis of cell cycle phases and progression in cultured mammalian cells. Methods 41: 143-150.

Vita

Steven C. Chen was born in Columbus, Ohio in July of 1985. He moved with his family to Seattle in 1988, where he attended his local elementary and junior high school. After 8th grade, he was accepted into the University of Washington Early Entrance Program and subsequently enrolled at the University of Washington in 1999. He earned a Bachelor of Science in Biochemistry, a Bachelor of Science in Cell and Molecular Biology, and a Bachelor of Arts in Music in 2004. After graduating, Steven pursued his interested in science by conducting research at Seattle Children's Hospital for 2 years with Dr. Carol Miao.

In 2006, Steven joined the Ph.D. program in the Department of Biochemistry at the University of Washington. He joined the lab of Dr. Brian Kennedy conducting research into the function of A-type lamins. Following the departure of Dr. Brian Kennedy to the Buck Institute for Research on Aging, he transitioned his research into the lab of Dr. Paul Lampe at the Fred Hutchinson Cancer Research Center. In 2012, he graduated with a Doctor of Philosophy in Biochemistry from the University of Washington. He will be moving to San Francisco to join his wife and is seeking a postdoctoral research position at the University of California San Francisco.